Author:
Lamb, Alex

Title:
A Novel Stomatal Mutant Implicates Clathrin Mediated Endocytosis as a Factor in Arabidopsis Carbon Dioxide Signalling

A Novel Stomatal Mutant Implicates Clathrin Mediated Endocytosis as a Factor in *Arabidopsis* Carbon Dioxide Signalling

Alexander Lamb

A dissertation submitted to the University of Bristol in accordance with the requirements for award of the degree of MSc by Research in the Faculty of Science.

School of Biological Sciences;

Submitted March 2019

Word Count: 26,725

Abstract

Screening of a mutant population of *Arabidopsis thaliana* identified a mutant, EO_2, that was insensitive to elevated atmospheric Carbon dioxide and further study found that the mutant had a wild type response to Abscisic Acid. These results indicated that the mutant was impaired in CO_2 perception upstream of the point of convergence with ABA signalling pathways at OST1/SnRK2. DRP1E was identified as the causative gene of the EO_2 mutant stomatal phenotype and corresponding phenotypes were found in 2 independent *drp1e* lines. EO_2 and *drp1e* mutants were found to have decreased transpiration rate, but increased carbon assimilation rate and water use efficiency compared to Col-0.

Based on an assessment of the collected results against the relevant literature, the role of DRP1E in clathrin mediated endocytosis (CME) was selected for further research in stomatal CO_2 responses. Inhibition of CME was found to strongly inhibit stomatal responses to elevated CO_2 but had only a moderate effect on responses to ABA. Confocal vesicle assays found that EO_2 exhibited similar vesicle formation rates to Col-0 in response to ABA and CO_2, indicating that rates of endocytosis were not the source of the CO_2 insensitivity displayed by EO_2 and in CME-inhibited Col-0. These results imply that targeted endocytosis of specific carbon dioxide signalling proteins at the cell membrane may act to regulate stomatal closure in response to elevated CO_2.

Dedication and Acknowledgements

I would first and foremost like to thank my supervisor, Professor Alistair Hetherington, for his insight, guidance, patience and support throughout my time in his research group; the completion of this thesis would not be possible if not for him and it has been a pleasure studying in his lab. I would also like to thank Dr Jean-Charles Isner and Dr Peng Sun for their assistance and expertise in molecular experiments and the long process of gene cloning and Dr Deirdre McLachlan for her invaluable guidance with confocal microscopy experiments. A big thank you to Professor Mike Mickelbart, Dr Mike Gosney and Mr Uday Mitsuyasu from Purdue University, Indiana, USA for their help, guidance and fantastic hospitality, it was a pleasure working with you all! I would also like to thank Dr Dan Lan, Mr Ashley Pridgeon and the rest of the guard cell group for their enthusiasm, ideas and good company; this thesis would not have been possible without you. Lastly, I would like to thank my wonderful friends and family for their support and encouragement throughout.

Author’s Declaration

I declare that the work in this dissertation was carried out in accordance with the requirements of the University's *Regulations and Code of Practice for Research Degree Programmes* and that it has not been submitted for any other academic award. Except where indicated by specific reference in the text, the work is the candidate's own work. Work done in collaboration with, or with the assistance of, others, is indicated as such. Any views expressed in the dissertation are those of the author.

SIGNED: ……. DATE:…….

Table of Contents

Figures and Tables

Chapter 1 - Introduction

Chapter 2 – Materials and Methods

Chapter 3 – Characterisation of the Stomatal Phenotypes of the Novel EO_2 Mutation.

Abbreviations

Abbreviation	Definition
ABA	Abscisic Acid (+/-)
ABA2	ABA Deficient 2
ABI1	ABA Insensitive 1
ABI2	ABA Insensitive 2
ADL	Arabidopsis Dynamin-Like Protein
ADP	Adenine Di-Phosphate
AP1	Apetala 1
AP2	Apetala 2
AP2 complex	AP2 Adaptor Complex
ARF	ADP-Ribosylation Factor
ARF-GAP	ARF GTPase Activating Protein
ARF-GEF	ARF Guanine Nucleotide Exchange Factor
ATP	Adenine Tri-Phosphate
AtRBOHD	*Arabidopsis thaliana* NADPH Repiratory Burst Oxidase D (RBOHD)
AtRBOHF	*Arabidopsis thaliana* NADPH Repiratory Burst Oxidase F (RBOHF)
βCA1	β-Carbonic Anhydrase 1
βCA4	β-Carbonic Anhydrase 4
BiFC	Bimolecular Fluorescence Complementation Assay
BSE	Bundle-Signalling Element
Caf4	CCR4-Associated Factor 4
CBL	Calcineurin B-Like 1
CCP	Clathrin-Coated Pit
CCV	Clathrin-Coated Vesicle
CDS	Coding DNA Sequence
CFP	Cyan Fluorescent Protein
CHC	Clathrin Heavy Chain
CLC	Clathrin Light Chain
CLSM	Confocal Laser-Scanning Microscopy
CME	Clathrin-Mediated Endocytosis
CO_2	Carbon Dioxide (Gaseous)
co-IP	Co-Immunoprecipitation
Col-0	Columbia-0 *Arabidopsis* Ecotype
CPK23	Calcium-Dependent Protein Kinase 23
CPK6	Calcium-Dependent Protein Kinase 6
DLP	Dynamin-Like Protein
DNA	De-Oxyribonucleic Acid
Dnm1	Dynamin-Related Protein DNM1
DRM	Detergent-Resistant Membrance Fractions
DRP1A (A-E)	Dynamin Related Protein 1A (1A-1E)
DRP1E	Dynamin Related Protein 1E
DRP2A	Dynamin Related Protein 2A
DRP2B	Dynamin Related Protein 2B
DRP3A	Dynamin Related Protein 3A
DRP3B	Dynamin Related Protein 3B
DRP4A (A-D)	Dynamin Related Protein 4A (4A-4D)
DRP5A	Dynamin Related Protein 5A
DRP5B	Dynamin Related Protein 5B
DRP6	Dynamin Related Protein 6

Abbreviation	Definition
eCFP	Enhanced Cyan Fluorescent Protein
ELM1	Elongated Mitochondria 1
EMS	Ethyl methanesulphonate
EPSIN1	Clathrin Interactor EPSIN 1
FBD	Ferrous Iron Transport Protein-B Homology Domain
FCHo	Fer/Cip4 Homology Domain Only
Fis1	Mitochondrial Fission Protein 1
FRET	Förster Resonance Energy Transfer
G Domain	GTPase Domain
GDV	Golgi-Derived Vesicle
GED	GTPase Effector Domain
GFP	Green Fluorescent Protein
GK08	GABI-KAT GK168C11.08 Arabidopsis Line
GORK	Guard Cell Outward Rectifying Potassium Channel
GTP	Guanosine Tri-Phosphate
H_2DCFDA	2,7-Dichlorofluorescin Diacetate
HAB1	Hypersensitive to ABA 1
HCO_3^-	Carbonate Ion (aq)
HT1	High Leaf Temperature 1
IRGA	Infra-Red Gas Analyser
KAT1	Potassium Channel in Arabipdosis 1
KEULE	SNARE-Interacting Protein KEULE
KNOLLE	Syntaxin Related Protein KNOLLE
Ler-0	Landsberg Erecta *Arabidopsis* Ecotype
MAPK	Mitogen-Activated Protein Kinase
Mdv1	Mitochondrial Division Protein 1
MME	Membrane Microdomain-Associated Endocytosis
MPK12	Mitogen-Activated Protein Kinase 12
NADPH	Dihydronicotinamide-adenine dinucleotide phosphate
NCED3	Nine-Cis-Epoxycarotenoid Dioxygenase 3
NCED5	Nine-Cis-Epoxycarotenoid Dioxygenase 5
NPSN11	Novel Plant Snare 11
OST1	Open Stomata 1 (SnRK2.6)
PAKRP2	Phragmoplast-Associated Kinesin-Related Protein 2 (KIN10A)
PAR	Photosynthetically Active Radiation
PCR	Polymerase Chain-Reaction
PEX13	Peroxin 13
PH Domain	Pleckstrin-Homology Domain
PIP1;4	Plamsa-Membrane Intrinsic Protein 1;4 (PIP1E)
PIP2A	Plamsa-Membrane Intrinsic Protein 2A
PMD1	Peroxisome and Mitochondrial Division Factor 1
PMD2	Peroxisome and Mitochondrial Division Factor 2
PP2C	Protein Phosphatase Type 2C
ppm	Parts Per Million
PRD	Proline-Rich Domain
PYL1	PYR1-Like Protein 1
PYL2	PYR1-Like Protein 2
PYL4	PYR1-Like Protein 4

Abbreviation	Definition
PYL5	PYR1-Like Protein 5
PYL8	PYR1-Like Protein 8
PYR1	Pyrobactin Resistance 1
QUAC1	Quick Anion Channel 1
RBOHD	NADPH Repiratory Burst Oxidase D (AtRBOHD)
RBOHF	NADPH Repiratory Burst Oxidase F (AtRBOHF)
RCAR	Regulatory Component of ABA Receptor 1
RFP	Red Fluorescent Protein
RHC1	Resistant to High CO_2 1
ROS	Reactive Oxygen Species
S.E.	Standard Error
SH3 Domain	Src Homology 3 Domain
SH3P1	SH3-Domain Containing Protein 1
SK206	SALK_206052C Arabidopsis Line
SLAC1	Slow-Opening Anion Channel 1
SNAP23	Synaptosomal-associated protein 23
SNARE	SNAP-Receptor Protein
SNP	Single Nucleotide Polymoprhism
SnRK2	Sucrose non-fermenting Related Kinase 2.6 (OST1)
SSLP marker	Simple Sequence Length Polymorphism Marker
TAP	Tandem-Affinity Purification
TASH3	TPLATE-Associated SH3-Domain Containing Protein
T-DNA	Transfer DNA
TML	TPLATE Complex Muniscin-Like
TN	Tubular Network
TPC	TPLATE Adaptor Complex
TVN	Tubulo-Vesicular Network
tyrA23	Tyrphostin-A23
VAEM	Variable Angle Epifluorescsnce Microscopy
VAMP721	Vesicle-Associated Membrane Protein 721
VAMP722	Vesicle-Associated Membrane Protein 722
VIAFM	Variable Incidence Angle Fluorescent Microscopy
WT	Wild-Type
WUE	Water Use Efficiency
XFP	Unspecified Fluorescent Protein
Y2H	Yeast 2-Hybrid Assay
YFP	Yellow Fluorescent Protein

Chapter 1 - Introduction

1.1 Overview of Stomatal Function

Stomata are microscopic pores on the leaf surface that are flanked by a pair of guard cells and provide a channel for gas exchange between the leaf internal photosynthetic tissues and the external atmosphere **(Hetherington and Woodward, 2003)**. The gas exchange that occurs through stomatal pores is a constant compromise between rate of carbon dioxide uptake for photosynthesis and the concurrent rate of transpirational water loss. Stomatal guard cells have evolved to be able to rapidly shrink and swell by adjusting their turgor pressure in response to perceived environmental and internal factors **(Wilmer and Fricker, 1996; Hetherington and Woodward, 2003)**, thereby controlling the aperture of the stomatal pore and regulating rates of gas exchange in real time.

These rapid changes in guard cell turgor allow for the dynamic alteration of stomatal aperture to reflect the gas exchange priorities dictated by a complex sensory/signalling web. This sensory web allows plants to adjust stomatal aperture to account for fluctuations in environmental conditions such as relative humidity, light intensity, atmospheric CO_2 concentration, temperature, pollutants, ground water availability and mineral concentrations **(Wilmer and Fricker, 1996; Mcainsh *et al.*, 2002; Hetherington and Woodward, 2003).** Both abiotic and biotic factors, such as herbivorous predation and pathogens, have been shown to elicit changes in stomatal aperture **(Hetherington and Woodward, 2003; Gudesblat *et al.*, 2009)**. Stomatal responses to these factors have been shown to propagate within local tissues through messengers such as reactive oxygen species (ROS) and on a whole plant level via long range signals, including internal Ca^{2+} ion currents and plant hormones such as Abscisic acid (ABA) **(Mcainsh *et al.*, 1996; Webb and Hetherington, 1997; Hetherington and Woodward, 2003; Sanders and Dodd, 2010; Danquah *et al.*, 2014)**.

In addition to their effects on stomatal aperture, environmental factors have been shown to influence stomatal density on the leaf surface **(Lake and Woodward, 2008; Casson and Hetherington, 2010)**. Differences in stomatal density act as an additional, long-term, method for control of gas exchange rates and have a marked effect on rates of transpirational water loss and assimilation of carbon dioxide **(Hetherington and Woodward, 2003)**.

The work detailed in this thesis will focus on investigating the *eo₂* mutation: a novel mutation discovered through infra-red thermography of a population of ethyl methanesulphonate (EMS) *Arabidopsis thaliana* mutants **(Tagliavia, 2006; Peng, 2008)**. The *eo₂* mutation was found to be allelic to Dynamin Related Protein 1E (*DRP1E*) and inhibited stomatal responses to elevated atmospheric [CO_2], but had no discernible impact on responses induced by other promoters of stomatal closure.

1.2 Stomatal Closure Signalling Pathways

As the EO_2 mutant was found to be inhibited in elevated [CO_2] induced stomatal closure but have wild type stomatal responses to ABA and exogenous Ca^{2+}, this introduction to established stomatal closure signalling pathways will focus on ABA, CO_2 and calcium induced closure pathways, as there is significant interaction between these pathways (**Webb and Hetherington, 1997**).

1.2.1 Abscisic Acid-Dependent Stomatal Closure and Inhibition of Stomatal Opening

Abscisic acid (ABA) was first identified in 1965 by **Cornforth *et al.*, 1965** as an inducer of seed dormancy and accelerator of seed abscission **(Cornforth *et al.*, 1965; Mittelheuser and Van Steveninck, 1969)**. It was later established that ABA played a significant role in inducing stomatal closure in wheat (*Triticum vulgare*) and barley (*Hordeum vulgare*) **(Mittelheuser and Van Steveninck, 1969)**, was synthesised in roots and leaves in response to water stress and formed a mobile systemic signal that affected ion uptake and starch content of stomatal guard cells (various species) **(Mansfield and Jones, 1971; Milbarrow and Robinson, 1973; Wang *et al.*, 1984; Loveys and Robinson, 1987; Wolf *et al.*, 1990)**. It has since been established that ABA is a critical promotor of stomatal closure **(Vahisalu *et al.*, 2008; Danquah *et al.*, 2014; Chater *et al.*, 2015**).

Cutler *et al.*, 2010 proposed a unified model of ABA action in which the PYR (Pyrobactin Resistance), PYL (Pyrobactin Resistance 1-Like) and RCAR (Regulatory Component of ABA Receptor 1) protein families directly bind ABA via a hydrophobic binding pocket(**Melcher *et al.*, 2009**). PYR/PYL/RCAR binding of ABA (**Ma *et al.*, 2009; Park *et al.*, 2009**) causes a conformational change to the protein, exposing a protein-binding loop that docks to the active site of the PP2Cs (Protein Phosphatase Type 2Cs) ABI1 (ABA Insensitive 1), ABI2 and HAB1 (Hyper Sensitive to ABA 1), inhibiting PP2C binding of OST1 **(Melcher *et al.*, 2009**). The inhibition of PP2Cs by ABA-bound PYR/PYL/RCAR proteins relieves inhibition of SnRK2s (Sucrose Non-Fermenting Related Kinase 2), such as OST1 (Open Stomata 1), thereby, allowing OST1 to be phosphorylated and restoring the kinase activity of the SnRK2s (**Umezawa *et al.*, 2009; Vlad *et al.*, 2009**). Dephosphorylated SnRK2 kinases are then free to phosphorylate the transmembrane ion channels SLAC1 (Slow Opening Anion Channel 1), QUAC1 (Quick Anion Channel 1) and KAT1 (Potassium Channel in Arabidopsis 1) activating SLAC1 and QUAC1, but inhibiting and promoting relocation of KAT1 from the cell membrane. (**Geiger *et al.*, 2009; Lee *et al.*, 2009; Sato *et al.*, 2009; Sasaki *et al.*, 2010; Imes *et al.*, 2013)**. Activation of SLAC1 and the Inhibition of KAT1 results in activation of the voltage gated, outward-rectifying K^+ channel GORK (Guard Cell Outward Rectifying Potassium Channel), causing an efflux of K^+ from the cytoplasm and further decreasing cytoplasmic solute potential (**Ache *et al.*, 2000; Imes *et al.*, 2013**). SLAC1 has been shown to be a key component in ABA mediated guard cell closure and its activation by OST1

results in efflux of anions from the cytoplasm, cell membrane depolarisation and efflux of water to decrease cell turgor **(Negi *et al.*, 2008; Vahisalu *et al.*, 2008**).

OST1 has also been shown to directly interact with the NADPH Respiratory Burst Oxidase Homologues AtRBOHD/RBOHF, resulting in their activation and generation of Reactive Oxygen Species (ROS) as secondary messengers in stomatal closure (**Sirichandra *et al.*, 2009; Acharya *et al.*, 2013**). ROS have been shown to enhance stomatal closure, inhibit stomatal opening and promote an increase in cytosolic Ca^{2+}, thereby increasing the persistence of another important secondary messenger of stomatal closure **(Mcainsh *et al.*, 1990; 1996; Pei *et al.*, 2000; Waidyarathne and Samarasinghe, 2018**).

Calcium ion currents have been shown to play an important role in stomatal closure, the maintenance of stomatal closure and inhibition of stomatal opening. This has been shown to occur through Ca^{2+} dependent activation of SLAC1 via the CPKs (Calcium-Dependent Protein Kinase), CBLs (Calcineurin B-Like) protein families and indirect activation of SLAC1 through a Ca^{2+} mediated Mitogen Activated Protein Kinase (MAPK) cascade (**Mcainsh *et al.*, 1990; Webb and Hetherington, 1997; Sanders and Dodd, 2010; Maierhofer *et al.*, 2014**).

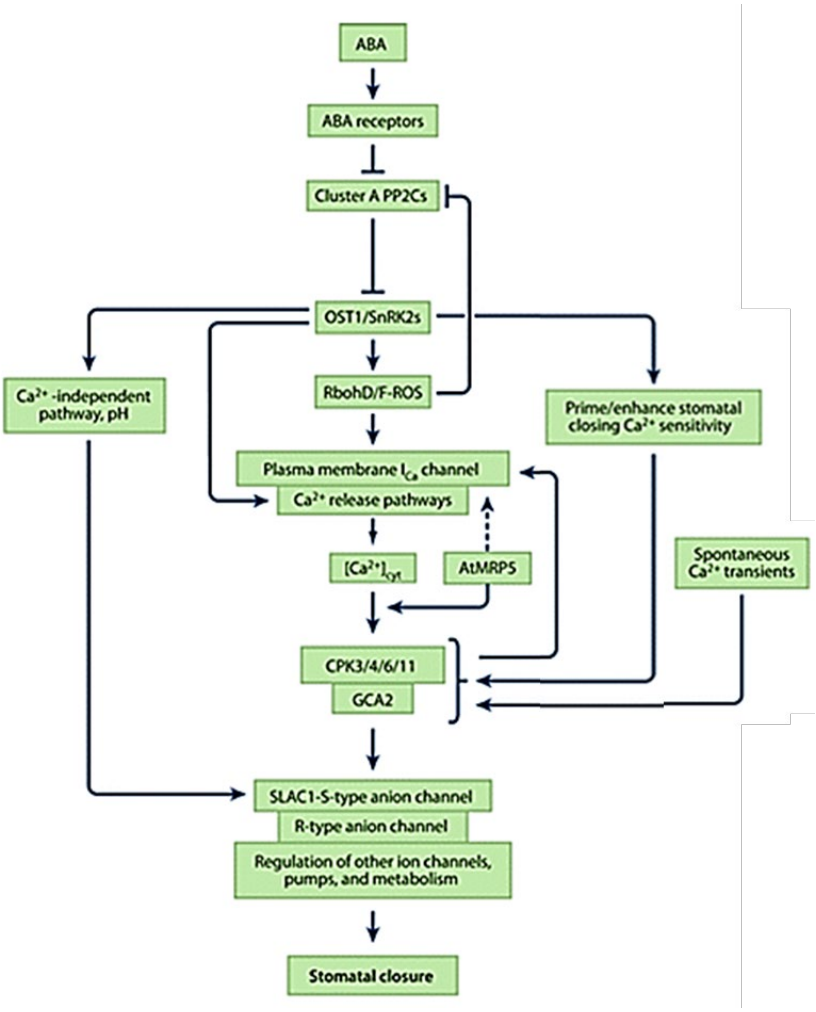

Figure 1.A) ABA-induced stomatal closure signalling pathways. ABA binds to PYR/PYL ABA receptor proteins which dimerise with PP2C kinases, inactivating the PPC2 kinase activity. This relieves inhibition of SnRK2s such as OST1, which then phosphorylates and activates the ion channels SLAC1 and QUAC1. The change in membrane potential then activates the voltage dependent K^+ channel GORK. This summative ion channel activity decreases cytoplasmic solute potential, resulting in an efflux of water and stomatal closure.

Taken from **Kim *et al.*, 2010**.

1.2.2 Carbon Dioxide Dependent Signalling Pathways in Stomatal Closure

Carbon dioxide is partially soluble in water and is present as aqueous CO_2 ($(CO_2)_{aq}$), at a concentration dependent on the $[CO_2]_{atm}$ and the pH and salt content of the water, amongst other factors. Increased $[CO_2]_{atm}$ will result in an increased apoplastic $[(CO_2)_{aq}]$ in fluid coating the sub-stomatal cavity. The PIP2A aquaporin, amongst other aquaporins, allows translocation of small uncharged molecules, principally H_2O, across the cell membrane. PIP2A has been shown by **Wang *et al,* 2016** to not only allow diffusion of H_2O across the membrane but to also be strongly implicated in the translocation of extra-cellular $(CO_2)_{aq}$ into the cytoplasm, as *Xenopus laevis* oocytes expressing transgenic *A.thaliana* PIP2A exhibited significantly higher cell surface pH than non-expressing oocytes. The dissociation of a proton from carbonic acid, which is formed through the reaction of water and $(CO_2)_{aq}$, to form carbonate (HCO_3^-), acidifies the surrounding medium proportion all to the concentration of dissolved CO_2. Cell surface pH can therefore be used as a measure of $(CO_2)_{aq}$ uptake by the cell, as increased cell surface pH indicates a lower local $[(CO_2)_{aq}]$ and increased $(CO_2)_{aq}$ uptake by the cell **(Musa-Aziz et al., 2009, 2014)**.

β-Carbonic Anhydrase 4 (βCA4) was found, via 4 separate methods, to interact with PIP2A in *Nicotiana benthamiana* and *X.laevis* oocytes co-expressing transgenic PIP2A and βCA4 were found to have a significantly increased pH in the vicinity of the cell membrane compared to both non-expressing oocytes and oocytes expressing PIP2A alone, indicating increased uptake of $(CO_2)_{(aq)}$ by the cell (**Wang *et al*, 2016**). βCA4 catalyses the equilibrium **E1.1**, with subsequent dissociation of a proton from carbonic acid via a second equilibrium: **E1.2**. The interaction of PIP2A, an apparent $(CO_2)_{aq}$ channel, with βCA4 and the decreased cell membrane pH in response to extracellular carbonate when PIP2A and βCA4 are co-expressed in *X.laevis* oocytes (**Wang *et al*, 2016**) leads to the likely conclusion that βCA4 and PIP2A act cooperatively as a carbon dioxide concentrating mechanism through rapid of conversion of membrane permeable $(CO_2)_{aq}$ to membrane impermeable HCO_3^- in the cytoplasm.

E1.1 $H_2O + (CO_2)_{aq} \rightleftarrows (H_2CO_3)_{aq}$

E1.2 $(H_2CO_3)_{aq} \rightleftarrows H^+ + HCO_3^-$

E1.1 – formation of carbonic acid from water and dissolved CO_2. **E1.2** – dissociation of a proton from carbonic acid to form a carbonate ion

Anabolism of CO_2 through photosynthesis creates a deficiency in $(CO_2)_{aq}$ in the chloroplast stroma leading to an increased $(CO_2)_{aq}$ diffusion gradient for $(CO_2)_{aq}$, that is likely converted from imported cytoplasmic HCO_3^- via potential chloroplast-localised aquaporins (**Uehlien *et al*, 2008**) and β-carbonic anhydrase 1 (βCA1), which is localised to the chloroplast stroma (**Fabre *et al*, 2007**). The diffusion of cytoplasmic HCO_3^- towards the chloroplasts will cause a gradient for diffusion of carbonate away from the cell membrane causing an effective decreased $[HCO_3^-]$ near the cell

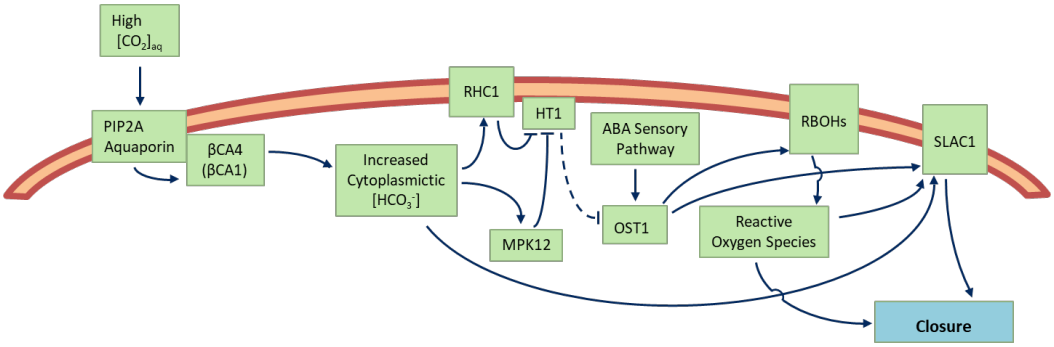

Figure 1.B) Diagram of the current putative carbon dioxide signalling pathways for elevated carbon dioxide induced stomatal closure. OST1 and SLAC1 are the major points of convergence of carbon dioxide specific signalling, ABA induced signalling and other closure responses. SLAC1 has a major role in effecting stomatal closure through the efflux of Cl^- and NO_3^- ions, hyperpolarising the cell membrane and activating outward rectifying K^+ channels, thereby reducing the cytoplasmic solute potential and resulting in efflux of water from the guard cells and stomatal closure.

membrane and causing skew of (**E1.2**) in the forward direction, thereby lowering cytoplasmic $[(CO_2)_{aq}]$ and creating a $(CO_2)_{aq}$ flux into the cell and having the knock on effect of removing $(CO_2)_{aq}$ from the fluid coating the apoplastic substomatal cavity, causing increased dissolution of $(CO_2)_{atm}$. Increased $[(CO_2)_{atm}]$ will thereby increase cytoplasmic $[HCO_3^-]$ via the above steps, including PIP2A/ βCA4 **(Hu *et al*, 2010; Xue *et al*, 2011)**. It is worth noting that *pip2a* T-DNA knockout mutants have no pronounced CO_2 induced stomatal closure phenotype, likely due to redundancy of aquaporins in *A.thaliana* as the aquaporin PIP1;4 has also been found to allow translocation of $(CO_2)_{aq}$ across the plasma membrane in *A.thaliana* (**Li *et al*, 2015**).

Elevated cytosolic $[HCO_3^-]$ increases the proportion of active RHC1, a plasma membrane protein that is activated by increased $[HCO_3^-]$ via an unknown mechanism, which in turn phosphorylates HT1, a plasma membrane associated (**Hashimoto-Sugimoto *et al*, 2016**) serine-threonine kinase, thereby relieving inhibition of OST1 **(Hashimoto *et al*, 2006; Tian *et al*, 2015)**. **Wang *et al*, 2016** found that elevated cytosolic $[HCO_3^-]$ induced activity of SLAC1 in *X.laevis* oocytes co-expressing either OST1 & SLAC1 or CPK6/23 & SLAC1 independently of other plant proteins, indicating that HCO_3^- may influence SLAC1 directly.

Jakobson *et al*, 2016 found that *mpk12* mutants are inhibited in both decreased $[CO_2]$ induced stomatal opening & elevated $[CO_2]$ induced stomatal closure, yet exhibit a WT response to ABA. *mpk12* mutants were also found to be hypersensitive to ozone and to have constitutively more open stomata than wild type Col-0. **Jakobson *et al*** conducted water use efficiency (WUE), stomatal index & density experiments and measured stomatal length in a variety of *mpk12* lines and lines expressing non-functional mpk12 and found no significant difference in index, density or stomatal length yet a decreased WUE. MPK12 was found by Y2H, BiFC and split luciferase assay in

N.benthamiana to interact with HT1 at the cell membrane and was shown by *in vitro* kinase assays to inhibit HT1. HCO_3^- induced S-type anion currents were significantly reduced in *mpk12* mutants and lines expressing non-functional MPK12, indicating reduced HCO_3^- induced SLAC1 activation (**Jackobson *et al*, 2016**).

Chater *et al*, 2015 showed that elevated [CO_2]-induced stomatal closure required ROS production for proper reduction of stomatal aperture. Previous studies had shown that *rbohD/rbohF* double mutants are impaired in ABA induced stomatal closure and have reduced ROS production and Ca^{2+} currents in response to ABA (**Kwak *et al*, 2003**). RBOHD and RBOHF are partially redundant plasma membrane NADPH oxidases that produce apoplastic H_2O_2 in response to a variety of stimuli including ABA, salt stress, pathogen associated molecular patterns and elevated atmospheric [CO_2] (**Kwak *et al*, 2003; Xie *et al*, 2011, 2016; Kadota *et al*, 2014; Torres *et al*, 2002; Chater *et al*, 2015**). **Chater *et al*, 2015** demonstrated, using the fluorescent ROS indicator H2DCFDA, that effective elevated [CO_2] induced stomatal closure requires production of reactive oxygen species and that elevated [CO_2] induced stomatal closure is severely impaired in *rbohD/rbohF* double mutants. This phenotype was rescued upon addition of exogenic H_2O_2. Further unpublished data from **McLachlan D *et al*** (Guard Cell Group) using *rbohD* and *rbohF* single mutants indicates that ROS production induced by elevated [CO_2] acts preferentially through RBOHD and that *rbohD*, but not *rbohF*, mutants exhibit reduced closure in response to elevated atmospheric [CO_2].

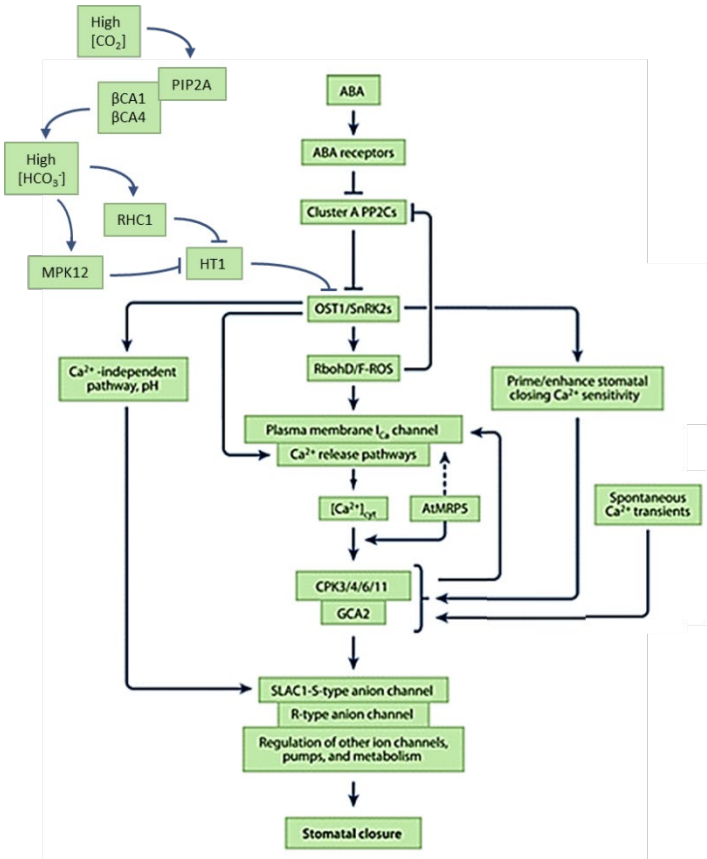

Figure 1.C) Convergence of the ABA-independent CO_2 signalling pathway with ABA mediated stomatal closure apparatus. Dissolved CO_2 enters the cell via aquaporins and is converted in to H_2CO_3 by associated βCA4. H_2CO_3 in the cell cytoplasm rapidly dissociates to form HCO_3^-, increasing [HCO_3^-] in the cytoplasm and stimulating RHC1 kinase activity. RHC1 phosphorylates HT1, relieving inhibition of OST1 by HT1. OST1 sensitivity to ABA is increased after relief of inhibition by HT1, increasing the proportion of active OST1, which can then stimulate stomatal closure via the ABA induced stomatal closure pathway, ROS and Ca^{2+} signalling.

Adapted from **Kim *et al.*, 2010**.

1.3 Convergence of CO_2 Signalling Pathways with ABA Closure Pathways.

The currently accepted model for Carbon Dioxide signalling in stomatal closure provides several points of convergence with ABA-dependent signalling pathways that effect stomatal closure. The principal point of convergence is thought to be the inhibition/relief of inhibition of OST1 by HT1, thereby increasing the proportion of active OST1 in response to elevated [CO_2] and effectively increasing the sensitivity and magnitude of a response to ABA in stomatal closure pathways (**Hashimoto *et al.*, 2006; Tian *et al.*, 2015; Hõrak *et al.*, 2016**). It has also been shown by **Wang *et al.*, 2016** that increased cytoplasmic [HCO_3^-] induced SLAC1 activity when a SLAC-activating kinase (OST1/CPK6/CPK23) was present in *Xenopus* oocytes, raising the possibility that SLAC1 or the activating kinases are directly sensitive to HCO_3^- concentration. **Chater *et al.*, 2015** demonstrated that stomatal responses to elevated [CO_2] required functional ABA signalling and closure pathways, showing a dependency on ABA induced stomatal closure for proper reduction of stomatal aperture in response to elevated CO_2.

Hsu *et al.*, 2018 showed, via stomatal conductance time-courses, that ABA synthesis (*nced3/5* double, *aba2-1* mutant) and sensory (*pyr1pyl1/2/4* quadruple*, pyr1pyl4/5/8* quadruple, *pyr1,pyl2/4/5/8* quintuple, *pyr1,pyl1/2/4/5/8* hextuple) mutants exhibited rapid reductions in stomatal conductance in response to elevated [CO_2]. The stomatal conductance of the ABA synthesis mutants was found to gradually increase over the period of high [CO_2], whilst the magnitude of the reduction in normalised stomatal aperture varied amongst the ABA sensory mutants: all but *pyr1,pyl1/2/4* showed a substantially reduced response to elevated CO_2 using normalised data and the *pyr1,pyl1/2/4/5/8* hextuple showed no response to elevated [CO_2] (**Hsu *et al.*, 2018)**. These results indicate that ABA is likely required to maintain a stomatal response to elevated CO_2 and that ABA sensing is necessary for a full stomatal response to elevated [CO_2]. The rapid reduction in stomatal conductance exhibited in ABA synthesis mutants is strong evidence against the hypothesis that elevated [CO_2] induces rapid synthesis of ABA to induce closure (**Merilo *et al.*, 2013; Chater *et al.*, 2015**) and the diminished response of the majority of the ABA sensory mutants instead implies that CO_2 induced stomatal responses reply on perception of basal ABA levels (**Hsu *et al.*, 2018**).

Interestingly, **Hsu *et al.*, 2018** also found, via in-gel kinase assays, that there was no increase in OST1 kinase activity in guard cell protoplast cell extract after incubation for 30 minutes with 13.5mM $NaHCO_3$ or 900ppm CO_2 equilibrated buffer, but found a substantial increase in kinase activity in response to 10µM ABA. These results appear to contradict the findings of several other papers (**Matrosova *et al.*, 2015; Tian *et al.*, 2015; Hõrak *et al.*, 2016**), however stomatal closure in response to CO_2 is thought to act by enhancing OST1 sensitivity to ABA, not by directly increasing OST1 activity and **Hsu *et al.*, 2018** themselves show that CO_2 induced stomatal closure acts via perception of basal

ABA levels, not via ABA synthesis. Enhancement of OST1 kinase activity in the above kinase assay would therefore be dependent on a basal ABA concentration being present in the reaction buffer, however the ABA concentration in the reaction buffer is likely to be orders of magnitude lower than in functional guard cells and so no increased activation of OST1 should be expected after exposure to HCO_3 or CO_2 equilibrated buffer alone. A repeat of the kinase assay with a low (≈0.1µM) concentration of exogenous ABA in the reaction buffer, with an appropriate control, could provide further insight into the role of OST1 of in CO_2 induced stomatal closure.

Stomatal closure in response to elevated [CO_2] therefore likely acts by increasing the sensitivity of the established ABA-induced closure pathway by increasing the amount of active OST1 that is able to respond to basal ABA concentrations, however synthesis of ABA is likely required to maintain reduced stomatal aperture under prolonged exposure to high [CO_2]. Elevated CO_2 may also, acting through MPK12 via an unknown mechanism, increase SLAC1 activity/sensitivity through HCO_3^- dependent priming of SLAC1, OST1 or CPK6/CPK12 (**Hõrak *et al.*, 2016**).

1.4 *Arabidopsis* Dynamin Related Proteins

1.4.1 Structure and Functions of Dynamin and *Arabidopsis* Dynamin Related Proteins

1.4.1.1 Protein Domain structure of Dynamin and Arabidopsis DRPs

Human dynamin is a well-studied large GTPase that can form large helical polymers around truncated lipid membranes, through the GTP-dependent polymerisation of dynamin dimers. Dynamin macromolecules have been found to contract around the tubulated membrane in a GTP dependent manner, with the hydrolysis of GTP causing a conformational change within each dimer unit, thus causing the macromolecule to contract and resulting in scission of the encompassed membrane **(Ford *et al*, 2011; Ferguson & De Camilli, 2012; Reubold *et al*, 2015)**. In this role, human dynamins and dynamin like proteins (DLPs) have been found to effect changes in membrane

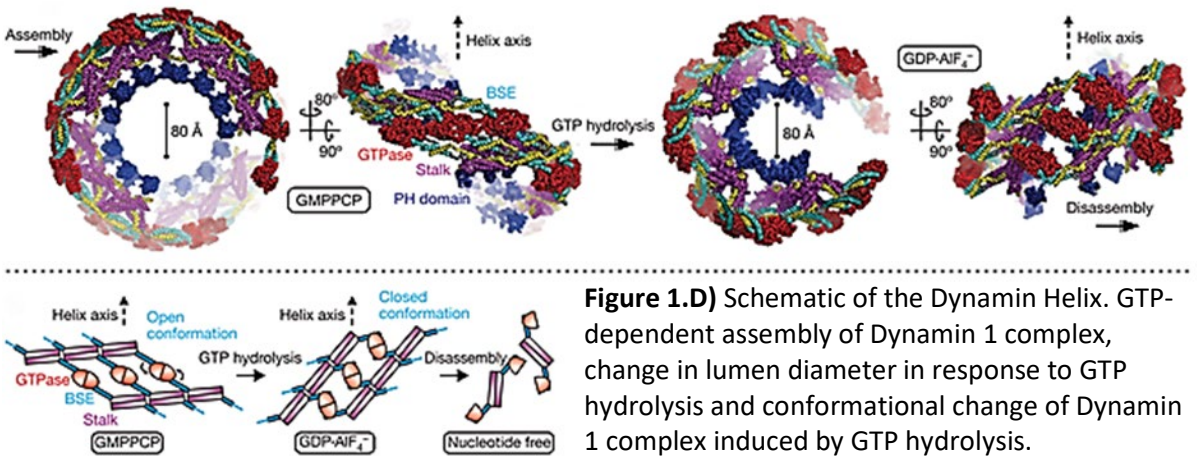

Figure 1.D) Schematic of the Dynamin Helix. GTP-dependent assembly of Dynamin 1 complex, change in lumen diameter in response to GTP hydrolysis and conformational change of Dynamin 1 complex induced by GTP hydrolysis. Adapted from **Ford *et al*, 2011**

organisation and structure to various ends, including organelle fusion and division, regulation of cell architecture in conjunction with actin microfilaments, vesicle formation, endocytosis and cell division **(Ferguson & De Camilli, 2012)**. Human dynamin monomers possess 5 domains: GTPase domain (G domain), GTPase effector domain (GED), 'middle' or 'stalk' region, pleckstrin homology (PH) domain and proline rich domain (PRD). The N-terminal GTPase domain binds GTP freely but does not possess GTPase activity in its monomeric form. The stalk region is involved in stalk-stalk dimerization between dynamin molecules, while a section of the GED combines with elements of the GTPase domain to form a 'neck' or 'bundle signalling element' (BSE) that is structurally essential for correct GTPase function. The PH domain is involved in the selective binding of certain phospholipids and phosphoinositides, thereby facilitating specificity in the association of specific dynamins with specific lipid moieties through the variation of PH domain structure in different dynamin and DLP isoforms. Lastly the PRD is thought to be involved in interaction with proteins responsible for the localisation and coordination of dynamin action, specifically proteins that possess an Src homology 3 (SH3) domain **(Ford *et al*, 2011; Ferguson & De Camilli, 2012; Fujimoto & Tsustumi, 2014; Reubold *et al*, 2015)**.

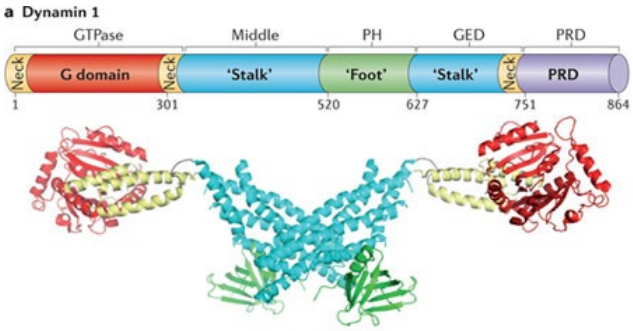

Figure 1.E) Linear domain structure and ribbon structure of human Dynamin 1. Dynamin is dimerised GTP-independently through stalk-stalk interactions.

Adapted from Ferguson & De Camilli, 2012.

In the past *Arabidopsis thaliana* Dynamin Related Proteins (DRPs) have been referred to by a variety of acronyms including ADLs, DLPs and DRPs. This leaves room for confusion and therefore the DRP system of nomenclature, as stated in **Hong *et al*, 2003a**, will be the sole nomenclature used. In *A.thaliana*, 16 DRPs have been identified and are separated into 6 distinct subfamilies (DRP1-6) based on their structural similarity and phylogeny **(Fujimoto & Tsustumi, 2014)**. The G domain, GED and Middle domains are conserved throughout, however the presence of PH and PRD domains varies depending on the DRP subfamily (**Figure 1.F**) **(Hong *et al*, 2003a; Fujimoto & Tsustumi, 2014)**.

1.4.1.2 Overview of *Arabidopsis* Dynamin Related Protein Functions

The *Arabidopsis* DRP1 subfamily comprises 5 relatively low molecular weight DRPs: DRP1a-e, that lack PH and PRD domains. Only DRP1a/c/e have been the subject of significant research and are hypothesised to be involved in formation of the cell plate during cytokinesis **(Lauber *et al*, 1997; Kang *et al*, 2003a,b; Hong *et al* 2003b**) and cell membrane trafficking, specifically in endocytosis **(Kang *et al*, 2003a,b; Konopka *et al*, 2008; Minami *et al*, 2015)**. DRP1a/c/e are able to associate with the cytoskeleton **(Hong *et al*, 2003b)** and potentially mitochondria **(Jin *et al*, 2003; Tang *et al*, 2006)**. The DRP2 subfamily has only 2 members and are 'true dynamins' in that they possess both PH and PRD domains. DRP2s are thought to be involved in clathrin-coated vesicle formation **(Jin *et al*, 2001; Minami *et al*, 2015)** and trafficking at both the cell membrane and at the cell plate during cytokinesis **(Minami *et al*, 2015; Fan *et al*, 2015)**. The two members of the DRP3 subfamily appear similar to the DRP1s in structure due to their lack of PH and PRD domains, however the DRP3s share only 29% sequence homology to DRP1a. DRP3a and 3b act in concert to create a heteropolymeric DRP helix which plays a key role in both mitochondrial and peroxisomal division **(Hong *et* al, 2003a; Fujimoto *et al*, 2009; Zhang & Hu, 2009; Aung & Hu, 2012)**. The DRP4s are orthologues of the Mx proteins that exhibit antiviral activity in animals **(Verma & Hong, 2005; Haller & Kochs, 2002)** although the DRP4s are thought to be predominantly pseudogenes in *A.thaliana* and their function is

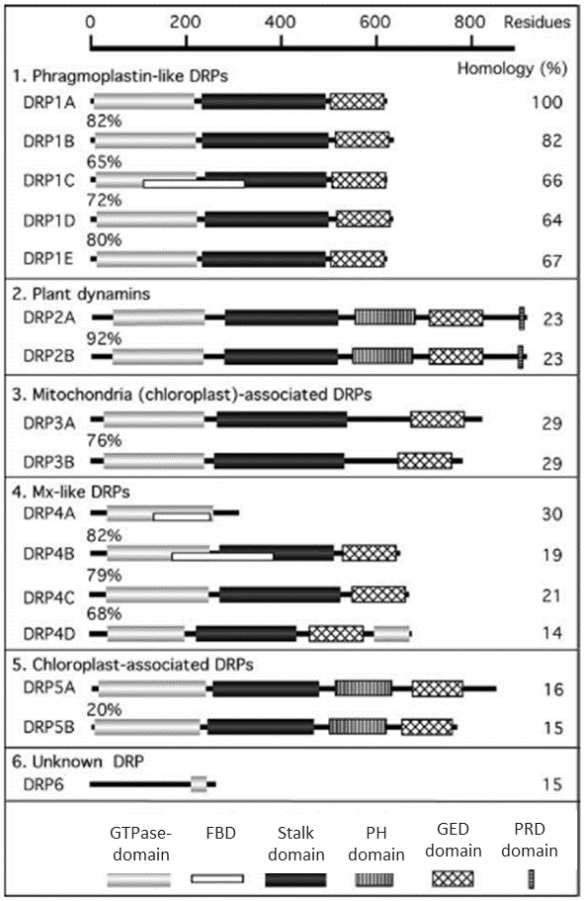

Figure 1.F) Domain structure of the Arabidopsis DRP subfamilies. The DRP1 and DRP3 subfamilies have only the GTPase, Stalk and GTPase-Effector Domain (GED) domains. The DRP2 subfamily comprise the largest proteins and are most similar to human Dynamin, as DRP2A/DRP2B possess all five of the domains present in human Dynamin.

The DRP4 subfamily has the least homology between its members; DRP4B/DRP4C have GED, stalk and GED domains similarly to the DRP1s and DRP3s, whilst DRP4A comprises only a GTPase domain and DRP4C has stalk and GED domains but a split GTPase domain. The DRP5s have GTPase, stalk, PH and GED domains, while DRP6 has little homology to the other DRPs and has only a severely truncated GTPase domain.

The 'FBD' domain indicates homology to the GTP binding domain of Ferrous Iron Transport Protein B (FeoB), a bacterial Fe^{2+} transporter. This is not conserved across DRPs and is effectively a GTP binding pocket.

Adapted from **Hong *et al*, 2003a**

as yet unknown **(Hong *et al*, 2003a; Fujimoto & Tsutsumi, 2014; Minami *et al*, 2015)**. Of the two members of the DRP5 subfamily, DRP5b has been found to play a critical role in chloroplast and peroxisomal division **(Zhang & Hu, 2010; Aung *et al*, 2010; Aung & Hu, 2012)** while DRP5a is thought to be involved purely in cytokinesis **(Miyagishima *et al*, 2008)**. It is unknown whether the single *DRP6* gene is transcribed, although the gene product would be a protein approximately half the size of virtually all other *A.thaliana* DRPs and is unlikely to display GTPase activity **(Hong, 2003a)**.

1.4.2 DRP1a/c/e and DRP2s are Involved in Cell Plate Formation During Cytokinesis

In higher plants, cytokinesis involves the formation of a pair of new lipid bilayers in the plane of the cell equator. These bilayers will expand laterally in the equatorial plane until they fuse with the cell membrane, thus dividing the cell totally in half along the cell equator **(Jurgens, 2005)**. The lipid vesicles that are fused together to form the *de novo* cell plate originate in the trans-Golgi network, where lipid vesicles of 51nm are produced from the lipid of the Golgi membrane. These vesicles then fuse to form larger 66nm vesicles, which are the principal building blocks of the forming cell plate **(Jurgens & Geldner, 2002; Segui-Simarro *et al*, 2004; Jurgens, 2005)**. Although the exact mechanism for the formation of these vesicles is not known, it seems likely that they are generated in a format analogous to other plant vesicle budding pathways such as clathrin mediated endocytosis. A guanine nucleotide exchange factor (ARF-GEF) activates its respective ADP ribosylation Factor (ARF) small-type GTPase through exchange of the bound GDP for GTP. The GTP-ARF/ARF-GEF complex recruits coat protein to form a coat-ARF complex, which is then bound by the associated GTPase activating protein (ARF-GAP). Upon binding of this complex to its specific cargo or phospoholipid/phospho-inositide, ARF undergoes GTP hydrolysis and dissociates the complex, leaving the cargo-bound coat complex to polymerise with adjacent complexes leading to invagination of the membrane. This membrane invagination is then cleaved from the membrane by a DRP to form a separate vesicle and the coat protein complex dissociates **(Jurgens & Geldner, 2002; Kirchhousen, 2000; Nee & Randazzo, 2006)**.

The 66nm Golgi-derived vesicles (GDV) are transported along the phragmoplast microtubule network to the forming cell plate by a putative Kinesin-related protein, PAKRP2 **(Otegui *et al*, 2001, Lee *et al*, 2001)**. Interestingly DRP1a has been found by confocal microscopy, using GFP-DRP1a fusions, to co-localise with cortical microtubules in G1 and S phase cells; with the mitotic spindle in metaphase cells and the phragmoplast microtubule network in late anaphase cells. This co-localisation of DRP1a, at various stages of the cell cycle, with microtubules perhaps implicates a role for DRP1a in the microtubule mediated transport of golgi-derived and endocytic vesicles **(Hong *et al*,**

2003b). Upon reaching the cell plate assembly matrix, the 66nm vesicles undergo homotypic fusion to form membrane tubules which will go on to form the tubulo-vesicular network (TVN).

This fusion process is executed by soluble N-ethylmaleimide-sensitive factor adaptor protein receptor (SNARE) complexes consisting of the syntaxin KNOLLE, the t-SNARE SNAP23 or NPSNII, the r-SNARE VAMP721/722 and the SM protein KEULE **(Jahn, 2003; Jurgens, 2005, Jurgens *et al*, 2015)**. DRP1a mediates the fusion of GDV in the cell plate assembly matrix by forming a helical superstructure around the resultant membrane tubules, thereby forcing the growing lipid body into a cylindrical conformation as opposed to simply forming a larger spherical vesicle **(Otegui *et al*, 2001)**. These diameter restricted membrane tubules amalgamate to form a lattice structure in the plane of the cell equator: the TVN. Excess membrane is removed from the TVN via endocytosis of clathrin coated vesicles, thereby reducing both the volume and surface area of the TVN **(Otegui *et al*, 2001; Segui-Simarro *et al*, 2004*;* Konopka *et al*, 2006; Fujimoto, 2010)**. Callose is deposited into the lumen of the TVN, most likely via DRP1a associated callose synthase complex **(Otegui *et al*, 2001; Hong *et al*, 2003a,b)**, laterally enlarging the TVN tubule network over time and forcing the tubules to flatten and merge to form an intricate, continuous Tubular Network (TN). With the continued deposition of callose and cellulose in to the TN lumen, the TN flattens and matures into a flattened, disk-like, planar fenestrated sheet **(Samuels *et al*, 1995; Otegui *et al*, 2001; Miart *et al*, 2014)**.

DRP1a has been found to associate with micro tubules in various phases of the cell cycle, including phragmoplast microtubules in cytokinesis **(Kang *et al*, 2001, 2003a,b; Hong *et al*, 2003b)**. DRP1a is thought to confine KNOLLE and the SNARE complex to the cell plate **(Hong *et al*, 2001a,b; Konopka *et al*, 2006; Bouette *et al*, 2010)**; to restrict the diameter of membrane tubules in the TVN and to assist GDV fusion in the cell plate assembly matrix **(Otegui *et al*, 2001; Segui-Simmaro *et al*, 2004; Konopka *et al*, 2006)**. DRP1a/e localise primarily to the growing edge of the cell plate, but also localise to the TVN, whilst DRP1c appears to localise to both the growing edge of the cell plate and to the TVN at a similar level. DRP1a/e are partially redundant: a *drp1e* mutant shows no discernible phenotype whereas *drp1a* mutant seedling require germination on 1% sucrose plates to survive past 5 days but otherwise show minimal abnormal phenotype. However, *drp1a*/*e* double mutant seedlings are embryo lethal and display pronounced plasma membrane invaginations and disturbed cell expansion and cytokinesis. **(Otegui *et al*, 2001; Hong *et al*, 2003b Segui-Simmaro *et al*, 2004; Collings *et al*, 2008; Bednarek & Backues, 2010)**.

DRP2a is targeted to the plasma membrane, the TVN and to punctate structures in the cytoplasm. It has been implicated in golgi trafficking and clathrin mediated endocytosis (CME) **(Jin *et al*, 2001; Lam *et al*, 2002; Fujimoto *et al*, 2008, 2010)**. DRP2b localises to the cell plate during cytokinesis and

has been shown to colocalise with DRP1a and clathrin light chain (CLC), a component involved in CME **(Fujimoto *et al*, 2008, 2010; Collings *et al*, 2008)**. DRP2a/b are functionally redundant and neither *drp2a* or *drp2b* knock-out mutants display any discernible phenotype, however *drp2a*/*b* double mutants produce unviable male and female gametes that arrest development prior to cell division, have an altered cell wall composition and structure and elongated golgi cisternae **(Backues *et al*, 2010; Taylor, 2011)**. This functional redundancy, similar localisation to the cell plate and association with DRP1a and CLC make it likely that DRP2a/b are involved in the "pinching-off" of clathrin coated vesicles (CCVs) from both the trans-golgi body and the TVN, thereby regulating and shaping the nascent cell plate and TVN **(Jurgens, 2005; Backues *et al*, 2010; Bednarek & Backues, 2010; Taylor, 2011; Fujimoto & Tsutsumi, 2014)**.

1.4.3 DRP1E may be Implicated in Mitochondrial Fission, Alongside DRP3A/B and DRP5A/B

DRP action is not limited to the cell plate and cell membrane: DRP3a/b and DRP5a/b have become widely accepted as playing pivotal roles in mitochondrial, perixisomal and chloroplastic replication, specifically in the division of these replicating organelles **(Hong, 2003a; Zhang & Hu, 2010; Aung *et al*, 2010; Aung & Hu, 2012)**. Mitochondrial division and replication has predominantly been studied in *Saccharomyces cerevisiae*, which has been used as a model organism for the study of mitochondrial division. In yeast Dnm1, a yeast DRP homologue, polymerises to form a helical ring around the mitochondrial division site to constrict the mitochondrial membrane and execute division of the conjoined mitochondria **(Arimura & Tsutsumi, 2016)**. Other *S.cerevisiae* mitochondrial division factors Fis1, Mdv1 and Caf4 are responsible for the localisation of Dnm1 to the mitochondrial membrane. Fis1 is localised to the mitochondrial division site by a specific C-terminal transmembrane domain, this allows the cytoplasmic N-terminal of Fis1 to interact with the N-terminal of Mdv1 or Caf4, a paralogue of Mdv1 that exhibits redundancy with Mdv1. The C-terminal of Fis1-localised Mdv1 or Caf4 then interacts with Dnm1, effectively limiting Dnm1 to the mitochondrial division site via Fis1 and Mdv1/Caf4 **(Arimura & Tsutsumi, 2016)**.

In *A.thaliana*, DRP3a/b have been found to fulfil the role of Dnm1 in yeast and are the primary DRPs involved in mitochondrial fission **(Arimura *et al*, 2004; Logan *et al*, 2004; Fujimoto *et al*, 2009)**. DRP3a/b interact with themselves and each other, dual localise to the division plane of dividing mitochondria, function redundantly and form both hetero or homo dimers and oligomers **(Arimura *et al*, 2008; Fujimoto *et al*, 2009; Zhang & Hu, 2010)**. Although DRP3a is thought to be the major component of the DRP3 homo-oligomer in organelle replication, both *drp3a* and *drp3b* single

mutants possess decreased numbers of mitochondria, which are elongated compared to wild type (WT), but are otherwise normal, whilst *drp3a*/*b* double mutants exhibit grossly elongated, conjoined mitochondria. **(Fujimoto *et al*, 2009; Aung & Hu, 2012; Arimura & Tsutsumi, 2016)**. FIS1a/b, the two *A.thaliana* homologues of Fis1, interact with DRP3a/b and are thought to aid localisation of DRP3a/b to the mitochondrial division site. FIS1a/b play a significant role in mitochondrial division: both *fis1a* and *fis1b* single mutants exhibit lower numbers of slightly elongated mitochondria compared to WT **(Scott *et al*, 2006; Zhang & Hu, 2008; Fujimoto *et al*, 2009)**.

ELM1 was identified through screening of *A.thaliana* for aberrant mitochondrial phenotypes, it localises to the outer mitochondrial membrane and is essential for the localisation of DRP3a/b to mitochondria despite being found to have little or no interaction with DRP3a/b or FIS1a/b **(Arimura *et al*, 2008; Logan, 2010)**. PMD1 and PMD2 are coiled-coil proteins that insert specifically into the mitochondrial membrane via a C-terminal domain. They form hetero and homo-complexes and have been found to be essential for correct mitochondrial division through a mechanism independent of DRP3a/b and FIS1a/b **(Aung & Hu, 2011)**. PMD1/2 have been found to have no interaction with DRP3a/b or FIS1a/b and *pmd1/2* mutants do not affect the localisation of DRP3a/b but do exhibit aberrant mitochondrial morphology **(Aung & Hu, 2011)**.

DRP5b has been implicated in mitochondrial division and morphogenesis and has been found, by co-immuno precipitation (co-IP) and bi-molecular fluorescence complementation (BiFC) experiments, to associate closely with DRP3a/b and with FIS1a/b-PEX13 complexes on the surface of peroxisomes through interaction with FIS1a **(Zhang & Hu, 2010)**. Despite this, DRP5b has not been found to interact with DRP3a/b or FIS1a/b on the mitochondrial membrane or to localise to mitochondria, yet has still been found to play a role in mitochondrial division, since *drp5b* mutants exhibit smaller numbers of elongated mitochondria **(Aung & Hu, 2012)**.

N-terminal GFP-DRP1e fusions under the control of 35S viral promoter have been shown to localise to mitochondria in *A.thaliana* root cells, as was DRP1c **(Jin *et al*, 2003; Tang *et al*, 2006)**. Furthermore, RFP-DRP1c and GFP-DRP1e were found to colocalise to punctate spots in the cytoplasm, which may indicate localisation to an organelle **(Jin *et al*, 2003)**. T7-DRP1c[K48E], a mutant with knocked out GTPase activity, was found to colocalise with F1-ATPase-γRFP, which is localised specifically to mitochondria. T7-DRP1c[K48E] was found to substantially increase the proportion of cells with elongated mitochondria in *A.thaliana* root cell protoplasts **(Jin *et al*, 2003)**. T-DNA knockout *drp1e* root cell protoplasts transformed with 35S::F1-ATPase-γRFP mutants were found, by transmission electron microscopy and confocal laser microscopy, to have an increased proportion of cells with an elongated mitochondrial phenotype, similar to that found in T7-

DRP1c[K48E] expressing lines. This effect was largely rescued by overexpression of T7-DRP1c or T7-DRP1e **(Jin *et al*, 2003)**. The elongated mitochondrial phenotype of drp1e has not been shown consistently and there are several accounts that GFP-DRP1e both does and does not localise to mitochondria **(Kang *et al*, 2003a; Tang *et* al, 2006; Minami *et al*, 2015)**.

1.4.4 DRP1A/C/E and DRP2A/B are Involved in Clathrin-Mediated Endocytosis

Clathrin mediated endocytosis (CME) is the primary method of internalisation into plant cells through the invagination of sections of the plasma membrane or golgi membrane resulting from the cooperation of the adaptor protein 2 (AP2) complex with its specific cargo, elements of the actin cytoskeleton and clathrin triskelia **(Chen *et al*, 2011)**. It is not yet known as to how clathrin coated pit (CCP) nucleation is carried out in plants: the cargo-bound AP2 complex may be directly responsible for the initiation of CCP formation or it may be that AP2 complexes are recruited to a pre-determined nucleation site **(Kelly *et al*, 2014; Fan *et al*, 2015)**. There is evidence for the latter theory as, in mammals and yeast, AP2 complexes are recruited to the site of the CCP initiator protein Fer/Cip4 Homology domain-only (FCHo) **(Henne *et al*, 2010)**, although no FCHo homologue has so far been identified in plants **(Fan *et al*, 2015)**. AP2 complexes consisting of 4 subunits: α, β2, σ2 and μ2 **(Fan *et al*, 2013; Kelly *et al*, 2014)** localise to the membrane around specific cargo proteins, which may occur through AP2 complex association with TPLATE complexes (TPC) **(Gadeyne *et al*, 2014)**. TPCs are hetero-octomeric protein complexes that interact with various cargo proteins, DRPs and both clathrin light chain (CLC) and clathrin heavy chain (CHC) **(Gadeyne *et al*, 2014)**. TPCs localise to CCP nucleation sites concomitantly with, or marginally before, AP2 complexes and both AP2 and TPC complexes are responsible for cargo binding **(Bonifacino & Traub, 2003; Chen *et al*, 2011)**. TPC complexes have been shown to possess subunits that directly interact with actin microfilaments and may act as an attachment point for the forming CCP to the polarised actin filament skeleton that surrounds the CCP site and helps to extrude the CCP into the cytoplasm.

The cargo-TPC-AP2 complex proceeds to recruit clathrin triskelia to the CCP initiation site, thereby stabilising the CCP as it is extruded into the cytoplasm through the action of actin **(Gadeyne *et al*, 2014)**. Clathrin triskelia each consist of 3 CLC and 3 CHC monomers, with the 3 CLC as spokes to which the CHC are attached **(McMahon & Boucrot, 2011)**. Continued recruitment of clathrin and action of the CCP associated actin filaments causes sustained invagination of the membrane until a mature CCP is formed **(Lam *et al*, 2001; McMahon & Boucrot, 2011)**. DRP1s and DRP2s are recruited to the mature CCP through the concerted effects of interaction with TPCs, SH3-containing Protein 1 (SH3P1) and through the specific lipid and phosphoinositide interactions of the DRP variable lipid

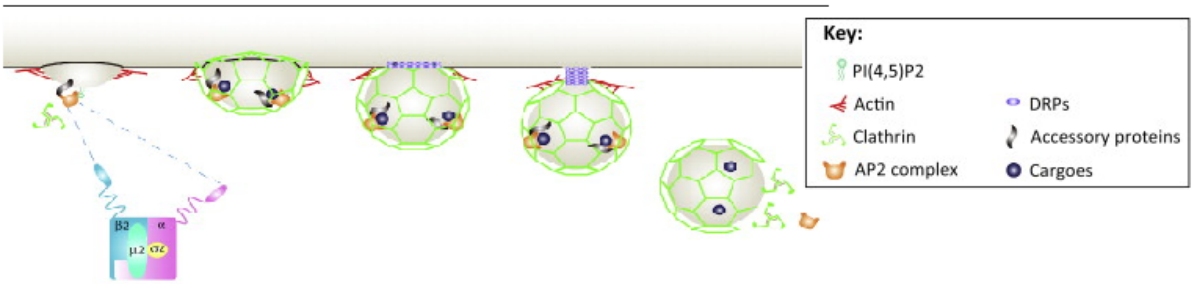

Figure 1.G) Diagram of Clathrin Coated Pit (CCP) formation, budding and scission to form a Clathrin Coated Vesicle (CCV). AP2 is recruited to the site of CCP formation, potentially via lipid specificity or cargo recognition, binding cargo proteins and TPCs. The cargo-AP2-TPC complexes begin to recruit clathrin triskelia to the CCP formation site, whilst actin micro filaments form at the edges of the CCP. Coordinated action by actin microfilaments extrudes the membrane around the CCP into the cytoplasm and continued recruitment of clathrin stabilises the forming CCP by creating a rigid clathrin sheath. DRPs bind to the join between the CCP and the cell membrane, polymerising to form a macromolecular helix in a GTP-dependent fashion. As the CCP is further extruded into the cytoplasm, the lengthening DRP helix restricts the membrane joining the forming CCV to the cell membrane into a membrane tubule. The CCV is then 'pinched off' to form a free CCV by contraction of the DRP helix induced by hydrolysis of bound GTP. The associated protein complexes, DRPs and actin filaments then begin to dissociate.

Taken from (Fan *et al.*, 2015).

binding sequence or PH domain and are thought to form a hetero-polymer **(Lam *et al*, 2001, 2002; Bednarek & Backues, 2010; Minami *et al*, 2015)**. The membrane joining the mature CCP to the cell membrane/golgi membrane is restricted by the GTP-bound helical DRP polymer to form a membrane tubule. This membrane tubule is further constricted by a conformational change in the DRP polymer upon GTP hydrolysis, causing scission of the membrane tubule and forming a free Clathrin Coated Vesicle (CCV) **(Fujimoto *et al*, 2010, 2014; Bednarek & Backues, 2010; McMahon & Boucrot, 2011; Taylor *et al*, 2011)**.

Gadeyne *et al* recently identified the octomeric TPLATE protein complex (TPC) through series of tandem affinity purification (TAP), Y2H, co-IP and BiFC experiments in which each of the 8 subunit proteins interacted with each other on multiple occasions, providing convincing evidence for the TPLATE complex assembly. During reverse-TAP experiments with each of the 8 constituent proteins of the TPLATE complex, TAP experiments using TML or TASH3 as bait detected positive interaction between DRPs 1a/c/e, 2a/b and both TML and TASH3 **(Gadeyne *et al*, 2014)**. TML was also found to interact with CLC2, CHC1/2 and AP2α1 subunit, thereby linking DRP1a/c/e and DRP2a/b to clathrin, the cell membrane and CCP formation sites **(Gadeyne *et al*, 2014)**. **Fujimoto *et al*, 2010** found by variable incidence angle fluorescent microscopy (VIAFM) that DRP1a and DRP2b colocalise with CLC at the plasma membrane, accumulate at sites at which CLC is already present and disappear from the plasma membrane in tandem with CLC. **Fujimoto *et al*, 2010** also found that application of

Tyrphostin A23 (tyrA23) disrupted localisation of DRP1a to DRP2b and CLC but had little effect on the localisation of DRP2b to CLC. tyrA23 is a disrupter of interactions between the AP2 complex µ2 subunit and the YXXΦ motifs that commonly provide binding interaction sites in cell membrane proteins and is a proven inhibitor of CME **(Banbury *et al*, 2003; Dhonukshe *et al*, 2007)**. **Konopka *et al*, 2008** found that DRP1c colocalises with CLC by variable angle epifluorescence microscopy (VAEM), that DRP1c and CLC share similar localisation, dynamics and lifetime and that application of tyrA23, or similar disruption of CME machinery, disrupts localisation of both DRP1c and CLC. **Jin *et al*, 2001** showed that DRP2a interacts with the AP1complex γ-subunit whilst **Song *et al*, 2006** demonstrated that AP1γ interacts with both with EPSIN1, an adaptor protein associated with AP2 complex and CCP formation, and clathrin. Together these two papers demonstrate that DRP2a likely interacts indirectly with clathrin and so is likely associated with CME.

Furthermore, **Huang *et al*, 2014** identified, by confocal laser scanning microscopy (CLSM), that both DRP2a and DRP2b colocalise with CLC and showed by Y2H, co-IP and VIAFM that DRP2a and DRP2b colocalise and interact with themselves and each other. **Huang *et al*, 2014** go on to propose that DRP2a and DRP2b are likely to form both hetero and homo polymers *in vivo*. **Fujimoto *et al*, 2010** found by Y2H that DRP1a and DRP2b interact with themselves and each other and infer that DRP1a and DRP2b form hetero-polymers at the cell membrane, since RFP-DRP1a and GFP-DRP2b displayed similar rates of fluorescent accumulation and disappearance during VIAFM experiments. **Minami *et al*, 2015** showed that GFP-DRP1e localised to the cell plate, a few punctate cytoplasmic structures and localised non-uniformly to the plasma membrane, with GFP-DRP1e foci at the plasma membrane displaying dynamics comparable to that observed with DRP1a/c and CLC **(Konopka *et al*, 2008; Fujimoto *et al*, 2010)**. **Minami *et al*, 2015** found by confocal fluorescence microscopy that GFP-DRP1e colocalised with PIP2A-mcherry at the plasma membrane and, by immunoblot analysis, isolated CHC and over expressed GFP-DRP1e from detergent resistant membrane fractions (DRM) rich in sphingolipids and sterols. Sphingolipid and sterol enriched membrane microenvironments and the PIP2A aquaporin channel are associated with sites of membrane microdomain-associated endocytosis (MME), a mechanism of clathrin independent endocytosis in *A.thaliana* **(Li X. *et al*, 2011; Li R. *et al*, 2012; Wang *et al*, 2013)**, implicating that DRP1e may have a role in MME.

The likely role of DRP1e in CME, and potentially MME, provides the possibility for regulatory interaction between DRP1E and CO_2 signalling pathways through the endocytosis of membrane-bound CO_2 signalling elements. The possibility of such interactions is investigated in this thesis through experiments conducted on a novel *drp1e* mutant that was identified as having an inhibited stomatal response to elevated atmospheric CO_2 concentrations.

Chapter 2 – Materials and Methods

2.1 Plant Materials and Growth Conditions

2.1.1 Seed Stocks

All plant material used was *Arabidopsis thaliana* in the Columbia-0 (Col-0) background. The Col-0 wild-type and EO_2 mutant line were obtained from Dr Jean-Charles Isner, Guard Cell research group, University of Bristol. T-DNA insertion lines in the genes *DRP1e* (AT3G60190), *PIP2;1* (AT3G53420) and *RBOHD* (AT5G47910) were obtained from the Nottingham Arabidopsis Stock Centre (NASC) and are listed in **Table 2A** below. All seed stocks were genotyped as described in **2.5.2.2** using the primer pairs and border primers listed in **Table 2A**. "Genotyping Primer Combinations" numbers in **Table 2A** refer to primers listed in **Table 2B**, which contains full primer descriptions, including sequence, T_m value and target sequence location.

Table 2.A) *Arabidopsis* seed stocks

Gene	Accession No.	Line	Type	N number	Genotyping Primer Combinations
DRP1e	AT3G60190	SALK_206052C	Confirmed homozygous line	N695462	1,2,15
		GK-168C11	Segregating line set	N741607	3,4,16
		GK-168C11.08	Homozygous line isolated from set	N742074	
		EO_2	Homozygous SNP mutant isolated from EMS lineage		11,12,13,14
PIP2A	AT3G53420	SALK_040961	Heterozygous line	N540961	5,6,15
RBOHD	AT5G47910	SALK_083046	Heterozygous line	N583046	7,8,15
		SALK_128800C	Confirmed homozygous line	N676885	9,10,15

2.1.2 Plant Growth Conditions

Seeds were surface sterilised with 70% v/v Ethanol for 5 mins followed by sterilisation in 20% v/v Household Bleach, 1% v/v TWEEN-20 for 5 mins. Seeds were then washed thoroughly in autoclaved MiliQ water. Potting media was a 3:1 mixture of Sinclair multi-purpose compost: Horticultural Silver Sand (both William Sinclair Horticultural, UK) that was well mixed. 4l portions of potting media were divided into clean autoclave bags, which were sealed and baked for 3 days at 60^oC before cooling to room temperature. Sterilised seeds were stratified for 3 days at 4^oC before being sown under light on prepared potting media in 8x5 plug trays, which were well-watered with reverse-osmosis distilled water (ro-dH_2O). Seeded trays were transferred into a Microclima growth cabinet (Snijders Scientific,

Netherlands) with growth conditions as follows, unless otherwise specified: 10hr/14hr light/dark cycle, 22°C/20°C light/dark, 70% Relative Humidity (RH), 120 µmol $m^{-2}s^{-1}$ average light intensity (PPFD), ambient [CO_2] (380-400ppm CO_2). Seven days after transferral of trays into the growth cabinet, pots with multiple germinated seedlings were thinned to leave the single most central seedling in each individual pot. These growth conditions apply to all plants and experiments unless specifically stated otherwise.

2.1.3 Plant Crosses

For plant crosses, eight – nine weeks old plants with mature, un-opened buds were selected to be female parents for plant crosses, buds were artificially opened using thin, pointed, metallic tweezers and the bud was disassembled to leave nothing but the pistils. These pistils were artificially pollinated using mature anthers taken from a selected male parent and the pollinated pistil was covered with clingfilm for 3 days. Seed were collected from mature siliques and either sterilised and sown directly, or stored in the dark at 4°C.

2.2 Stomatal Assays Using Epidermal Strips

2.2.1 Preparation of Epidermal Strips

Fully expanded leaves were taken from 4-5 week old plants and carefully cut and peeled to produce abaxial epidermal strips, which were floated cuticle-side up in 5cm single vent petri dishes (Sterilin, UK) containing 10mM MES (pH 6.15 /KOH) at 22°C.

2.2.2 Stomatal Bioassay of Epidermal Strips

Stomatal bioassays were performed on *Arabidopsis thaliana* abaxial epidermal strips according to the protocol described in **Webb and Hetherington, (1997)**, with minor modifications. Results were tested for statistical significance by two-tailed t-test (between 2 treatments) or 2 way Analysis of Variance (ANOVA) (between two lines, multiple treatments).

2.2.2.1 Abscisic Acid-Induced Promotion of Stomatal Closure Bioassay

Prepared abaxial epidermal strips (**2.2.1**) were floated cuticle-side up in 5cm single vent petri dishes (Sterilin, UK) containing KCl-MES buffer (50mM KCl, 10mM MES, pH 6.15 /KOH) (abbreviated to KCl-MES 10:50 buffer) and were incubated for 2 hours at 22°C, 120 µmol $m^{-2}s^{-1}$ average light intensity (PPFD), ambient [CO_2] (380-400ppm CO_2). At 2 hours, strips were transferred to control dishes or dishes containing the stated concentration of ABA and were incubated for a further 2 hours under the same conditions. Treatments with stated concentrations of ABA were made by addition of the respective volume of 10mM ABA stock solution in EtOH to KCl-MES 10:50 buffer, resulting in an

EtOH concentration of ≤0.1% v/v. Additional EtOH was added to make the total EtOH concentration in treatment and control dishes up to 0.1% v/v. Three epidermal strips from each dish were mounted on slides on a drop of buffer from the respective dish and covered with a cover slip. The mounted slide was gently pressed, cover slip down, onto lab-roll to remove excess buffer before being visualised at 400x magnification using a Leica DM-IRB inverted microscope (Leica) fitted with a side port-mounted CCD camera (JVC-TKC1381, JVC Ltd.) to allow visualisation of stomatal apertures on a colour computer monitor. Stomatal aperture was measured directly from the monitor screen using an acetate ruler, calibrated to the screen and magnification using a stage micrometer. The apertures of ten randomly selected, healthy, stomata were measured from each peel to give 30 measurements from each treatment. Each peel was taken from a separate plant and the experiment was repeated three times, giving a total of 90 measurements from 9 biological replicates per treatment. Experiments were conducted blind to genotype.

2.2.2.2 Calcium Chloride-Induced Promotion of Stomatal Closure Bioassay

Prepared abaxial epidermal strips (**2.2.1**) were floated cuticle-side up in 5cm single vent petri dishes (Sterilin, UK) containing KCl-MES 10:50 buffer and were incubated for 2 hours at 22°C, 120 µmol $m^{-2}s^{-1}$ average light intensity (PPFD), ambient [CO_2] (380-400ppm CO_2). At 2 hours, strips were transferred to control dishes or dishes containing the stated concentration of CaCl2 and were incubated for a further 2 hours under the same conditions. Treatments with stated concentrations of $CaCl_2$ were made by addition of the respective volume of 1M $CaCl_2$ stock solution in water to KCl-MES 10:50 buffer. Measurements of stomatal apertures were as stated in **2.2.2.1**.

2.2.2.3 Elevated Atmospheric Carbon Dioxide-Induced Promotion of Stomatal Closure Bioassay

Prepared abaxial epidermal strips (**2.2.1**) were floated cuticle-side up in 5cm single vent petri dishes (Sterilin, UK) containing KCl-MES 10:50 buffer that had been bubbled with air, containing 400ppm CO_2, by means of a hypodermic needle through a small hole in the lid of the dish. Upon the addition of epidermal strips to the dish, the needle was lifted just above the surface of the buffer to provide an atmosphere of 400ppm CO_2 air within the dish. Epidermal strips were incubated for 2 hours at 22°C, 120 µmol $m^{-2}s^{-1}$ average light intensity (PPFD) under 400ppm CO_2 before being transferred to dishes containing KCl-MES 10:50 buffer that had been bubbled with 400ppm CO_2 (control) or 1000ppm CO_2 (treatment) air through the same means as described above. Upon transferral of peels into these dishes the hypodermic needles were lifted above the buffer to provide an atmosphere with CO_2 at the stated concentration within the dish. Control and treatment dishes were incubated under the above conditions for a further 2 hours before measurement of stomatal aperture, which was conducted as described in **2.2.2.1**.

2.2.2.4 Dark-Induced Promotion of Stomatal Closure Bioassay

Prepared abaxial epidermal strips (**2.2.1**) were floated cuticle-side up in 5cm single vent petri dishes (Sterilin, UK) containing KCl-MES 10:50 buffer and were incubated for 2 hours at 22^{o}C, 120 µmol $m^{-2}s^{-1}$ average light intensity (PPFD), ambient [CO_2] (380-400ppm CO_2). At 2 hours, strips were transferred to transparent control dishes or light-excluding black dishes treatment and were incubated for a further 2 hours under the same conditions. Measurements of stomatal apertures were as stated in **2.2.2.1**.

2.3 Physiological Techniques

2.3.1 Infra-Red Gas Analysis

2.3.1.1 Light to Dark Transition Infra-Red Gas Analysis using WALZ GFS-3000

Fully expanded leaves of 4-5 week old *Arabidopsis* were inserted into the leaf clamp of a WALZ GFS-3000 Infrared gas analyser (WALZ, Germany), with an insert exposing a 2.5cm^2 area of the leaf for gas exchange analysis, the experiment was conducted *in-situ* in the growth cabinet with conditions as listed in **2.1.2**. IRGA program was as follows: 2hours, sampling is 10-second average, 300µmols^{-1} flow rate, temp 22^{o}C, 70% Relative Humidity, 400ppm CO_2. For the first hour of the program the leaf area was illuminated with ambient light at 110-130µM m^{-2} s^{-1} PPFD from the cabinet through a glass partition, at one hour a metal plate was affixed to the glass partition to exclude light and the data was recorded for a further hour at 0-3 µM m^{-2} s^{-1} PPFD. The experiment was repeated 3 times with data collected from 2 biological replicates per repeat to give a total of 6 (Col-0) or 5 (EO_2) biological replicates per line. The average of these replicates was used to calculate transpiration and carbon assimilation data at each time point. Due to the large amount of noise in the mean carbon assimilation rate, the data shown is a plot of a 2-minute moving average of the mean carbon assimilation rate.

2.3.1.2 Ambient to Elevated [CO_2] Transition Infra-Red Gas Analysis using Li-COR 6400XT

Plants were grown in a Conviron E15 growth cabinet (Conviron, USA) at 22^{o}C, 70% RH, 10hr/14hr light/dark cycle, 110-120µmol m^{-2} s^{-1} PPFD, in 1.5" LI-COR 'cone-tainers' (Prod.no. 610-09645, LI-COR, USA), compatible with the circular Li-Cor gas exchange chamber for a flush seal. The potting media of 4-5 week old *Arabidopsis* plants were covered with polyethylene wrap to isolate the aerial tissue of the plants and eliminate potting media surface evaporation. Prepared plants were inserted into the whole plant *Arabidopsis* chamber (prod.no. 6400-17, LI-COR, USA) of a LI-COR 6400XT infra-red gas analyser with light-source attachment (prod.no. 6400-18A, LI-COR, USA) and subjected to the

following program: 400µmols^{-1} flow rate, temp 22^{o}C, 60-70% Relative Humidity, 300µmolm^{-2}s^{-1} PPFD. CO_2 concentration was kept at 400ppm for 8 minutes before increasing to 1000ppm over a period of 1 minute. [CO_2] was then maintained at 1000ppm for a further 9 minutes. Sampling occurred at 21 second intervals and plant leaf area was subsequently calculated for area correction on an individual basis using Image J (version 1.8). The experiment was repeated in triplicate over three consecutive days, giving a total of 7 (Col-0) or 8 (other lines) biological replicates per line.

2.3.1.3 Light to Dark Transition Infra-Red Gas Analysis using Li-COR 6400XT

Plants were grown in a Conviron E15 growth cabinet (Conviron, USA) at 22^{o}C, 70% RH, 10hr/14hr light/dark cycle, 110-120µmol m^{-2} s^{-1} PPFD, in 1.5" LI-COR 'cone-tainers' (Prod.no. 610-09645, LI-COR, USA), compatible with the circular Li-Cor gas exchange chamber for a flush seal. The potting media of 4-5 week old *Arabidopsis* plants was covered with polyethylene wrap to isolate the aerial tissue of the plants and eliminate potting media surface evaporation. Prepared plants were inserted into the whole plant *Arabidopsis* chamber (prod.no. 6400-17, LI-COR, USA) of a LI-COR 6400XT infra-red gas analyser with light-source attachment (prod.no. 6400-18A, LI-COR, USA) and subjected to the following program: 400µmols^{-1} flow rate, temp 22^{o}C, 60-70% Relative Humidity, 400ppm CO_2. PPFD was kept at 300µmolm^{-2}s^{-1} for 2 minutes before reduction to 0-1 µmolm^{-2}s^{-1}, which was then maintained for a further 4 minutes. Sampling occurred at 21 second intervals and plant leaf area was subsequently calculated for area correction on an individual basis using Image J (version 1.8). Three biological replicates were used per line.

2.3.2 Whole-Plant Gravimetric Transpiration Analysis

Plants were grown in a Conviron E15 growth cabinet (Conviron, USA) at 22^{o}C, 70% RH, 10hr/14hr light/dark cycle, 110-120µmol m^{-2} s^{-1} PPFD, in 1.5" LI-COR 'cone-tainers' (Prod.no. 610-09645, LI-COR, USA). The bottom drainage hole and potting media of 4-5 week old *Arabidopsis* plants grown in 1.5" LI-COR 'cone-tainers' were covered with polyethylene wrap to isolate the aerial tissue of the plants and minimise evaporation from the potting media. A set of twenty matched EK410i balances (A&D, USA) were set up in a growth cabinet with identical growth conditions and synchronised to the same dusk/dawn times. Three plants of the same line were randomly selected and mounted together on a randomly selected balance, this was repeated 3 times for each line to give 3 sets of 3 plants per experimental repeat. Mass readings from each balance were electronically recorded at 5-minute intervals over a 36-hour dark-light-dark supra-diurnal cycle. Rate of water loss was calculated for each balance based on weight loss over the time period between readings and this value was area corrected for the total leaf area of all three plants (Image J version 1.8), giving the average transpiration rate for each balance in mmol m^{-2} s^{-1}. A 12 point (60 minute) moving average of

transpiration rate was calculated for each balance to smooth the data and cubic curves were separately fitted to dark period 1, light period and dark period 2 data for each balance to give fitted transpiration rate values. Mean fitted transpiration rate values for each line were calculated at each time point and the result presented as final transpiration rate data. Transpiration rate values were calculated from the first derivative of the curve of water loss against time. The experiment was repeated 3 times for a total of 9 balances (n=9) and 27 biological replicates per line.

2.3.3 Water Use Efficiency Experiments

Nine 4 mm holes were drilled into the bottom of 465 ml white, opaque, disposable, specimen containers (Berry Plastics Corporation, IN, USA) for sub-irrigation and drainage. A single 5 mm hole was drilled into the centre of the container lids and the lids were spray painted matt-black with 2X Ultra-Cover Flat black Spray (249127 , Rust-Oleum, USA). Empty containers were weighed, then filled with Sungro Sunshine Mix #2 soilless media (Sun Gro Horticultural, MA, USA), the lid fastened and containers, complete with lid and media, were weighed again. The filled and assembled containers were saturated with water and weighed to determine mass of water added. Sterilised seed was sown onto the surface of the saturated media in the 5mm lid-hole and containers were placed under intermittent mist for ten days, before transferral to the Purdue Plant-Growth facility greenhouses. Containers were again saturated with water before being placed inside a further identical container with no holes drilled into the bottom, to minimise water loss by this means. Plants were grown under 10hr/14hr light/dark photoperiod (controlled with electronic blinds) with no water for 21-days. Light intensity and temperature were variable although temperature was somewhat controlled by an inbuilt air conditioning system. To ameliorate these factors, containers were randomly distributed, blind to genotype, within a specified area to remove bias from variation in localised conditions. At 3-weeks, the containers were weighed and the aerial tissue of each plant removed. The aerial tissue of each plant was weighed and the total leaf area calculated using Image J (version 1.8) for area correction, before being desiccated and weighed again. WUE was calculated as plant dry weight/total water loss in g l^{-1}.

2.3.4 Stomatal Development Under Ambient and Elevated Atmospheric Carbon Dioxide

Fully expanded, healthy leaves were taken from 8-9 week old *Arabidopsis* plants and impressions of the abaxial leaf epidermis made using a Polyvinylsiloxane-based dental putty (prod.no. ICC065, The Dental Directory, UK). The dental putty was left to cure for 30 minutes before careful application of clear “60 seconds supershine” nail polish (shade-740 ‘clear’, Rimmel London, UK) to the dental putty epidermal impression. The clear nail varnish was left to dry for 10 minutes before mounting of the nail varnish impressions on microscope slides using transparent ‘Scotch Crystal Tape’ (Cat.no. 600,

3M, UK), resulting in a slide-mounted replica of the leaf epidermis. Slides were visualised using a Zeiss Axiovert 200M inverted microscope (Zeiss, Germany) with side-port mounted Hamamatsu ORCA-ER C4742-80 camera. Images of the impressions were taken halfway along the leaf blade and midway between the midrib and leaf edge, avoiding leaf veins and any bubbles or tears in the impression. Images were taken at 200x Magnification as 5µm-interval image stacks that were analysed using the Image J (version 1.8) cell counter plugin (version 2.2.2). Stomatal density was calculated as the number of stomata in a 0.64mm^2 (800µm x 800µm) area and normalised to number of stomata in a 1mm^2 area; stomatal index was calculated as number of stomata in a 0.64mm^2 (800µm x 800µm) area divided by the total number of cells in the same area.

2.4 Inhibitor Assays and Confocal Microscopy Experiments

2.4.1 Stomatal Bioassay of Epidermal Strips with Application of Tyrphostin-A23

2.4.1.1 Abscisic Acid-Induced Promotion of Stomatal Closure Bioassay with Application of Tyrphostin-A23.

Prepared abaxial epidermal strips (**2.2.1**) were floated cuticle-side up in 5cm single vent petri dishes (Sterilin, UK) containing KCl-MES 10:50 buffer and were incubated for 90 minutes at 22^{o}C, 120 µmol $m^{-2}s^{-1}$ average light intensity (PPFD), ambient [CO_2] (380-400ppm CO_2). At 90 minutes, strips were transferred to dishes containing KCl-MES 10:50 buffer with 0µM or 30µM Tyrphostin-A23 (from a 30mM stock in DMSO), giving a final DMSO concentration of 0.1%. At 120 minutes epidermal strips were transferred to dishes containing Tyrphostin-A23 at the stated concentrations and 0 µM or 5µM Abscisic Acid (from 10mM stock in EtOH, giving 0.05% EtOH by volume). All dishes were made up to 0.1% DMSO and 0.05% EtOH by volume to control for the added solvents and were incubated for 2 hours before assessment of stomatal apertures as described in **2.2.2.1**. Epidermal strips were incubated under the above conditions throughout the experiment.

2.4.1.2 Elevated Atmospheric Carbon Dioxide-Induced Promotion of Stomatal Closure Bioassay with Application of Tyrphostin-A23.

Prepared abaxial epidermal strips (**2.2.1**) were floated cuticle-side up in 5cm single vent petri dishes (Sterilin, UK) containing KCl-MES 10:50 buffer that had been bubbled with air, containing 400ppm CO_2, by means of a hypodermic needle through a small hole in the lid of the dish. Upon the addition of epidermal strips to the dish, the needle was lifted just above the surface of the buffer to provide an atmosphere of 400ppm CO_2 air within the dish. Epidermal strips were incubated for 90 minutes at 22^{o}C, 120 µmol $m^{-2}s^{-1}$ average light intensity (PPFD) under 400ppm CO_2 before being transferred to dishes, that had been bubbled with 400ppm CO_2, containing KCl-MES 10:50 buffer with 0µM or

30µM Tyrphostin-A23 (from 30mM stock in DMSO). At 120 minutes epidermal strips were transferred to dishes that had been bubbled with 400ppm or 1000ppm CO_2 air and 0µM or 30µM Tyrphostin-A23. All dishes were made up to 0.1% DMSO by volume and were incubated for a further 2 hours before measurement of stomatal aperture, which was conducted as described in **2.2.2.1**. Epidermal strips were incubated under the above conditions throughout the experiment with the exception of stated changes in [CO_2].

2.4.2 Stomatal Closure Vesicle Assays with Application of Tyrphostin-A23

2.4.2.1 Abscisic Acid-Induced Stomatal Closure Vesicle Assay with Application of Tyrphostin-A23

Prepared abaxial epidermal strips (**2.2.1**) were floated cuticle-side up in 5cm single vent petri dishes (Sterilin, UK) containing KCl-MES 10:50 buffer and were incubated for 90 minutes at 22^{o}C, 120 µmol $m^{-2}s^{-1}$ average light intensity (PPFD), ambient [CO_2] (380-400ppm CO_2). At 90 minutes, strips were transferred to dishes containing KCl-MES 10:50 buffer with 0µM or 30µM Tyrphostin-A23 (from a 30mM stock in DMSO), giving a final DMSO concentration of 0.1%. At 120 minutes epidermal strips were transferred to dishes containing Tyrphostin-A23 at the stated concentration and 0 µM or 5µM Abscisic Acid (from 10mM stock in EtOH), giving 0.05% EtOH by volume. All dishes were made up to 0.1% DMSO and 0.05% EtOH by volume to control for the added solvents and were incubated for 15 minutes before transferral to dishes containing 15 µM FM4-64 styryl membrane dye (Biotium, Prod. No. 70021) (from 15 mM stock in MiliQ water). Epidermal strips were loaded with FM4-64 dye for 10 minutes and washed for 5 minutes before being mounted on slides as described in **2.2.2.1**. Loading and washing of FM4-64 dye occurred under the stated concentrations of Tyrphostin-A23 and ABA and epidermal strips were incubated under the above conditions throughout the experiment. Imaging of slides was conducted using a Leica TCS SP5 confocal microscope, exciting with an argon laser at 488 nm, collecting emissions at 600-630 nm. Image stacks were taken with 0.5 µm intervals, collecting at 680-800nm for autofluorescence and vesicle numbers were computed using ImageJ (version 1.8) with the 3D object counter plugin (version 2.3).

2.4.2.2 Elevated Atmospheric Carbon Dioxide-Induced Stomatal Closure Vesicle Assay with Application of Tyrphostin-A23

Prepared abaxial epidermal strips (**2.2.1**) were floated cuticle-side up in 5cm single vent petri dishes (Sterilin, UK) containing KCl-MES 10:50 buffer that had been bubbled with air, containing 400ppm CO_2, by means of a hypodermic needle through a small hole in the lid of the dish. Upon the addition of epidermal strips to the dish, the needle was lifted just above the surface of the buffer to provide an atmosphere of 400ppm CO_2 air within the dish. Epidermal strips were incubated for 90 minutes at

22°C, 120 µmol $m^{-2}s^{-1}$ average light intensity (PPFD) under 400ppm CO_2 before being transferred to dishes, that had been bubbled with 400ppm CO_2, containing KCl-MES 10:50 buffer with 0µM or 30µM Tyrphostin-A23 (from 30mM stock in DMSO). At 120 minutes epidermal strips were transferred to dishes that had been bubbled with 400ppm or 1000ppm CO_2 air and 0µM or 30µM Tyrphostin-A23. All dishes were made up to 0.1% DMSO by volume to control for the added solvents and were incubated for 15 minutes before transferral to dishes containing 15 µM FM4-64 styryl membrane dye (from 15 mM stock in MiliQ water). Epidermal strips were loaded with FM4-64 dye for 10 minutes and washed for 5 minutes before being mounted on slides as described in **2.2.2.1**. Loading and washing of FM4-64 dye occurred under the stated concentrations of Tyrphostin-A23 and CO_2 and epidermal strips were incubated under the above conditions throughout the experiment. Imaging of slides was conducted using a Leica TCS SP5 confocal microscope, exciting with an argon laser at 488 nm, collecting emissions at 600-630 nm. Image stacks were taken with 0.5 µm intervals, collecting at 680-800nm for autofluorescence and vesicle numbers were computed using ImageJ (version 1.8) with the 3D object counter plugin (version 2.3).

2.4.3 Confocal Experiments with Fluorescent Protein Expressing *Arabidopsis* Protoplasts

2.4.3.1 PIP2A, RBOHD and DRP1E Preliminary Confocal Experiments

These experiments were carried out in 16-hour-old *Arabidopsis* protoplasts expressing fluorescently tagged DRP1E-XFP, RBOHD-XFP or PIP2A-XFP, transformed according to the protocol described in **2.5.7**. Three slices from each stack were selected at the middle, upper quartile and lower quartile between the top of the stack and loss of focus. ROIs were defined, comprising the cell membrane, in each slice and the fluorescent intensity of each ROI calculated using the ImageJ ROI Manager tool. Data from the ROI manager tool was corrected for background fluorescence values to give Corrected Total Cellular Fluorescence (CTCF) values for the selected ROIs. These values were then averaged to give mean CTCF intensities for each treatment at each time point. Confocal images were collected at 0.5µm slice intervals with brightfield active and collecting at 680-800nm for autofluorescence, excitation was accomplished using an argon laser. Laser settings for CFP was as follows: excitation at 458nm Argon laser, collecting at 464-499nm in addition to autofluorescence. For YFP, excitation was at 514nm Argon laser, collecting at 525-555nm in addition to autofluorescence.

2.4.3.2 Preliminary FRET Experiments

These experiments were carried out as detailed in **2.4.3.1** using dual transformed *Arabidopsis* protoplasts expressing CFP and YFP tagged DRP1E or YFP tagged DRP1E and CFP tagged PIP2A. Confocal images were collected at 0.5µm slice intervals with brightfield active and collecting at 680-

800nm for autofluorescence, excitation was accomplished using an argon laser. Laser settings for CFP was as follows: excitation at 458nm Argon laser, collecting at 464-499 in addition to autofluorescence. For YFP, excitation was at 514nm Argon laser, collecting at 525-555nm in addition to autofluorescence. Settings for FRET were excitation at 458nm using an Argon laser, collecting at 463-500nm, 524-560nm, 680-800nm with brightfield active.

2.5 Molecular Methods

2.5.1 DNA and RNA Extractions

2.5.1.1 Tissue Collection and Sample Preparation

Leaf tissue was collected from healthy 4-5 week old plants, inserted into sterile 2ml lock-cap centrifuge tubes and flash frozen in liquid nitrogen. Sterile 5mm diameter stainless steel beads were added to each lock-cap tube and the tissue was homogenously macerated at -80˚C using a Qiagen Tissue Lyser II (Prod.No. 85300, Qiagen).

2.5.1.2 Genomic DNA Extractions

Tissue samples were prepared according to **2.5.1.1**. Genomic DNA extractions were carried out using Promega Wizard Genomic DNA Purification kit (Prod.No. A1120, Promega) according to the manufacturer's protocol (Wizard Genomic DNA Purification Kit Technical Manual, Protocol 3E). Rehydrated gDNA samples were stored at -20˚C.

2.5.1.3 RNA Extractions

Tissue samples were prepared according to **2.5.1.1**. RNA extractions were carried out using Machery-Nagel NucleoSpin RNA Plant and Fungi kit (Prod.No. 740120.50, Machery-Nagel) according to the manufacturers protocol. RNA samples were kept on ice and used immediately for cDNA synthesis reactions (**2.5.2.4**).

2.5.2 Polymerase Chain Reactions

2.5.2.1 Primer Design and Catalogue of Primers

DNA accession sequences were taken from the TAIR and NCBI websites. Primers for genotyping were designed using the T-DNA Express Primer design tool (**SIGnAL (SALK Institute Genomic Analysis Laboratory)**, **2005**) for SALK and GABI-KAT seed stocks and manually checked using the nucleotide BLAST sequence alignment tool (**NCBI (National Centre for Biotechnology Information), 2009)** against gDNA sequences available from TAIR (**Garcia-Hernandez *et al.***, **2002**; **TAIR (The Arabidopsis Information Resource)**, **2018**). Primers for site directed mutagenesis were designed using the

NEBase Changer online tool (**NEB (New England Biolabs)**, **2011**). Other primers were designed using the Primer3 online tool (**V 4.1.0**) (**ELIXIR**, **2006**). All primers were from Eurofins Genomics and were stored at -20˚C as 100pmol μl^{-1} stocks in Nuclease-Free water (Prod.No. R0581, ThermoFisher Scientific). All primers are listed in the below **Table 2B**.

Table 2.B) – Catalogue of Primers

Primer Name	Primer No.	Sequence	Decription
SK206052 LP	1	5’ CCAAATGTCCTCTCACCTGAG	Genotyping Primer
SK206052 RP	2	5’ GGGAAATCTTCGGTTCTTGAG	Genotyping Primer, Posn. 154 f DRP1E CDS
GK168C11 LP	3	5' AGTGTCAAATTCACAACTGTTTCC	Genotyping Primer
GK168C11 RP	4	5' TAGGATACAGAGAGCATGTACCGT	Genotyping Primer
PIP2A LP	5	5'-AGCGGAGCTAAAGAAGTGGTC	Genotyping Primer
PIP2A RP	6	5'-ATGTTGGTTTGGTTTGCTTTG	Genotyping Primer
RBOHD SK083046 f	7	5'-ATCAGTGCCGCATATTCTTTG	Genotyping Primer, Posn. 894 r RBOHD cDNA
RBOHD SK083046 r	8	5'-ATCTTTCTTCCGAAGCACCTC	Genotyping Primer, Posn. 378 f RBOHD cDNA
RBOHD SK128800 f	9	5'-GCATGTCCACTCTTTTTAGCG	Genotyping Primer
RBOHD SK128800 r	10	5'-CGAGTCGTCCCTGATGTCTAG	Genotyping Primer, Posn. 241 r RBOHD cDNA
EO2 G794 f	11	5'-GTTGCAGACGAAGGAGAAGC	Genotyping Primer, Posn. 1569 r DRP1E CDS
EO2 G794 r	12	5'-TGGCGGGTAAACATCTTTGC	Genotyping Primer
EO2 G1567 f	13	5'-TAACCATCTGCCTCGGACAC	Genotyping Primer, Posn. 1206 r DRP1E CDS
EO2 G1567 r	14	5'-CAGCGTGCTTTCCAGTTCTT	Genotyping Primer
SALK LBb1.3	15	5' ATTTTGCCGATTTCGGAAC	Genotyping Primer
GABI KAT LBP	16	5' ATAATAACGCTGCGGACATCTACATTTT	Genotyping Primer
DRP1e cDNA f	17	5'-ATGACGACTATGGAGAGTTTGATTG	CDS Cloning Primer
DRP1e cDNA r	18	5'-TCATCTTACCCAAGCAACAGCAAT	CDS Cloning Primer
DRP1e cDNA f RES	19	5'-GAATTCAACAATGACGACTATGGAGAGTTTGATTG	CDS Cloning Primer with EcoRI restriction site
DRP1e cDNA r RES	20	5'-ATCGATTCTTACCCAAGCAACAGCATCAAT	CDS Cloning Primer with ClaI restriction site
DRP1e prom f	21	5’- ACGTTGGATGGTAAAAGCCG	Promoter Cloning Primer
DRP1e prom r	22	5’ CTTCCTTCTCCTTCAGTTTCAGA	Promoter Cloning Primer
DRP1e prom f res	23	5’-ACGCGTACGTTGGATGGTAAAAGCCG	Promoter Cloning Primer with MluI restriction site
DRP1e prom r res	24	5’- GAATTCCTTCCTTCTCCTTCAGTTTCAGA	Promoter Cloning Primer with EcoRI restriction site
PIP2A cDNA f	25	5'-ATGGCAAAGGATGTGGAAGCC	CDS Cloning Primer
PIP2A cDNA r	26	5'-TTAGACGTTGGCAGCACTTCTG	CDS Cloning Primer
PIP2A cDNA f RES	27	5'-GAATTCAACAATGGCAAAGGATGTGGAAGCC	CDS Cloning Primer with EcoRI restriction site
PIP2A cDNA r RES	28	5'-ATCGATGACGTTGGCAGCACTTCTGAA	CDS Cloning Primer with ClaI restriction site
PIP2A prom f	29	5’ GGTCGGTCCTAAAGAAAATGACA	Promoter Cloning Primer
PIP2A prom r	30	5’ AGTTAACTTCTTCTTCTTTCAAACAATAGC	Promoter Cloning Primer
PIP2A prom f res	31	5’ ACGCGTGGTCGGTCCTAAAGAAAATGACA	Promoter Cloning Primer with MluI restriction site
PIP2A prom r res	32	5’ GAATTCAGTTAACTTCTTCTTCTTTCAAACAATAGC	Promoter Cloning Primer with EcoRI restriction site
RBOHD cDNA f	33	5'-ATGAAAATGAGACGAGGCAATTCAAG	CDS Cloning Primer
RBOHD cDNA r	34	5'-CTAGAAGTTCTCTTTGTGGAAGTCAA	CDS Cloning Primer
RBOHD cDNA f RES	35	5' GAATTCAACAATGAAAATGAGACGAGGCAATTCAAG	CDS Cloning Primer with EcoRI restriction site
RBOHD cDNA r RES	36	5' ATCGATGAAGTTCTCTTTGTGGAAGTCAAACT	CDS Cloning Primer with ClaI restriction site
RBOHD prom f	37	5’ TCAGTGCCCAAGAGACAAAT	Promoter Cloning Primer
RBOHD prom r	38	5’ TCTCACTAGATTTGGCCAAGA	Promoter Cloning Primer
RBOHD prom f res	39	5’ ACGCGTTCAGTGCCCAAGAGACAAAT	Promoter Cloning Primer with MluI restriction site
RBOHD prom r res	40	5’ GAATTCTCTCACTAGATTTGGCCAAGA	Promoter Cloning Primer with EcoRI restriction site
pART7 f	41	5’ ATGCGATCATAGGCGTCTCG	Vector Insertion Site Primer
pART7 OCS r	42	5’ CAATCCCACTATCCTTCGTAAGA	Vector Insertion Site Primer
XFP front r	43	5’ GCTGAACTTGTGGCCGTTTA	Vector Sequence Primer, Posn. 181 r in C/YFP
XFP mid f	44	5’ GACGACGGCAACTACAAGAC	Vector Sequence Primer, Posn. 421 f in C/YFP
LacZα f	45	5’ TGACCATGATTACGCCAAGC	Vector Sequence Primer, Posn. 2 f in LacZα
LacZα r	46	5’ GTTGTAAAACGACGGCCAGT	Vector Sequence Primer, Posn. 208 r in LacZα
DRP CDS 1455 f	47	5’ TGTTGACATGGAATCTGCGT	Vector Insertion Primer, Posn. 1455 f DRP1E CDS
DRP CDS 79 r	48	5’ CACCACCATAGTCACCGAGT	Vector Insertion Primer, Posn. 79 r DRP1e CDS
PIP CDS 107 r	49	5’ GACCACTTCTTTAGCTCCGC	Vector Insertion Primer, Posn. 107 r PIP2A CDS
RBOHD CDS 2236 f	50	5’ ATTGGAGCCACGCCTATGAT	Vector Insertion Primer, Posn. 2236 f RBOHD CDS
RBOHD CDS 152 r	51	5’ TTCTTGGACGCACGTTTAGG	Vector Insertion Primer, Posn. 152 r RBOHD CDS
DRP1e C929T f mut	52	5’ AGTATACTATtCTTAATAAACAAAAGCATTG	Site Directed Mutagenesis Primer, Posn. 919 f DRP CDS
DRP1e C929T r mut	53	5’ TGGAATACGGGTCCTGAT	Site Directed Mutagenesis Primer, Posn. 918 r DRP CDS

2.5.2.2 PCRs for Genotyping, Colony PCR and Construct Border Checking

These PCRs were carried out using Dream Taq Green PCR Master Mix (2x) (Prod.No. K1081, ThermoFisher Scientific) and reaction mixtures were made-up according to the manufacturer's instructions, substituting a swab of the bacterial culture for the 1µl DNA sample in the case of colony PCR. Polymerase Chain Reactions were carried out using an Eppendorf Mastercycler Nexus Gradient PCR cycler (Prod.No. 6331, Eppendorf) using the following program:

Initial Denaturation	95˚C, 5 minutes
30 Cycles	{Denaturation 95˚C, 30s;
	Annealing 55˚C, 30s;
	Extension 72˚C, (60s/kb Product Size) + 20s};
Final Extension	72˚C, 10 minutes;
Product Hold	4˚C, Continuous.

2.5.2.3 PCRs for Promoter/CDS Cloning and SNP Confirmation

These PCRs were carried out using Q5 High-Fidelity 2X Master Mix (Prod.No. M0492S, New England Biolabs Inc.) and reaction mixtures were made-up according to the manufacturer's instructions. Polymerase Chain Reactions were carried out using an Eppendorf Mastercycler Nexus Gradient PCR cycler (Prod.No. 6331, Eppendorf) using the following program:

Initial Denaturation	98˚C, 2 minutes
35 Cycles	{Denaturation 98˚C, 20s;
	Annealing **TM**˚C, 30s;
	Extension 72˚C, (30s/kb Product Size) + 20s};
Final Extension	72˚C, 2 minutes;
Product Hold	4˚C, Continuous.

Annealing temperature (**TM**) during cycles was determined separately for each reaction using the New England Biolabs T_m Calculator online tool based on primer sequences.

2.5.2.4 cDNA Synthesis Polymerase Chain Reactions

RNA samples for cDNA synthesis reactions were prepared as described in **2.5.1.3**. cDNA synthesis reactions were carried out using Agilent AffinityScript QPCR cDNA Synthesis Kit (Prod. No. 600559) according the manufacturer's instructions with minor modifications:

20µl Reaction - 10µl First Strand Mastermix (2x)

3µl RNase Free Water

3µl Primers (**P1-3**)

1µl AffinityScript RT/RNase Block Enzyme Mixture

3µl RNA Sample

5 Separate reaction mixtures were made up using different primer combinations (**P1-3**):

P1 - 3µl oligo(dT) primers (100ng μl^{-1}); **P2** - 3µl random primers (100ng μl^{-1}); **P3** – separate reaction mixtures containing 1.5µl forward and 1.5µl reverse primers (10µM) specific to the CDS of DRP1E, PIP2A and RBOHD respectively.

cDNA synthesis products were used directly as subject DNA samples for PCR with Q5 High-Fidelity 2X Master Mix (**2.5.2.3**) to amplify the CDS of DRP1E, PIP2A and RBOHD.

2.5.3 Agarose Gel Electrophoresis and Gel Extraction Techniques

2.5.3.1 Making and Running of Agarose Gels

Agarose gels were made using 0.9% Agarose in TAE buffer, the mixture was heated to a rolling boil and allowed to cool to 65˚C before addition of 5µl/100ml Midori Green Advance DNA Stain (Prod.No MG04, Nippon Genetics) to the molten agar. The DNA ladder used was New England Biolabs 2-Log DNA Ladder (0.1-10.0kb) (Prod.No. N3200L, New England Biolabs) made up according to the manufacturer's instructions with Gel Loading Dye Purple 6X (Prod.No. B7024S, New England Biolabs) and Nuclease Free Water (Prod.No. R0581, ThermoFisher Scientific) in a 1:1:4 ratio. PCR products from reactions using Dream Taq Green PCR Master Mix (2x) (Prod.No. K1081, ThermoFisher Scientific) (**2.5.2.2**) were loaded directly into the wells of the gel. All other DNA samples were mixed with Gel Loading Dye Purple 6X (Prod.No. B7024S, New England Biolabs) in a 5:1 ratio prior to loading onto the gel. Gels were run in TAE buffer at 100V, 300mA for 30 minutes or 45 minutes as appropriate to the length of the gel.

2.5.3.2 Visualisation of Agarose Gels after Electrophoresis

Agarose gels of DNA samples from genotyping, colony or construct border checking PCRs were visualised under 365nm UV light using a Fusion Pulse 6 Imaging System (Vilber Lourmat). Agarose gels of other DNA samples were visualised under blue light at 465nm, using a VisiBlue UV Transilluminator (Prod.No. 95-0461-02, UVP) to minimise DNA damage from exposure to UV light.

2.5.3.3 Gel Extraction Techniques

During visualisation under 465nm blue light (**2.5.3.2**), bands were excised from the agarose gel and frozen at -20˚C in sterile 1.5ml Eppendorf tubes. DNA products from SNP confirmation PCR were gel extracted using Qiagen QIAquick Gel Extraction Kit (Prod.No. 28704, Qiagen) according to the manufacturer's protocol. Frozen gel slices for other DNA products were inserted into sealed 50mm sections of MEMBRA-CEL dialysis membrane (Prod.No. 44314.01, Serva) with 250µl TAE buffer, air bubbles were removed and the tubing was sealed with sterile plastic clips. The dialysis membrane section containing each gel slice was run in TAE buffer in an electrophoresis tank at 70V, 300mA for 20 minutes, the electrical contacts on the power pack were reversed and the membrane was run backwards at 70V, 300mA for a further 20 minutes. After running of the membrane, the interior of the membrane was washed with the residual TAE buffer contained in the membrane pocket to resuspend DNA adhering to the membrane wall. The DNA was then purified using a Qiagen QIAquick PCR Purification kit (Prod.No. 28104, Qiagen) according to the manufacturer's protocol, treating the residual TAE buffer as a PCR reaction product.

2.5.4 DNA Ligation and Restriction Reactions

2.5.4.1 pJET Blunting and Ligation Reactions

Gel extracted PCR products (2.5.3.3) from Q5 PCR reactions (2.5.2.3) were ligated into pJET 1.2/blunt Cloning Vector from CloneJET PCR Cloning Kit (Prod.No. K1231, ThermoFisher Scientific) according to the Manufacturer's "Sticky End Cloning Protocol" with the following adaptions:

Blunting Reaction -	5µl 2x Reaction Buffer
	3µl gel Extracted PCR Product
	1µl DNA Blunting Enzyme
Ligation Reaction -	Added to Completed Blunting Reaction Mixture
	1µl pJET 1.2/blunt Cloning Vector
	0.5µl T4 DNA Ligase

The Ligation Reaction was incubated at 22˚C for 30 minutes before being placed on ice and used directly for transformation of competent cells (**2.5.5.1**).

2.5.4.2 Ligation of Restriction Products

Restriction products were ligated in 2x Reaction Buffer from CloneJET PCR Cloning Kit using T4 DNA Ligase (Prod.No. EC0011, ThermoFisher Scientific) according to the following protocol:

Set up on Ice - 6µl 2x Reaction Buffer

5µl Total of 2 Restriction Products (**RP**)

1µl T4 DNA Ligase

5µl of each restriction product was run on an agarose gel as stated in **2.5.3.1** to determine their approximate relative concentrations. A total of 5µl of the restriction products was then added to the ligation reaction in ratio **RP**, estimating an equal concentration of DNA as determined by the gel. The reaction mixture was incubated at 22˚C for 30 minutes before being placed on ice and used directly for transformation of competent cells (**2.5.5.1**).

2.5.4.3 Digestion of Plasmid DNA with Restriction Endonucleases

All restriction digests were carried out in CutSmart Buffer (Prod.No. B7204S, New England Biolabs using one or more of the following restriction endonucleases: ClaI (Prod.No. R0197S, New England Biolabs), EcoRI-HF (Prod.No. R3101L, New England Biolabs), MluI-HF (Prod.No. R3198S, New England Biolabs), NotI-HF (Prod.No. R3189S, New England Biolabs), SmaI (Prod.No. R0141S, New England Biolabs). Digestion of plasmid DNA with restriction endonucleases was conducted according to the following protocol:

Set up on Ice - 5µl CutSmart Buffer

2µg Purified plasmid DNA (2-6µl)

1µl Restriction Enzyme(s)

Nuclease-Free water (Prod.No. R0581, ThermoFisher Scientific) was added to the reaction mixture to 50µl total volume, restriction endonucleases were added last. The reaction mixture was briefly vortexed and centrifuged before incubation at 37˚C (operating temperature of all enzymes except SmaI) for 90 minutes and heat inactivation by incubating at 65˚C for 20 minutes. Restriction products were run on a gel and gel extracted as described in **2.5.3**. Certain restriction products were subjected to 5’ dephosphorylation as described in **2.5.4.5**.

2.5.4.5 Dephosphorylation of Restriction Product 5' Ends

Specified products of restriction endonuclease digest (**2.5.4.4**) were dephosphorylated at 5' ends using Quick CIP alkaline phosphatase (Prod.No. 0508S, New England Biolabs) by addition of 1µl Quick CIP to the completed restriction digest reaction. The Reaction was briefly vortexed, centrifuged and incubated at 37˚C for 20 minutes before heat inactivation at 80˚C for 2 minutes. The dephosphorylated restriction products were then run on a gel and gel extracted as described in **2.5.3**.

2.5.5 Bacterial Transformation, Culture and Mini/Midiprep

2.5.5.1 Transformation of Competent *E.coli* Cells

Transformation of competent *E.coli* cells was carried out using 50µl aliquots of chemically competent TOP10 *E.coli* cells that were prepared as described in **2.5.5.6**. Competent cell aliquots were removed from the -80˚C freezer and 5µl vector from ligation product or mini/midiprep added. The aliquot was defrosted at room temperature, tapping the tube gently to mix the aliquot and placed on ice for 30 minutes. The competent cells were heat shocked at 42˚C for exactly 75 seconds before being placed immediately back on ice for 5 minutes. 400µl SOC media, pre-warmed to 37˚C and prepared as described in **2.7.2.2**, was added to the heat-shocked cells and mixed by inverting the tube. Transformed cells in SOC media were incubated at 37˚C, shaking 180rpm for 60 minutes, plated on appropriate LB selective plates (**2.7.2.3**) and incubated at 37˚C overnight.

2.5.5.2 Liquid Culture of Transformed *E.coli* Cells

For miniprep, single *E.coli* transformant colonies were selected from overnight culture plates (**2.5.5.1**), the tip was ejected into a 50ml Falcon tube containing 5ml of the appropriate selective LB liquid media (**2.7.2.3**) and the culture was incubated overnight at 37˚C, 180rpm shaking. For plasmid midiprep, single *E.coli* transformant colonies were selected from overnight plates, the tip was ejected into a 50ml Falcon tube containing 3ml of the appropriate selective LB liquid media and this starter culture was incubated at 37˚C, 180rpm shaking for 2 hours. After the 2 hours incubation, 1ml culture medium was pipetted off into a 500ml Erlenmeyer flask containing 100ml of pre-warmed selective LB liquid media, which was cultured overnight at 37˚C, 180rpm shaking to an OD_{600} of 2-3. For midiprep cultures of *E.coli* cells transformed with vectors containing RBOHD gene constructs, 2 ml of starter culture was pipetted off into a 2l Erlenmeyer flask containing 300ml of pre-warmed selective LB liquid media and cultured at 37˚C, 180rpm shaking for 16 hours to an OD_{600} of 1.8-2.0.

2.5.5.3 Plasmid Miniprep

Plasmid minipreps were conducted with 5ml overnight *E.coli* cultures, as described in **2.5.5.2**, using Qiagen QIAprep Spin Miniprep Kit (Prod.No. 27104, Qiagen) according to the manufacturers protocol with an adjusted DNA elution step: Elution buffer EB was pre-heated to 55˚C before being applied to the column and left for 2 minutes before centrifuging at 16000rcf, 1 minute. The column was then centrifuged again at 16000rcf, 1 minute to obtain residual elution buffer and improve yield. Plasmid samples were stored at -20˚C.

2.5.5.4 Plasmid Midiprep

Plasmid midipreps were conducted with 100ml overnight *E.coli* cultures, as described in **2.5.5.2**, using Qiagen Plasmid Midi Kit (Prod.No. 12143, Qiagen) according to the manufacturer's protocol. Buffer EB (Prod.No. 19086, Qiagen) was preheated to 55˚C and 300µl was used to elute plasmid from QIAtips (Prod.No. 10043, Qiagen).

2.5.5.5 Preparation of Competent TOP10 *E.coli* Cell Aliquots

Competent *E.coli* aliquots were prepared according to an adapted version of the protocol by Michael Koelle, Yale School of Medicine: a 50µl TOP10 competent *E.coli* aliquot was allowed to defrost at room temperature and subjected to a 15x dilution in SOC media pre-warmed to 37˚C. The diluted aliquot was cultured for 30 minutes at 37˚C, 180rpm shaking before being plated on a Y-media agar plate (**2.7.3.1**), which were cultured overnight. A single colony from the overnight plate was selected and used to inoculate 5ml Y-liquid media (**2.7.3.1**) in a 50ml Falcon Tube, which was cultured at 37˚C, 180rpm shaking for 2 hours to an OD_{600} of 0.35. 1ml of this starter culture was used to inoculate 300ml Y-liquid media, pre-warmed in a 2l Erlenmeyer flask, which was cultured for 2-3 hours at 37˚C, 180rpm shaking to an OD_{600} of 0.5. The 300ml culture was divided into six 50ml Falcon tubes, which were chilled on ice for 10 minutes before being centrifuged at 6000rcf, 10 minutes, 4˚C. The supernatant was carefully poured off and residual supernatant removed by pipetting. Cell pellets were each resuspended in 20ml chilled TfbI buffer (**2.7.2.1**) and re-distributed into 4 x 30ml suspensions in 50ml Falcon tubes, which were kept on ice for 5 minutes and centrifuged at 6000rcf, 5 minutes, 4˚C. Supernatent was poured off and residual supernatant removed by pipetting. Cell pellets were each resuspended in 3ml chilled TfbII buffer (**2.7.2.2**) and left on ice for 15 minutes, before being pipetted into sterile 1.5ml Eppendorfs as 50µl aliquots which were flash frozen in liquid nitrogen and stored at -80˚C. All work was done under sterile conditions and all tubes, tips, solutions and Falcon tubes were pre-chilled to 4˚C.

2.5.6 Site Directed Mutagenesis

Site directed mutagenesis was carried out using Q5 Site-Directed Mutagenesis Kit (Prod.No. E05545, New England Biolabs) on a pJET 1.2 vector containing the CDS sequence of DRP1E to induce a C929T point mutation. Site directed mutagenesis was conducted according to the manufacturer's protocol using Q5 Hot Start High-Fidelity Master Mix (2x) and the PCR programme used was as follows:

Initial Denaturation	98˚C, 30s;
25 Cycles	{Denaturation 98˚C, 10s;
	Annealing 60˚C, 30s;
	Extension 72˚C, 3 minutes 30s};
Final Extension	72˚C, 5 minutes;
Product Hold	4˚C, Continuous.

2.5.7 Creation and Transformation of *Arabidopsis* Protoplasts

Arabidopsis protoplasts were created and transformed according to an adapted version of the protocol by Isner et al, 2018. The protocol was as follows: 2 fully expanded leaves from 4-5 week old plants were placed in a 50mm shallow petri dish and rinsed well with ro-dH_2O, water was poured off and 5ml plasmolysis buffer added. Leaves submerged in the plasmolysis buffer ad cut into thin uniform slices using a sterile scalpel and forceps, before gentle shaking to ensure coating in plasmolysis buffer. Plasmolysis buffer was poured off and 5ml Enzyme buffer added, leaf slices in enzyme buffer were incubated at 28˚C in the dark for 90 minutes. A 40µm mesh was wetted with plasmolysis buffer, leaf slices in enzyme buffer were swilled gently to dislodge protoplasts and buffer was poured into a 50ml Falcon tube through the wetted 40µm mesh. 5ml plasmolysis buffer was added to the leaf slices, which were again swilled and the buffer poured into the same Falcon tube through the 40µm mesh. The Falcon tube was centrifuged in an Allegra X-30R centrifuge (Prod.No. B06323, Beckman Coulter) at 4˚C, 3 minutes, 48rcf, accel/decel 4, the supernatant was carefully pipetted off and protoplasts were resuspended in 3ml W5 Buffer. Protoplasts in W5 were incubated at 4˚C in the dark for 45 minutes, during which time PEG-CMS solution was made up fresh. Protoplast density in W5 suspension was assessed by counting in a Fuchs-Rosendahl chamber. Protoplasts in W5 were centrifuged at 4˚C, 3 minutes, 48rcf, accel/decel 4, the supernatant was carefully pipetted off and MaMg Buffer added (1-2ml) to a protoplast density of ≈$1x10^6 ml^{-1}$. Protoplasts were re-suspended in MaMg and divided into 100µl aliquots, 3µg desired vector(s) was added to each protoplast aliquot and mixed by gentle tapping. A volume of freshly prepared PEG-

CMS, equal to 100µl + volume of vector solution added, was added to the protoplasts in MaMg and mixed by careful tapping, protoplasts were incubated at 28˚C for 25 minutes in the dark. Protoplasts tubes were transferred to room temperature and protoplast incubation media (PIM) added to each tube in increasing increments of 100µl, 200µl, 400µl, 800µl, 1ml, 2ml, 2ml mixing by gentle tapping after each addition and a single gentle inversion of the tube after the final addition of PIM. Transformed protoplasts were incubated at 28˚C in the dark for 16 hours, during which time protoplasts settled in the bottom of the Falcon. All but ≈500µl supernatant was carefully removed by pipetting, protoplasts were resuspended in remaining supernatant and immediately visualised by confocal microscopy (**2.4.3**) in 250µl aliquots.

2.5.8 Sanger Sequencing of Q5 High Fidelity Polymerase PCR Products

PCR products of certain PCR reactions with Q5 High-Fidelity 2X Master Mix (Prod.No. M0492S, New England Biolabs Inc.) were subjected to sanger sequencing using the Eurofins Mix2seq service (Mix2Seq Kit, Eurofins Genomics) according to the manufacturer's protocol. Analysis of the resultant ab1 trace files was conducted using Accelrys Gene (v2.5) sequence confirmation tool using wild type sequences obtained from TAIR (**TAIR (The Arabidopsis Information Resource)**, **2018**), SnapGene (**SnapGene**, **2017**) or modified pART7/pART27 (**Gleave**, **1992**) sequences obtained from Dr Jean-Charles Isner.

2.6 Preparation of Buffers and Media

2.6.1 Preparation of 0.1M MES pH5.6, MES pH6.15 and KCl – MES pH 6.15 Buffers for Epidermal Strip Experiments

0.1M MES pH 5.6 (KOH) buffer was prepared through addition of 0.976g MED to a 50ml Falcon tube, 45ml of MiliQ water was added, the pH measured and adjusted to pH 5.6 with 2M KOH. The total volume was made up to 50ml with MiliQ water.

MES 6.15 (KOH) buffer was prepared through addition of 800ml of MiliQ water to 1.952g MES, which was fully dissolved with stirring. The pH was measured and adjusted to pH 6.15 with 2M KOH and the final volume made up to 1l with MiliQ water.

KCl – MES pH 6.15 buffer was prepared as above with the addition of 3.728g KCl prior to addition of 800ml MiliQ water. Both MES pH 6.15 and KCl – MES pH 6.15 buffers were stored at room temperature.

2.6.2 Buffers for Preparation of Competent *E.coli* Cells

2.6.2.1 Preparation of Buffer TfbI

TfbI buffer was prepared as described in the protocol by Michael Koelle, Yale: MOPS (0.2g), Calcium Chloride Dihydrate (1.1g), Rubidium Chloride (0.12g) and Glycerol (15ml) were added to a 100ml volumetric flask and the total volume made up to ≈80ml. The pH was measured and adjusted to pH 6.5 with 1M KOH. The total volume was made up to 100ml with MiliQ water and the solution was filter sterilised and stored at 4˚C.

2.6.2.2 Preparation of Buffer TfbII

TfbII buffer was prepared as described in the protocol by Michael Koelle, Yale: Potassium Acetate (1.5g), Rubidium Chloride (6g), Calcium Chloride Dihydrate (0.74g), Manganese Chloride Tetrahydrate (4.95g) and Glycerol (75ml) were added to a 500ml volumetric flask and the total volume made up to ≈450ml.

2.6.3 Preparation of Buffers and Solutions for *Arabidopsis* Protoplasts

2.6.3.1 Preparation of Plasmolysis Buffer

Mannitol (6.83g), Calcium Chloride (50µl of 1M stock solution) and 0.1M MES pH 5.6 buffer (2.5ml of 0.1M stock) were added to a 50ml Falcon tube and the total volume made up to 50ml with MiliQ water. The solution was stored at 4˚C.

2.6.3.2 Preparation of Enzyme Buffer

Cellulase Onozuka R-10 (Prod.No. 16419, Serva) (0.375g), Macerozyme R-10 (Prod.No. 28302, Serva) (0.125g) MiliQ water (5ml), Mannitol (15ml of 1M stock solution and 0.1M MES pH 5.6 (2.5ml of 0.1M stock solution) were added to a 50ml Falcon tube, mixed well and incubated at 55˚C for 10 minutes. The solution was cooled to room temperature and Calcium Chloride (25µl of 1M stock solution), Bovine Serum Albumin (2.5ml of 10mg ml^{-1} stock solution) and Ampicillin (25µl of 100mg ml^{-1} stock solution) were added. The solution was mixed well and divided into 5ml aliquots, which were stored at -20˚C and defrosted at 4˚C overnight before use.

2.6.3.3 Preparation of W5 Buffer

MiliQ water (40.5ml), Calcium Chloride (6.25ml of 1M stock solution), Sodium Chloride (1.54ml of 5M stock solution), 0.1M MES pH 5.6 (1ml of 0.1M stock solution) and Potassium Chloride (0.25ml of 1M stock solution) were added to a 50ml Falcon tube, mixed well and stored at 4˚C.

2.6.3.4 Preparation of MaMg Buffer

Mannitol (5.465g), Magnesium Chloride (1.5ml of 0.5M stock) and 0.1M MES pH 5.6 (2ml of 0.1M stock solution) were added to a 50ml Falcon tube and MiliQ water added to a total volume of 50ml. The solution was stored at 4˚C.

2.6.3.5 Preparation of PEG-CMS Solution

Calcium Nitrate Tetrahydrate (0.236g) was added to a 15ml Falcon tube and the total volume made up to 1ml with MiliQ water to form a 1M Calcium Nitrate Solution. Poly-Ethylene Glycol (1g), MiliQ water (0.375ml), Mannitol (1ml of 1M stock solution) and Calcium Nitrate (0.25ml of 1M stock solution) were added to a 15ml Falcon tube and vortexed thoroughly until the PEG was completely dissolved. Both the 1M Calcium Nitrate solution and PEG-CMS solution were made up fresh for each transformation and used immediately.

2.6.3.6 Preparation of Protoplast Incubation Medium

Mannitol (55g), 0.1M MES pH5.6 (20ml of 0.1M stock solution), Potassium Chloride (2ml of 1M stock solution) and Calcium Chloride (1.5ml of 1M stock) were added to a 500ml volumetric flask. MiliQ water was added to ≈450ml, Ampicillin (500µl of 100mg ml^{-1} stock solution) was added and the solution was made up to 500ml with MiliQ water. The solution was aliquoted into 10 x 50ml Falcon tubes, filter sterilised and stored at -20˚C. Aliquots were defrosted at 4˚C overnight before use.

2.6.4 Bacterial Growth Media

2.6.4.1 Preparation of Y Media

Tris Base (3.029g) was added to a 50ml Falcon tube MiliQ water added to ≈20ml, the pH was measured and adjusted to pH 8.0 with 1M HCl. MiliQ water was added to a total volume of 25ml to give a 1M Tris-HCl stock solution (pH 8)

Y liquid media and Y agar plates were prepared according to the protocol of Michael Koelle, Yale university. Tryptone (10g), Magnesium Sulphate Heptahydrate (2.5g) and Tris-HCl (10ml of 1M stock) were added to a 500ml volumetric flask and MiliQ water added to ≈450ml. The pH was measured and adjusted to pH 7.6 with 0.1M HCl and MiliQ water was added to a total volume of 500ml. For Y agar, agar (7g $500ml^{-1}$) was included prior to addition of MiliQ water. Media was transferred to the desired vessels and autoclaved before use. Media for Y agar plates was cooled to 60˚C and poured under sterile conditions. Plates and media were stored at 4˚C under sterile conditions and were heated to 37˚C immediately prior to use.

2.6.4.2 Preparation of SOC Media

Tryptone (2g), Yeast Extract (0.5g), Sodium Chloride (1ml of 1M stock solution) and Potassium Chloride (250µl of 1M stock solution) were added to 80ml of MiliQ water and autoclaved. Magnesium Chloride (1ml of 1M stock solution) and Glucose (2ml of 1M solution), both filter sterilised, were added and autoclaved MiliQ water was added to a total volume of 100ml. The solution was divided into 800µl aliquots which were flash frozen in liquid nitrogen and stored at -20˚C. Sterile conditions were maintained throughout after autoclaving.

2.6.4.3 Preparation of LB Media and LB Selective Media

Tryptone (10g), Yeast Extract (5g) and Sodium Chloride (10g) were added to 800ml MiliQ water, the pH was measured and adjusted to pH 7 with 0.1M NaOH, MiliQ water added to a total volume of 1l and the solution was autoclaved. For LB Agar plates, Agar (14g l^{-1}) was included prior to addition of MiliQ water, autoclaved LB Agar was cooled to 60˚C and plates were poured under sterile conditions. Plates and media were stored at 4˚C under sterile conditions and were heated to 37˚C immediately prior to use. For selective media or plates, media was cooled to 60˚C after autoclaving and Ampicillin (from filter sterilised 100mg ml^{-1} stock solution) or Kanamycin (from filter sterilised 50mg ml^{-1} stock solution) was added to a concentration of 100µg ml^{-1} (Ampicillin) or 50mg ml^{-1} (Kanamycin).

Chapter 3 – Characterisation of the Stomatal Phenotypes of the Novel EO_2 Mutation.

3.1 Detail of EO_2 mutant background

The EO_2 mutant was identified by infrared thermography of an Ethyl Methanesulphonate (EMS) mutant population of *Arabidopsis thaliana* as part of a large scale genetic screen to identify guard cell carbon dioxide signalling mutants (**Merlot *et al.*, 2002**; **Wang *et al.*, 2004**; **Tagliavia, 2006**) . The screen was conducted under 1500ppm CO_2, with identification of CO_2 inhibited & CO_2 hypersensitive mutants relying on difference in leaf temperature compared to wild type Columbia-0 (Col-0) (**Merlot *et al.*, 2002**; **Tagliavia, 2006**). Higher or lower leaf temperatures are an indication of comparatively reduced or increased transpiration rates as a proxy of stomatal aperture and hence guard cell responsiveness to CO_2. The EO_2 mutant was found to have a lower leaf temperature than the Col-0 under elevated atmospheric [CO_2] which is indicative of inhibited stomatal closure in response to elevated atmospheric CO_2 (**Fig. 3.A**) (**Tagliavia, 2006**; **Peng, 2008**).

3.1.1 Elevated [CO_2] Infrared Thermography

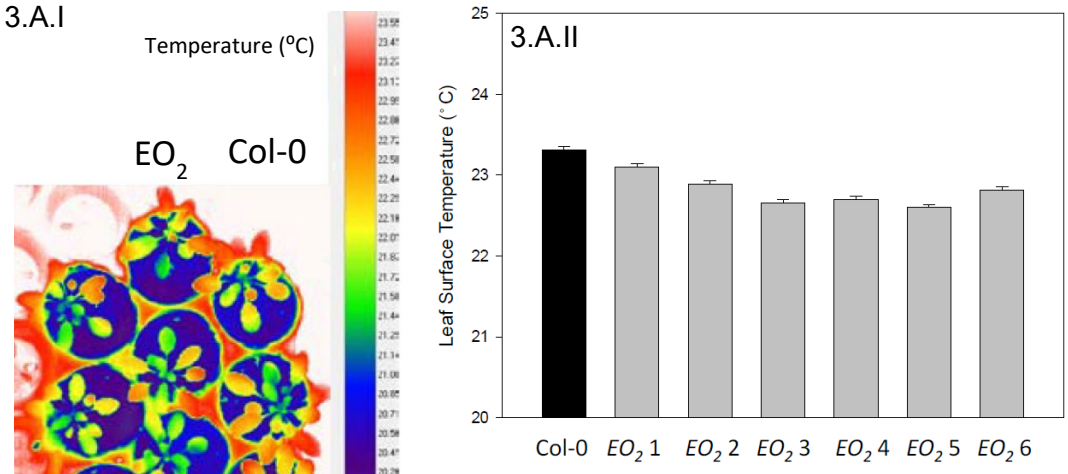

Figure 3.A.I) Colourised infrared image of the EO_2 mutant and Col-0 under 1700ppm CO_2. **3.A.II)** All six EO_2 mutant plants display decreased average leaf temperature compared to the Col-0 average under 1700ppm atmospheric CO_2. Adapted from (**Peng, 2008**).

Adapted from PhD thesis of Dr Kai Peng

3.2 Established mutant phenotype

Preliminary work from Dr Kai Peng and Dr Yun-Kuan Liang (**Peng, 2008**) identified the EO_2 mutant as having partially disrupted stomatal closure in response to elevated [CO_2] and wild type stomatal responses to ABA and external Ca^{2+}. The EO_2 mutant was found to have stomatal index and density

comparable to WT under ambient [CO_2], however stomatal density was significantly reduced compared to WT under elevated [CO_2] despite similar having stomatal index. Root elongation rate was found to be significantly increased compared to wild type (**Peng**, **2008**).

3.3 Isolation of Mutant Line, Sequencing, Gene Confirmation and Confirmation of Phenotype

3.3.1 Isolation and Sequencing

Selected EO_2 mutants were backcrossed twice to the Col-0, using the EO_2 mutant as the female and male in separate crosses to check for maternal inheritance. No maternal effects were observed (**Tagliavia**, **2006**). F2 seed was then sown on vertical plates and mutants were selected by root length assay and elevated CO_2 infra-red thermography. Mutants segregated in a 3:1 ratio which is indicative of a recessive mutation, thereby indicating that selected F2 mutants were homozygous. A mapping population was created by crossing of homozygous EO_2 mutants into *Landsberg erecta* (Ler-0) and mapping of SSLP markers was conducted according to the procedure of **Lukowitz *et al.*** (**2000**). Results indicated that the EO_2 mutation was located at approximately 13.24cM on chromosome 3 (**Peng**, **2008**). The EO_2 x Ler mapping population was subjected to next generation sequencing, from which a G->A single nucleotide polymorphism (SNP) at position 22245735 on chromosome 3 was identified as the likely cause of the EO_2 carbon dioxide insensitive stomatal closure phenotype. This equated to a C929T mutation in the DRP1E coding sequence (CDS), resulting in an S310F substitution in DRP1E. Searches of the NCBI Conserved Domain Database (**Marchler-Bauer *et al.***, **2017**; **NCBI (National Centre for Biotechnology Information)**, **2017**) indicated that the S310F amino acid substitution lies in the N terminal half of the, highly conserved, Dynamin 'Middle' domain, which is involved in dimerization, dimer-dimerization and GTP-dependent oligomerisation of assembled tetramers (**Smirnova *et al.***, **1999**; **Ramachandran *et al.***, **2007**; **Reubold *et al.***, **2015**). The presence of the homozygous SNP in the EO_2 mutant was confirmed by PCR of the target region (**2.5.2.3**), the PCR products of which were subjected to Sanger sequencing (**2.5.8**) with subsequent sequence analysis (**2.5.8**). Sixteen individual EO_2 mutants were subjected to PCR and Sanger sequencing for SNP confirmation, with 16 Col-0 control specimens sequenced in tandem. All EO_2 mutants were found to be homozygous for the C929T SNP in *DRP1E*, whilst all Col-0 specimens were found to be homozygous wild type at the same locus.

3.3.2 Confirmation of Established Mutant Phenotype

3.3.2.1 The EO_2 Mutant is Inhibited in Elevated [CO_2] Induced Stomatal Closure

To confirm the EO_2 mutant phenotype of being inhibited in CO_2 induced stomatal closure, the back-crossed EO_2 mutant line was subjected to stomatal bioassay under elevated atmospheric CO_2 as described in **2.2.2.3**. After 2 hours exposure to air containing 1500pm CO_2, the EO_2 mutant was

found to have no significant reduction in stomatal aperture, whilst the wild-type Col-0 was found to significantly reduce in aperture (**Fig.3.B**). This demonstrates that the observed carbon dioxide insensitive phenotype of EO_2, established through infra-red thermography, is supported by EO_2 stomatal movements and is present in the backcrossed EO_2 mutant line.

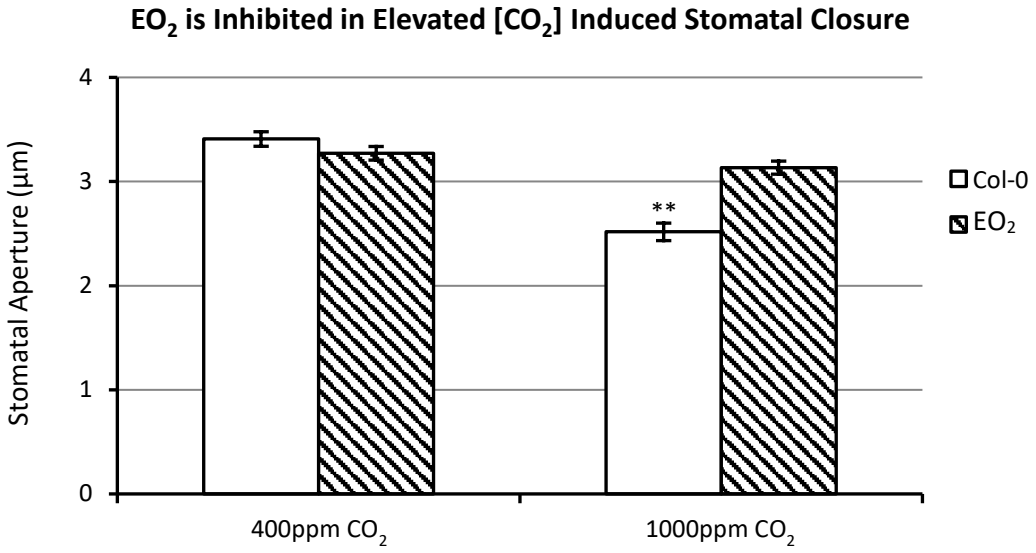

Figure 3.B) EO_2 stomatal aperture fails to significantly reduce in response to treatment with high atmospheric [CO_2] (1000ppm), whilst the stomatal aperture of Col-0 reduced significantly ($p<0.01$). Data values shown are mean values ± SE (n=90 from 9 biological replicates) from 3 independent experiments carried out on consecutive days. Two-tailed t-test. 10hr day, 120 µmol m-2s-1 PPFD; 70% RH, 380-400ppm CO2, 22^{o}C day/20^{o}C night.

3.3.2.2 EO_2 Exhibits a Wild Type Dose Response to Increased [ABA]

The EO_2 mutant was subjected to stomatal bioassay using 4 concentrations of Abscisic acid to determine the dose-dependent response to external ABA as described in **2.2.2.1**). The stomatal aperture of EO_2 was not found to differ significantly from that of the Col-0 control at any one ABA concentration (**Fig.3.C**). However, the stomatal aperture at each ABA concentration, for both EO_2 and Col-0, was found to be significant compared to every other ABA concentration (**Fig.3.C**). Carbon dioxide specific signalling pathways are thought to converge with abscisic acid mediated signalling pathways at OST1 (**Webb and Hetherington**, **1997**; **Leymarie, Lascève, *et al.***, **1998**; **Leymarie, Vavasseur, *et al.***, **1998**; **Hashimoto *et al.***, **2006**) via the inhibition of OST1 by HT1 (**Hashimoto *et al.***, **2006**). The confirmed EO_2 stomatal phenotype of an inhibited closure response to elevated [CO_2] and WT closure response to ABA therefore indicates that the EO_2 mutation acts in a CO_2 specific signalling or sensory pathway up-stream of convergence with ABA closure pathways.

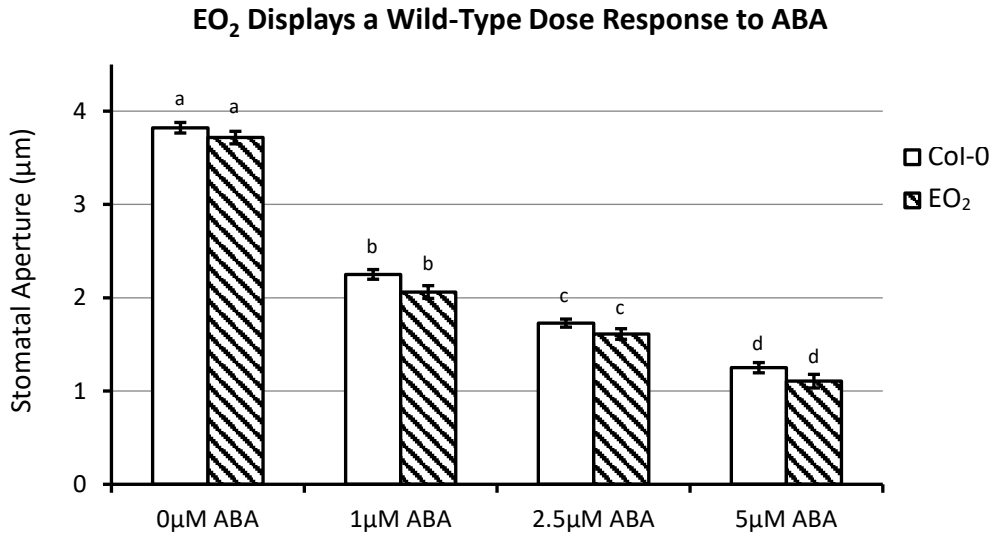

Figure 3.C) The stomatal aperture of EO_2 and Col-0 does not significantly differ at any specific ABA concentration, however the stomatal aperture of both EO_2 and Col-0 at each ABA concentration does differ significantly from the stomatal aperture of both EO_2 and Col-0 at every other ABA concentration ($p<0.01$). Data values shown are mean values ± SE (n=90 from 9 biological replicates) from 3 independent experiments carried out on consecutive days. Two-tailed t-test (between treatments), 2-way ANOVA (between lines, multiple treatments). 10hr day, 120 µmol m-2s-1 PPFD; 70% RH, 380-400ppm CO2, 22^{o}C day/20^{o}C night.

3.3.3 Confirmation that the EO_2 Mutation is Allelic to *DRP1E*

As the EO_2 mutation was found to be recessive (**3.3.1**), to determine whether the EO_2 mutation is allelic to *DRP1E* the EO_2 homozygous line was crossed (**2.1.3**) in to two separate T-DNA knockout *drp1e* lines: SALK_206052C (SK206) and GABI-KAT_168C11.08 (GK08) (homozygous line isolated from segregating T-DNA set). The EO_2 mutant and the F1 of the EO_2 → *drp1e* crosses were subjected to elevated [CO_2] induced stomatal closure bioassay (**2.2.2.3**) to assess whether the CO_2 insensitive phenotype was conserved. The stomatal aperture of EO_2 and the two EO_2 x *drp1e* F1 crosses, "EO_2 x GK08" and "EO_2 x SK206", failed to reduce in response to treatment with elevated [CO_2], whilst the Col-0 aperture was found to reduce significantly (**Fig.3.D**). The conservation of the EO_2 carbon dioxide insensitive phenotype in the F1 EO_2 x *drp1e* crosses, despite the recessive nature of the EO_2 mutation, indicates that the EO_2 mutation is allelic to *DRP1E* and that the SNP C929T in *DRP1E* is responsible for the aberrant stomatal phenotype.

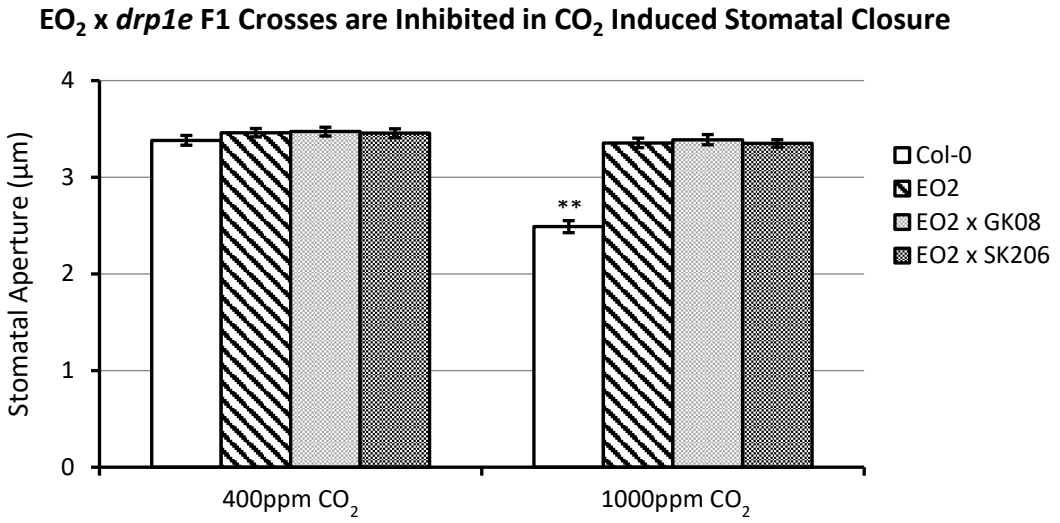

Figure 3.D) The stomatal aperture of EO_2 and EO_2 x *drp1e* crosses does not significantly reduce in response to treatment with elevated [CO_2] (1000ppm CO_2), whereas the stomatal aperture of Col-0 decreased significantly ($p<0.01$) in response to the same treatment. There is no significant difference between the stomatal aperture of EO_2, EO_2 x GK08 and EO_2 x SK206 under either ambient (400ppm CO_2) or after treatment with elevated [CO_2]. The EO_2 x *drp1e* crosses, EO_2 x GK08 and EO_2 x SK206, conserve the EO_2 carbon dioxide insensitive phenotype, thereby indicating that EO_2 and the mutation responsible for this phenotype is allelic to *DRP1E*. Data values shown are mean values ± SE (n=90 from 9 biological replicates) from 3 independent experiments carried out on consecutive days. Two-tailed t-test (between treatments), 2-way ANOVA (between lines, multiple treatments). 10hr day, 120 µmol m-2s-1 PPFD; 70% RH, 380-400ppm CO2, 22^{o}C day/20^{o}C night.

3.4 Characterisation of EO_2 Stomatal Phenotype Using T-DNA Knockout *drp1e* Lines

3.4.1 EO_2 and *drp1e* Lines Exhibit Wildtype Responses to ABA

To confirm that the *drp1e* T-DNA knockout lines, SALK_206052C (SK206) and GABI-KAT_168C11.08 (GK08), display the same wildtype response to ABA that was established for the EO_2 mutant in **3.3.2.2** (**Fig.3.C**), EO_2 and the two *drp1e* lines were subjected to ABA stomatal closure bioassay as described in **2.2.2.1**. Due to the number of lines involved, it was not possible to conduct an ABA bioassay with full dose responses as described in **3.3.2.2**, instead 5µM ABA was selected as an appropriate concentration for treatment based on the data obtained in **3.3.2.2**. The stomatal aperture of all lines was found to significantly reduce in response to treatment with 5µM ABA (**Fig.3.E**), indicating that the wildtype response of EO_2 to ABA is also present in the *drp1e* T-DNA knockout lines SK206 and GK08.

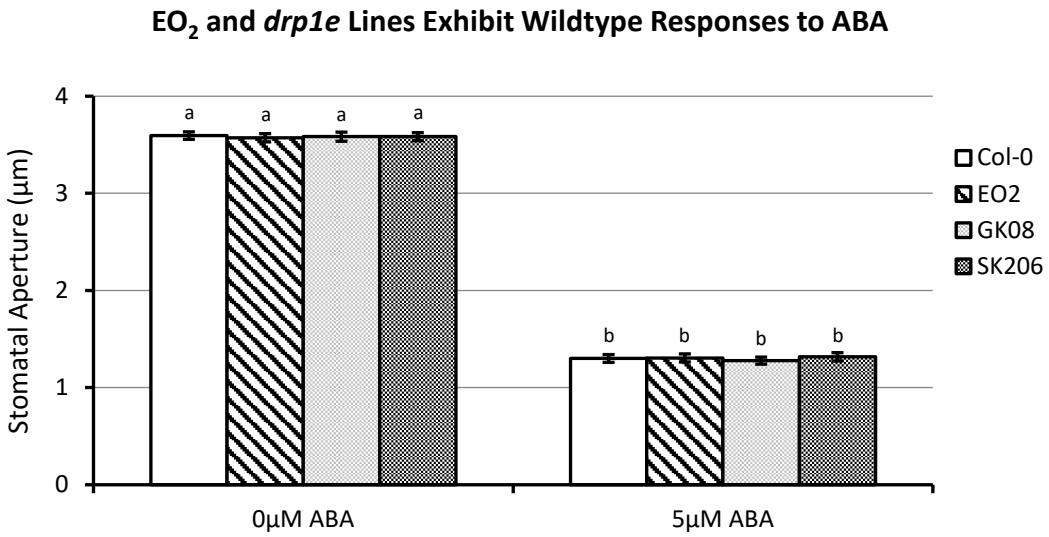

Figure 3.E) Results of ABA induced stomatal closure bioassay with EO_2 and the *drp1e* T-DNA knockout lines GABI-KAT_168C11.08 (GK08) and SALK_206052C (SK206). The stomatal aperture of all lines was found to significantly reduce in response to treatment with 5µM ABA ($p<0.01$). There was no significant difference in stomatal aperture between any of the lines at either 0µM ABA or 5µM ABA. This indicates that the EO_2 wildtype response to ABA is replicated in *drp1e* lines. Data values shown are mean values ± SE (n=90 from 9 biological replicates) from 3 independent experiments carried out on consecutive days. Two-tailed t-test (between treatments), 2-way ANOVA (between lines, multiple treatments). 10hr day, 120 µmol m-2s-1 PPFD; 70% RH, 380-400ppm CO2, 22^{o}C day/20^{o}C night.

3.4.2 EO_2 and *drp1e* T-DNA Knockout Lines are Inhibited in CO_2 Induced Stomatal Closure

The results of **3.3.3** indicated that *drp1e* lines should display a carbon dioxide insensitive stomatal phenotype. To confirm this putative phenotype, the *drp1e*T-DNA knockout lines SALK_206052C (SK206) and GABI-KAT_168C11.08 (GK08) were subjected, with EO_2, to stomatal bioassay under elevated atmospheric [CO_2] as described in **2.2.2.3**. The stomatal aperture of Col-0 was found to significantly decrease in response to treatment with elevated (1000ppm) CO_2 ($p<0.001$), however there was also a small but significant decrease in the stomatal aperture of EO_2, GK08 and SK206 in response to the same treatment (**Fig.3.F.I**). Despite the significant ($p<0.05$) reduction in stomatal aperture of EO_2, GK08 and SK206 after treatment with elevated [CO_2], the difference in stomatal aperture was much less for EO_2, GK08 and SK206 (**Fig.3.F.II**) and these lines were found to respond significantly less ($p<0.001$) than that of Col-0 after treatment with 1000ppm CO_2 (**Fig.3.F.I**). The significant decrease in stomatal aperture of EO_2, GK08 and SK206 may be partially attributed to very

low variance values of these lines (mean variance =0.16), which are reflected in the size of the error bars (**Fig.3.F.I**).

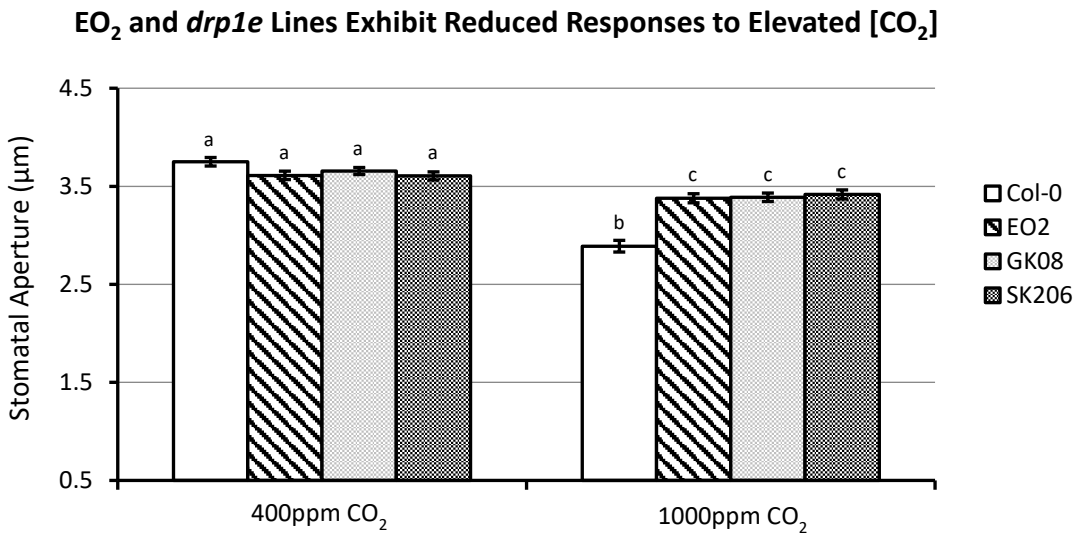

Figure 3.F.I) Results of elevated [CO_2] induced stomatal closure bioassay of EO_2 and the *drp1e* lines GABI-KAT_168C11.08 and SALK_206052C. Col-0 displayed a significantly reduced stomatal aperture in response to elevated [CO_2] ($p<0.001$), however EO_2, GK08 and SK206 also displayed significantly reduced stomatal aperture after treatment with elevated [CO_2] ($p<0.05$). Despite their significant reduction of stomatal aperture in response to treatment with 1000ppm [CO_2], EO_2, GK08 and SK206 exhibited significantly lower ($p<0.001$) reduction in stomatal aperture compared to the Col-0. Data values shown are mean values ± SE (n=90 from 9 biological replicates) from 3 independent experiments carried out on consecutive days. Two-tailed t-test (between treatments), 2-way ANOVA (between lines, multiple treatments). 10hr day, 120 µmol m-2s-1 PPFD; 70% RH, 380-400ppm CO2, 22^{o}C day/20^{o}C night.

	Col-0	EO_2	GABI-KAT_168C11.08	SALK_206052C
Change in Stomatal Aperture ± SE (µm)	-0.86 ± 0.07	-0.23 ± 0.06	-0.27 ± 0.06	-0.19 ± 0.06

Figure 3.F.II) Table detailing the change in stomatal aperture displayed in **Fig.3.F.I**. Values were calculated from the original data set by subtraction of stomatal aperture under 400ppm CO_2 from the stomatal aperture under 1000ppm CO_2 within each line. Standard Error (SE) for change in stomatal aperture was calculated from the standard error of stomatal aperture under 400ppm CO_2 (SE_1) and 1000ppm CO_2 (SE_2).

3.4.3 EO_2 and *drp1e* Lines Exhibit Wild-Type Responses to Apoplastic Calcium Chloride

The results of **3.4.1** and **3.4.2** demonstrate that EO_2 and the *drp1e* T-DNA mutants GABI-KAT_168C11.08 (GK08) and SALK_206052C (SK206) are inhibited in stomatal closure in response to elevated [CO_2] but respond normally in response to treatment with ABA (**Fig.3.E, Fig.3.F**). These results indicate that the EO_2 mutation does not affect ABA mediated closure pathways or ABA sensory pathways, which could be indicative of a mutation specific to carbon dioxide signalling or sensory pathways (**Kim *et al.*, 2010**). To further investigate this possibility EO_2, GK08 and SK206 were subjected to a calcium chloride induced promotion of stomatal closure bioassay, as described in **2.2.2.2**. All lines were found to reduce significantly in stomatal aperture when treated with 1µM $CaCl_2$ and when treated with 10µM $CaCl_2$ compared to treatment with 0µM $CaCl_2$. All lines also significantly reduced in stomatal aperture when treated with 10µM $CaCl_2$ compared to treatment with 1µM $CaCl_2$ (**Fig.3.G**). Within any treatment concentration there was no significant difference in stomatal aperture between lines, showing that both EO_2 and the *drp1e* lines GK08 and SK206 exhibit a completely wildtype response to calcium chloride treatment, which simulates apoplastic Ca^{2+} flux.

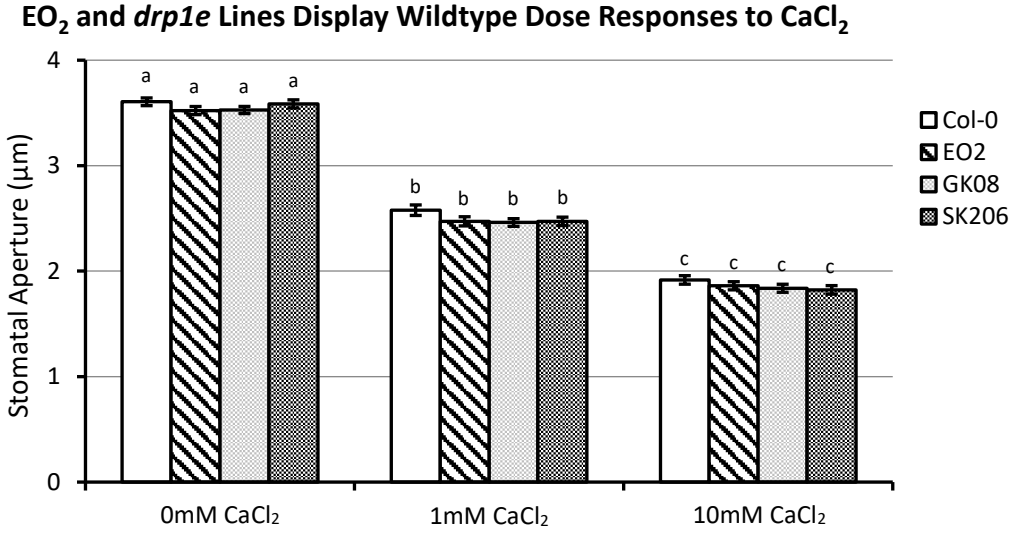

Figure 3.G) Results of calcium chloride induced promotion of stomatal closure bioassay with EO_2 and the *drp1e* T-DNA knockout lines GK08 and SK206. The stomatal apertures of EO_2, GK08 and SK206 were not found to differ significantly from the Col-0 within any treatment concentration of $CaCl_2$. All lines were found to have a significant ($p<0.01$) decrease in stomatal aperture upon treatment with either 1mM or 10mM $CaCl_2$ compared to the control treatment. The stomatal apertures of all lines were also found to decrease significantly ($p<0.01$) after treatment with 10mM $CaCl_2$ compared to treatment with 1µM $CaCl_2$. EO_2, GK08 and SK206 were all found to exhibit wildtype dose responses to treatment with $CaCl_2$. Two-tailed t-test (between treatments), 2-way ANOVA (between lines,

multiple treatments). 10hr day, 120 µmol m-2s-1 PPFD; 70% RH, 380-400ppm CO2, 22°C day/20°C night.

3.4.4 EO_2 and *drp1e* Lines a Display Wildtype Stomatal Closure Response to Darkness

Based on the current limited understanding of stomatal closure in darkness, it is likely that closure in darkness is largely dependent on ABA-dependent closure pathways, as it has been shown that mutants defective in ABA synthesis (**Pantin *et al.*, 2013**) and ABA receptors (**Merilo *et al.*, 2013**) display reduced stomatal closure in response to ABA, elevated [CO_2] and darkness (**Leymarie, Lascève, *et al.*, 1998**; **Merilo *et al.*, 2013**; **Pantin *et al.*, 2013**). Furthermore it has been shown that interrupted guard cell s-type anion channel SLAC1 activity results in greatly reduced stomatal responses to CO_2, ABA and darkness (**Negi *et al.*, 2008**; **Vahisalu *et al.*, 2008**; **Merilo *et al.*, 2013**), which may indicate common mechanisms of stomatal closure between the dark, carbon dioxide and ABA pathways. However **Costa *et al.*, 2015** identified several mutants that displayed reduced stomatal closure in response to darkness, yet also displayed wild type responses to ABA and elevated [CO_2], providing evidence for a distinct dark closure pathway. To examine the possibility of the EO_2 mutation playing a role in stomatal closure in response to darkness EO_2 and *drp1e* T-DNA knockout lines were subjected to stomatal bioassay with dark treatment as detailed in **2.2.2.4**. All lines were found to significantly reduce in stomatal aperture in response to treatment with darkness and there was no significant difference between lines within either the light or dark treatments. All lines displayed a wildtype stomatal response to treatment with darkness (**Fig.3.H**).

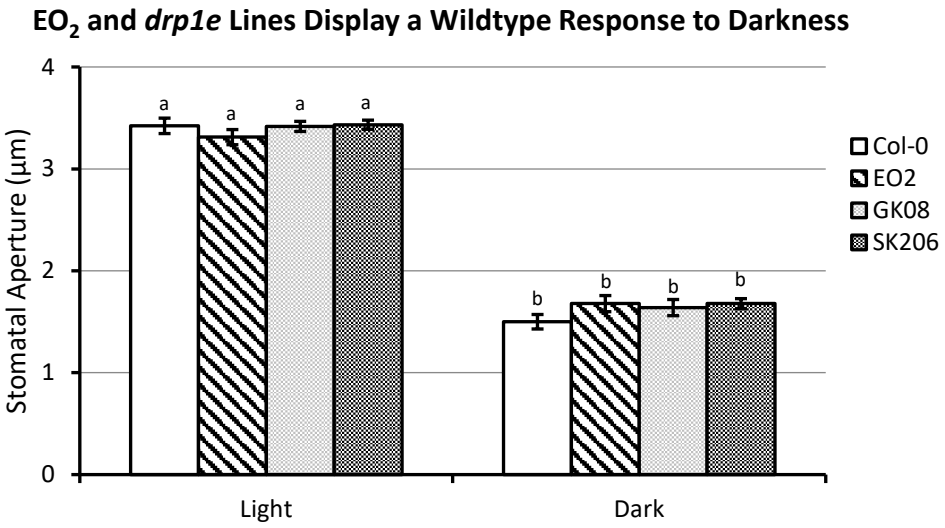

Figure 3.H) Results of dark induced promotion of closure bioassay including EO_2 and the *drp1e* lines GABI-KAT-168C11.08 (GK08) and SALK_206052C (SK206). All lines were found to significantly reduce ($p<0.001$) in stomatal aperture upon treatment with darkness. No significant difference in stomatal

aperture was found between lines within either the light treatment or dark treatment. EO_2, GK08 and SK206 all exhibited wildtype stomatal responses to dark induced promotion of closure. Two-tailed t-test (between treatments), 2-way ANOVA (between lines, multiple treatments). 10hr day, 120 µmol m-2s-1 PPFD; 70% RH, 380-400ppm CO2, 22^{o}C day/20^{o}C night.

3.5 Summary and Discussion

The EO_2 mutant was identified from an EMS population through screening by infrared thermography under elevated atmospheric [CO_2] and was found to have reduced average leaf temperature compared to Col-0 under the same conditions (**Tagliavia**, **2006**; **Peng**, **2008**). The EO_2 mutant was backcrossed to reduce the number of SNPs present, whilst conserving the leaf temperature under high [CO_2] phenotype, and bred to a homozygous line. An EO_2 mapping population was generated and the mutation tracked to approximately 13.24cM on chromosome 3 (**Peng**, **2008**). Next generation sequencing of the homozygous EO_2 population located a C929T SNP in *DRP1E* as the putative cause of the CO_2 insensitive phenotype of EO_2. Initial bioassay results indicated that the EO_2 mutant line had impaired stomatal closure responses to elevated [CO_2] but wildtype stomatal closure in response to the application of ABA. Elevated [CO_2] bioassay of 2 separate lines of F1 EO_2 x *drp1e*, in tandem with the EO_2 mutant line, showed that the [CO_2] insensitive stomatal phenotype was conserved in the F1 crosses and proved that the EO_2 mutation is allelic to *DRP1E*. Further characterisation of EO_2, using two independent T-DNA knockout lines in tandem, indicated that the EO_2 mutant and both *drp1e* mutant lines displayed wild type responses to ABA, darkness and the application of calcium chloride but were inhibited in elevated [CO_2] induced stomatal closure. These results strongly imply that *DRP1E* is involved in stomatal closure pathways specific to carbon dioxide and may be involved in the regulation of elements responsible for the perception of CO_2 or HCO_3^-. These findings make *DRP1E* and the EO_2 mutant promising subjects for further study.

Chapter 4 – Gas-Exchange and Physiological Assays

4.1 Introduction to Gas-Exchange and Physiology Experiments

The results of the previous chapter established that the EO_2 carbon dioxide insensitive stomatal phenotype was allelic to *DRP1E* and reported that both *eo₂* and *drp1e* T-DNA knockout mutants were inhibited in elevated CO_2-induced stomatal closure. It was further reported that EO_2 and *drp1e* mutants exhibited WT responses to exogenous abscisic acid, external Ca^{2+} and darkness, indicating that the *eo₂* mutation specifically affected CO_2 signalling pathways and making EO_2 a promising candidate for further research. As the EO_2 mutant had been found to be impaired in stomatal function, it seemed logical to investigate whether EO_2 was similarly inhibited in gas exchange parameters at the level of whole leaves. To this end, experiments were conducted using specialised gas exchange equipment to measure transpirational water loss and CO_2 assimilation rates and experiments conducted to calculate the water use efficiency of these mutant lines (**Mickelbart and Marler, 1998; Yoo *et al.*, 2009; 2010; Sandoval *et al.*, 2016)**. Stomatal development assays were conducted to determine the stomatal index and density of EO_2 and the *drp1e* lines, as gas exchange has been shown to be influenced by both stomatal function and number **(Casson and Hetherington, 2010)**.

In this chapter, the EO_2 mutant and the *drp1e* T-DNA knockout lines, GABI-KAT-168C11.08 (GK08) and SALK_206052C (SK206), were subjected to Infra-Red Gas Analysis (IRGA), stomatal development experiments, gravimetric transpiration assay and water use efficiency experiments in order to investigate the physiological impact of the *eo₂* mutation at a whole-plant level. The work in this chapter was carried out in collaboration with the research group of Dr Mike Mickelbart (Purdue University, USA).

4.2 Whole-Leaf Infra-Red Gas Analysis Experiments

4.2.1 Ambient to Elevated Carbon Dioxide Gas Exchange Experiments using a LiCor-x6400 Infra-Red Gas Analyser

To investigate the implications of the inhibited stomatal response of EO_2 to elevated atmospheric carbon dioxide concentrations, EO_2 and the *drp1e* T-DNA knockout lines GABI-KAT-168C11.08 (GK08) and SALK_206052C (SK206) were treated to elevated [CO_2] Infra-Red gas analysis. The experiments were conducted using a LiCor-x6400 model gas analyser, which used a whole-plant gas exchange cuvette attachment.

4.2.1.1 EO_2 and *drp1e* lines Display no Significant Reduction in Transpiration rate over an Ambient to Elevated Carbon Dioxide Transition

During Infra-Red Gas Analysis experiments, EO_2, GK08 and SK206 clearly showed no significant decrease in transpiration rate (E) in response to a transition from ambient (400ppm) to elevated (1000ppm) [CO_2]. In response to elevated [CO_2], the transpiration rate of Col-0 was found to significantly decrease, over a period of 6 minutes, to rates comparable with that of EO_2 and the *drp1e* lines. EO_2 and the *drp1e* lines display significantly lower transpiration rates under ambient [CO_2] than Col-0. These results confirm that that the inhibited stomatal response of EO_2 to elevated atmospheric [CO_2] affects whole-plant physiology and results in significant differences in whole-plant transpiration rates.

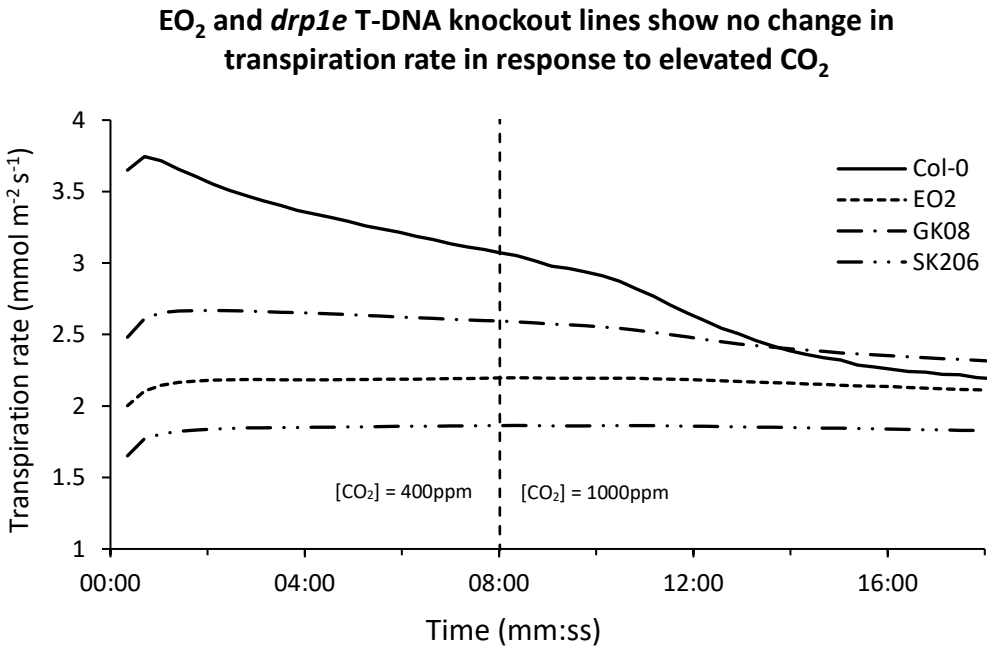

Figure 4.A) EO_2 and the *drp1e* T-DNA knockout lines GK08 and SK206 show no significant reduction in transpiration rate in response to a transition to elevated [CO_2]. Col-0 exhibited a significant reduction in transpiration rate in response to the transition to elevated [CO_2] over a period of 6 minutes. EO_2 and the *drp1e* lines exhibited significantly lower transpiration rates compared to the Col-0 under ambient [CO_2]. [CO_2] = 400ppm until 08:01, at which point [CO_2] increases to 1000ppm over one minute and [CO_2] is then maintained at 1000ppm for a further 9 minutes. For clarity, error bars are not included on plot. N=8 for all lines except N=7 for Col-0. 10hr day, 110-120 µmol m-2s-1 PPFD; 70% RH, 380-400ppm CO2, 22^{o}C day/20^{o}C night.

4.2.1.2 EO_2 and *drp1e* lines Display Substantially Increased Net CO_2 Assimilation rates Compared to Col-0 under both Ambient and Elevated CO_2 as Determined by Li-Cor x6400 IRGA Experiments.

EO_2 and the *drp1e* lines were similarly subjected to measurement of Carbon Assimilation rate (A) over an ambient (400ppm) to elevated (1000ppm) CO_2 transition. The carbon assimilation rate of all lines, including Col-0, was found to significantly increase in response to the transition to elevated [CO_2]. However, the carbon assimilation rate of Col-0 was found to increase by 101.9% ± 1.6 over the transition compared to increases of 55.1% ± 0.3, 57.6% ± 0.4 & 54.5% ± 0.04 for EO_2, GK08 and SK206 respectively. The carbon assimilation rate of EO_2 and both *drp1e* lines was found to be significantly higher than that of Col-0 under both ambient and elevated CO_2, despite the substantially greater increase in assimilation rate of Col-0 in response to the transition to elevated [CO_2].

Combined with the results of **4.2.1.1**, these results indicate that the EO_2 inhibited stomatal response to elevated [CO_2] similarly affects whole plant transpiration rates. Furthermore, EO_2 and *drp1e* lines exhibit significantly lower transpiration rates under ambient CO_2 and significantly increased carbon assimilation rates under both ambient and elevated CO_2 compared to the Col-0. These results indicate that EO_2 may have substantially improved water use efficiency compared to Col-0.

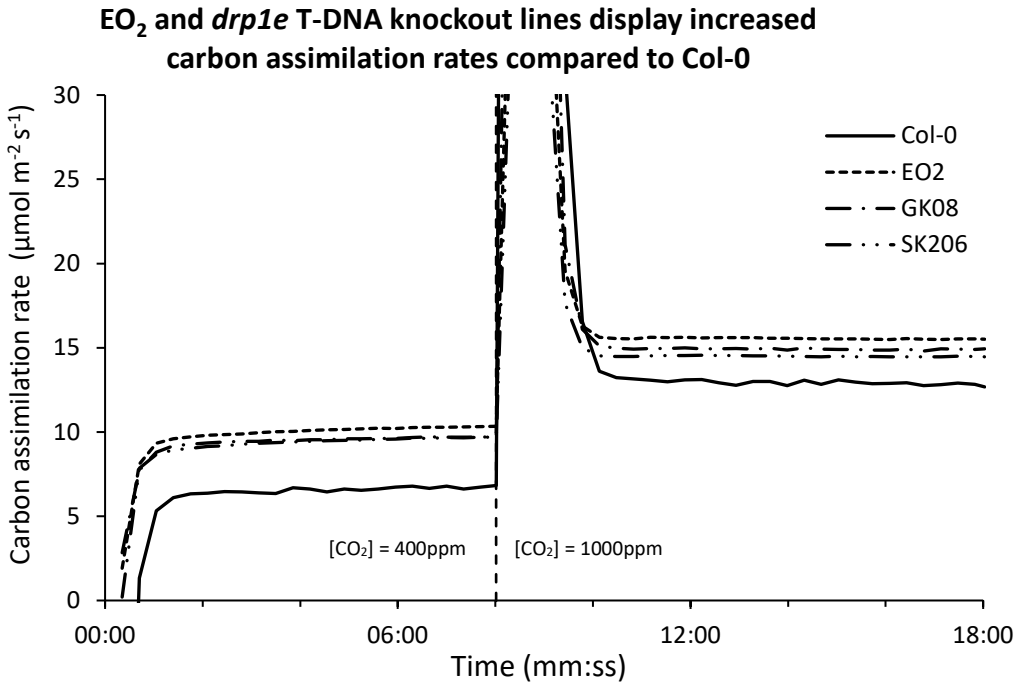

Figure 4.B) EO_2 and the *drp1e* T-DNA knockout lines GK08 and SK206 display significantly increased carbon assimilation rates compared to Col-0 under both ambient and elevated [CO_2]. The carbon assimilation rate of all lines was found to significantly increase in response to an ambient (400ppm) to elevated (1000ppm) [CO_2] transition, however the carbon assimilation rate of Col-0 was found to increase almost twofold compared to the increases of EO_2 and the *drp1e* lines. [CO_2] = 400ppm until 08:01, at which point [CO_2] increases to 1000ppm over one minute and [CO_2] is then maintained at 1000ppm for a further 9 minutes. For clarity, error bars are not included on plot. N=8 for all lines except N=7 for Col-0. 10hr day, 110-120 µmol m-2s-1 PPFD; 70% RH, 380-400ppm CO2, 22^{o}C day/20^{o}C night.

4.2.2 Gas Exchange Experiments over a Light to Dark transition using a WALZ GFS-3000 Infra-Red Gas Analyser

EO_2 was subjected to Infra-Red gas analysis experiments over a light-dark transition to investigate any differences in transpiration rate and carbon assimilation rate. The experiments were conducted using a WALKZ GFS-3000 model gas analyser, which used a 2cm^2 leaf clamp attachment.

4.2.2.1 EO_2 Displays a More Rapid Response to Darkness and has Constitutively lower Transpiration rates Compared to Col-0

The transpiration rates of both EO_2 and Col-0 were found to significantly decrease in response to darkness, however there was found to be no significant difference in the reduction of transpiration rate of EO_2 compared to Col-0. The transpiration rate of EO_2 was however found to decrease more rapidly in response to the light to dark transition compared to Col-0. EO_2 was found to have a significantly lower transpiration rate compared to the Col-0 under both light and dark conditions. These results indicate that EO_2 and Col-0 exhibit similar decreases in transpiration rate in response to darkness, however the EO_2 was found to respond more rapidly. The EO_2 was

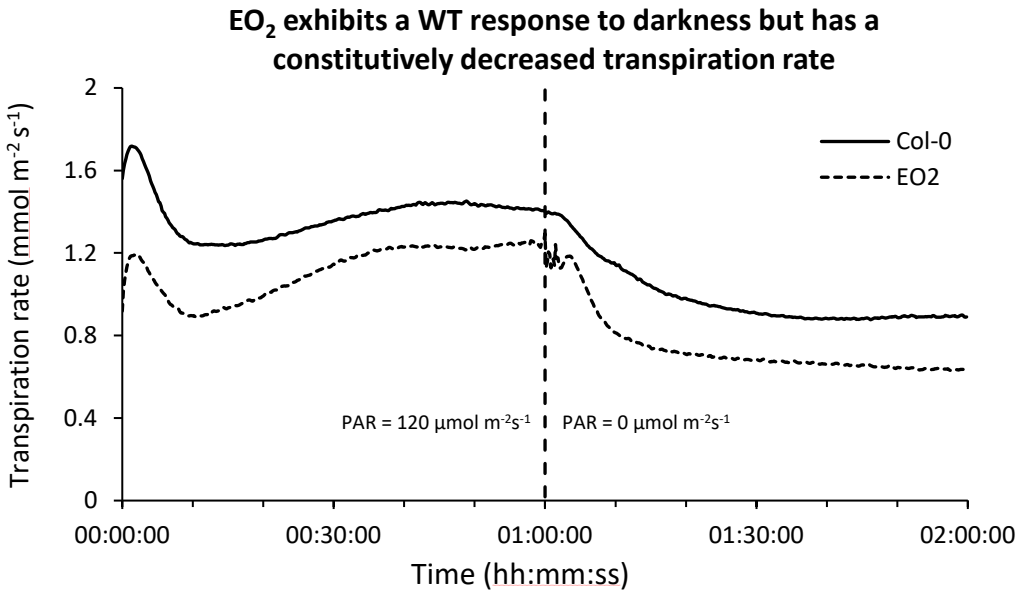

also found to have a constitutively decreased transpiration rate in both light and darkness compared to the Col-0.

Figure 4.C) There was found to be no significant difference in the response of EO_2 to the light to dark transition compared to Col-0, with changes in E of -0.65 ± 0.21 mmol m^{-2} s^{-1} (EO_2) and -0.51 ± 0.18 mmol m^{-2} s^{-1} (Col-0). However, the light to dark transition appeared to elicit a more rapid response in EO_2 over the initial ten minutes of darkness (01:00:00 - 01:10:00), with a decrease in transpiration rate of -0.48 ± 0.21 mmol m^{-2} s^{-1} in the EO_2 mutant compared to -0.26 ± 0.15 mmol m^{-2} s^{-1} in the Col-0 over this time period. The transpiration rate of EO_2 steadied after approximately 01:15:00, while the transpiration rate of Col-0 decreased by a further -0.16 ± 0.13 mmol m^{-2} s^{-1} and appeared to steady after approximately 01:20:00. Until 01:00:00 PAR = 110-120 µmol m^{-2} s^{-1}, from 01:00:00 to 02:00:00 PAR = 0-3 µmol m^{-2} s^{-1}. For clarity, error bars are not included on plot. N=6 (Col-0) N=5 (EO2). 10hr day, 120 µmol m-2s-1 PPFD; 70% RH, 380-400ppm CO2, 22°C day/20°C night.

4.2.2.2 EO_2 has an Elevated Carbon Assimilation Rate under 120 µmol m^{-2} s^{-1} PAR Light.

EO_2 was found to have an elevated carbon assimilation rate compared to Col-0 during periods of light, however EO_2 and Col-0 were found to have comparable, negative, carbon assimilation rates during darkness. These results indicate that the elevated carbon assimilation rate of EO_2 compared to Col-0 during periods of light is not likely to be due to differences in respiratory rate and could indicate an increased rate of photosynthesis or more efficient carbon dioxide/bicarbonate assimilation pathways, however it would require significant further work to determine if this is indeed the case.

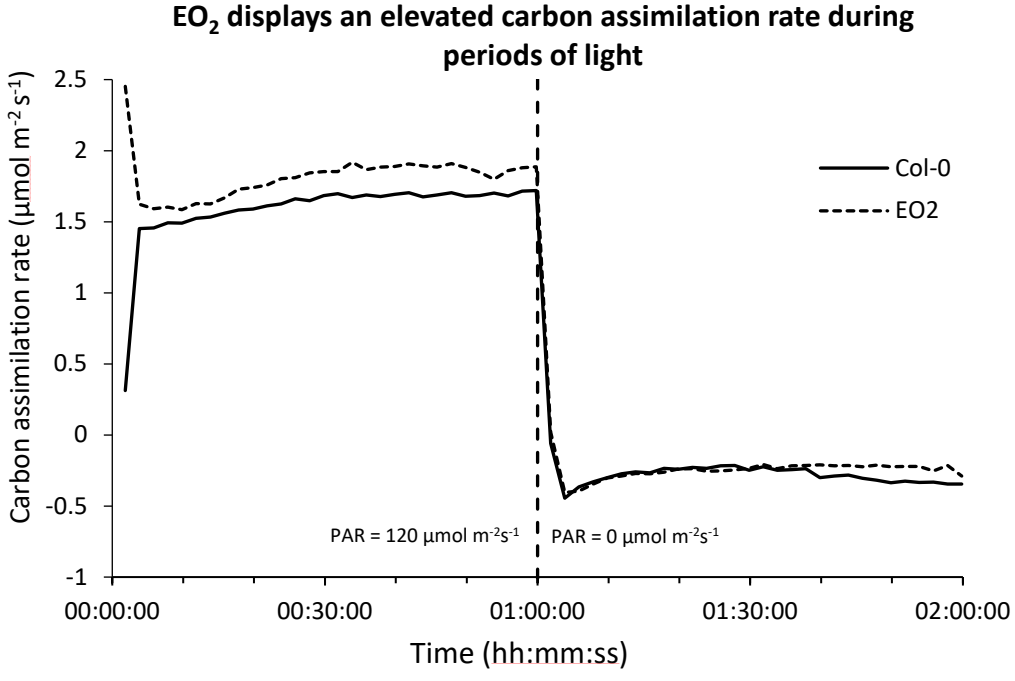

Figure 4.D) EO_2 displays an elevated carbon assimilation rate during periods of light and returns to WT rates during periods of dark. During the light period EO_2 had an average carbon assimilation rate 0.23 ± 0.04 µM m^{-2} s^{-1} higher than that of Col-0, however, during the dark period the difference in carbon assimilation rate was comparable. Until 01:00:00 PAR = 110-120µM m^{-2} s^{-1}; from 01:00:00 to 02:00:00 PAR = 0-3 µM m^{-2} s^{-1}. For clarity, error bars are not included on plot. Data shown is 2-minute moving average of the mean carbon assimilation rate. N=6 (Col-0), N=5 (EO2). 10hr day, 120 µmol m-2s-1 PPFD; 70% RH, 380-400ppm CO2, 22°C day/20°C night.

4.3 Characterisation of Stomatal Development Phenotype

To assess potential factors contributing to the decreased transpiration rate of EO_2 and the *drp1e* T-DNA knockout lines GABI-KAT 168C11.08 (GK08) and SALK_206052C (SK206) and to further investigate the perception of carbon dioxide in EO_2, the mutant lines were subjected to stomatal index and density assays. The assays were carried out with plants grown at either ambient (400ppm) or elevated (1500ppm) CO_2.

4.3.1 Evaluation of Stomatal Index when Grown under Ambient and Elevated [CO_2]

Calculation of stomatal index from abaxial leaf impressions found that there was no significant reduction in stomatal index for any line in plants grown at 1500ppm CO_2 compared to plants grown at ambient (400ppm) CO_2. Variation between lines lead to a significant difference in stomatal index between EO_2 and SK206 at 400ppm and between SK206 and both EO_2 & GK08 at 1000ppm CO_2. However, when the data was normalised there was found to be no significant decrease in stomatal index and no significant difference in stomatal index between any of the lines at 1500ppm CO_2 compared to ambient CO_2.

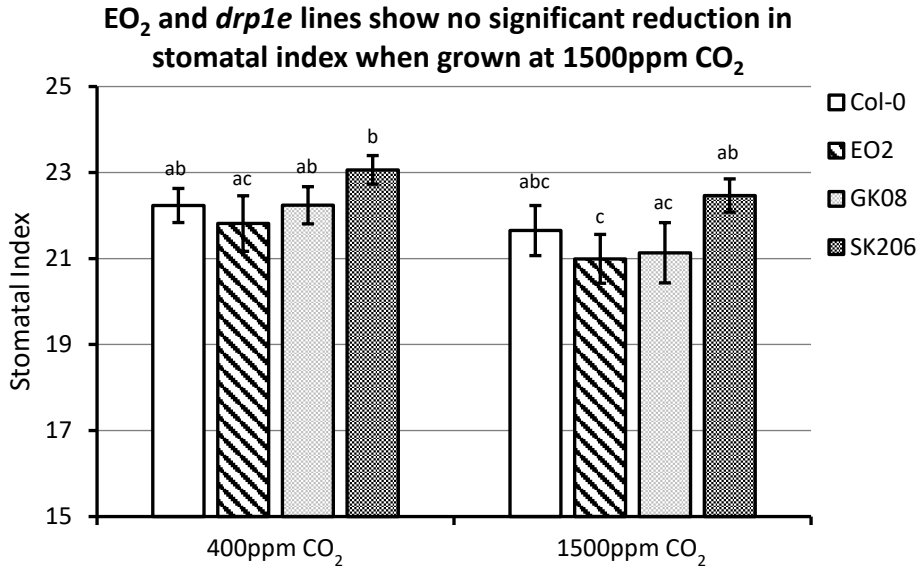

Figure 4.E) None of the mutant lines or Col-0 displayed any significant decrease in stomatal index when grown under elevated (1500ppm) [CO_2] compared to growth at ambient (380ppm) [CO_2], however all lines were found to exhibit minor, non-significant, decreases in stomatal index under elevated [CO_2]. The stomatal index of SK206 was found to be marginally significantly ($p<0.05$) different from EO_2 at 400ppm CO_2. The stomatal of index of SK206 was found to be significantly different ($p<0.01$) from that of EO_2 and marginally significantly different ($p<0.05$) from that of GK08 at 1500ppm CO_2 (two-tailed t-test). N = 10 for all lines. Stomatal indices were calculated from abaxial impressions. Two-tailed t-test (between treatments), 2-way ANOVA (between lines, multiple treatments). 10hr day, 120 µmol m-2s-1 PPFD; 70% RH, 22°C day/20°C night.

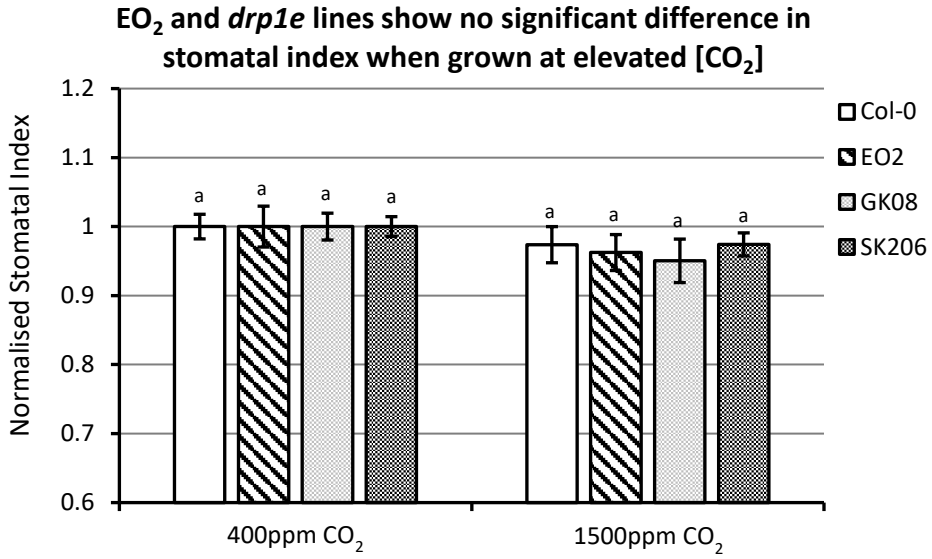

Figure 4.F) Data displayed in **Fig.4.E** after normalising for stomatal index at 400ppm [CO_2]. There was found to be no significant decrease in stomatal index for any line at 1500ppm CO_2 compared to 400ppm CO_2. There was found to be no significant difference in stomatal index between any two lines after growth at 1500ppm in the normalised data despite finding significant difference between SK206 and both EO_2 and GK08 in the un-normalised data (two-tailed t-test). N = 10 for all lines. Stomatal indices were calculated from abaxial impressions. Two-tailed t-test (between treatments), 2-way ANOVA (between lines, multiple treatments). 10hr day, 120 µmol m-2s-1 PPFD; 70% RH, 22°C day/20°C night.

4.3.2 Calculation of Stomatal Density after Growth at Ambient and Elevated [CO_2]

Stomatal density calculations found that the stomatal density of EO_2 significantly increased when grown at elevated (1500ppm) [CO_2] compared to ambient (400ppm) [CO_2], however no other line displayed significant change in stomatal density under elevated [CO_2]. The stomatal densities of EO_2

and GK08 were found to be significantly lower than that of Col-0 at 400ppm CO_2. At 1500ppm CO_2 the stomatal density of GK08 was found to be significantly lower than that of Col-0 and EO_2.

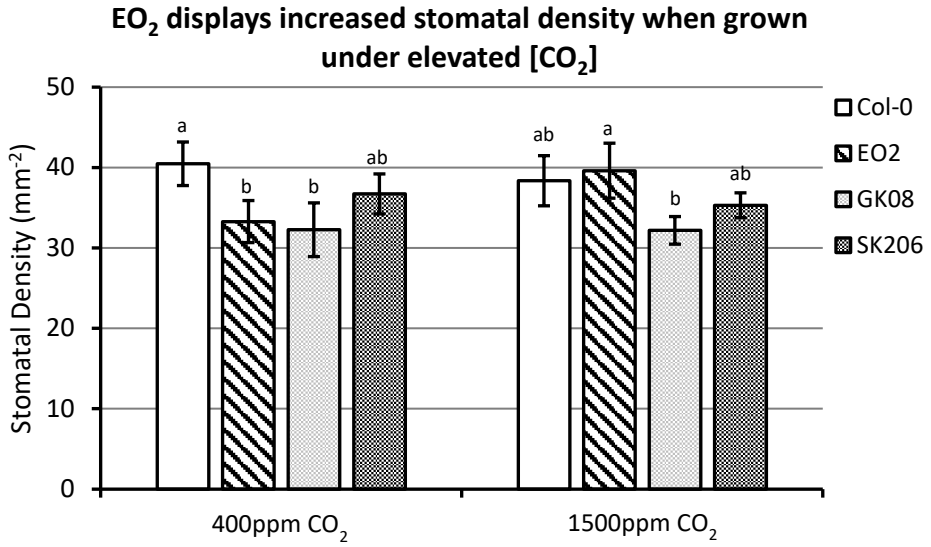

Figure 4.G) The stomatal density of EO_2 was found to significantly ($p<0.05$) increase when grown at 1500ppm CO_2 compared to 400ppm CO_2. The stomatal density of the other lines was not found to change significantly when grown at 1500ppm CO_2 compared to at 400ppm CO_2, however the stomatal density of Col-0 and SK206 was found to slightly decrease as a result of growth at 1500ppm CO_2. The stomatal densities of EO_2 and GK08 were found to be significantly ($p<0.01$) lower than that of Col-0 at 400ppm CO_2. At 1500ppm CO_2, the stomatal density of GK08 was found to be significantly less than that of both Col-0 and EO_2 (two-tailed t-test). N = 10 for all lines. Stomatal densities were calculated from abaxial impressions. Two-tailed t-test (between treatments), 2-way ANOVA (between lines, multiple treatments). 10hr day, 120 µmol m-2s-1 PPFD; 70% RH, 22°C day/20°C night.

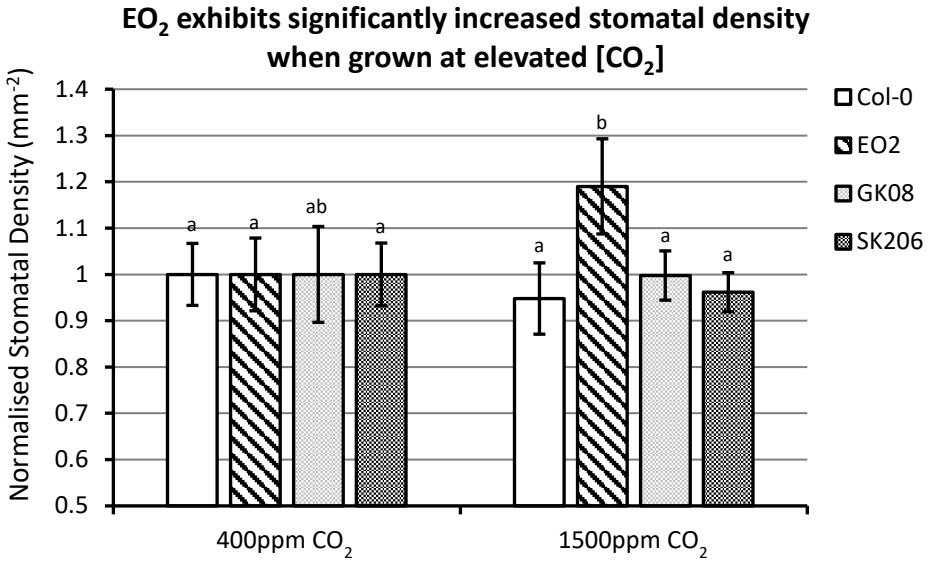

Figure 4.H) Normalised stomatal density. The stomatal density of EO_2 was found to significantly ($p<0.01$) increase after growth under elevated (1500ppm) [CO_2] compared to growth under ambient (400ppm) [CO_2] (two-tailed t-test). All other lines were found to have no significant difference in stomatal density when grown at ambient and elevated [CO_2], however the stomatal density of Col-0 and SK206 were found to decrease slightly when grown at 1500ppm [CO_2] compared to growth at ambient CO_2 levels. N = 10 for all lines. Stomatal indices were calculated from abaxial impressions. Two-tailed t-test (between treatments), 2-way ANOVA (between lines, multiple treatments). 10hr day, 120 µmol m-2s-1 PPFD; 70% RH, 22^{o}C day/20^{o}C night.

These results show that a significantly ($p<0.05$) lower stomatal density under ambient [CO_2] could contribute to the constitutively lower transpiration rates of EO_2 found in **4.2.1.1** and **4.2.2.1**. However, the lower stomatal density of EO_2 when grown at ambient [CO_2] does not explain and is even contradictory to the increased carbon assimilation rate that was observed under conditions with light. The significant increase in stomatal density of EO_2 after growth under elevated [CO_2] could indicate that EO_2 and potentially DRP1E, are involved in pathways that regulate stomatal development or leaf cell expansion in response to increasing CO_2 concentrations (Gray *et al.*, 2000; Lake and Woodward, 2008). However this phenotype was not replicated in the *drp1e* T-DNA knockout lines GK08 and SK206 and so could be as a result of expression of a defective or truncated gene product of *eo₂* or even be due to a second SNP that was inadvertently selected for in the EO_2 mutant line alongside the *drp1e* mutation, due to it having an effect on CO_2-dependent pathways. An assessment of stomatal and epidermal cell size could provide further explanation for the observed differences in stomatal density in EO_2.

4.4 EO_2 and *drp1e* lines Display Consistently Decreased Transpiration Rates Over a Night-Day-Night Diurnal Cycle at Ambient [CO_2]

EO_2 and the *drp1e* lines GABI-KAT 168C11.08 (GK08) and SALK_206052C (SK206) were treated to gravimetric transpiration assays using a set of matched balances to determine transpiration rates over both light to dark and dark to light transitions. EO_2 and both *drp1e* lines were found to have significantly reduced transpiration rates compared to the Col-0 during both dark and light periods.

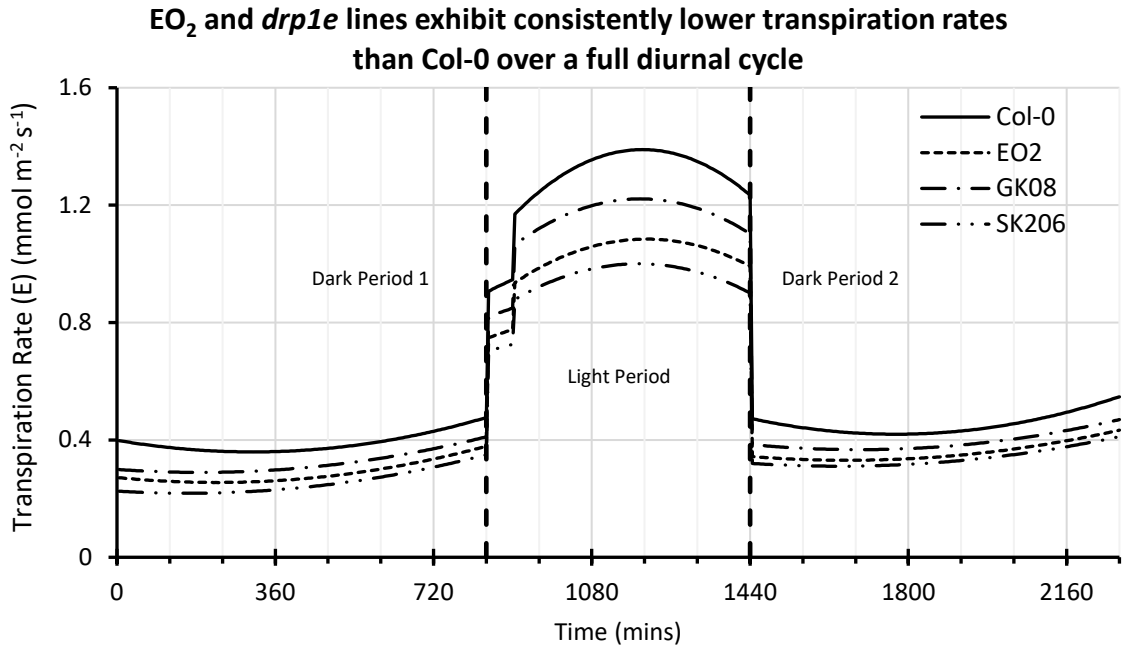

Figure 4.I) Plot of the average transpiration rate of EO_2, GK08 and SK206 over a 14:10:14 hour Night:Day:Night diurnal cycle as determined by gravimetric transpiration assays. EO_2, GK08 and SK206 were all found to have consistently decreased transpiration rates compared to Col-0 during both day and night periods. During the dark periods the transpiration rate of Col-0 fell to rates that more closely matched the 3 mutant lines, however the mutant lines still exhibited lower transpiration rates than the Col-0 (**Table 4.A**). N=27 for all lines, the above results are from 3 separate experimental repeats. Please note that the "step" between hours 14 and 15 in **Figure 4.I** is due to a technical error that made the day cycle start one hour later for one of the experimental repeats. 10hr day, 110-120 µmol m-2s-1 PPFD; 70% RH, 380-400ppm CO2, 22°C day/20°C night.

These results confirm the findings of **4.2.1.1** and **4.2.2.1** that EO_2 and *drp1e* lines have constitutively lower transpiration rates compared to Col-0.

Table 4.A) Average Transpiration Rate of EO_2 and *drp1e* Lines in Dark and Light Periods as Determined by Gravimetric Transpirations Assays.

Period	Transpiration rate (E) Col-0 (mmol m^{-2} s^{-1})	Transpiration rate (E) EO_2 (mmol m^{-2} s^{-1})	Transpiration rate (E) GK08 (mmol m^{-2} s^{-1})	Transpiration rate (E) SK206 (mmol m^{-2} s^{-1})
Dark 1	0.39 ± 0.01	0.29 ± 0.01	0.32 ± 0.01	0.25 ± 0.01
Light	1.28 ± 0.01	1.01 ± 0.01	1.14 ± 0.01	0.94 ± 0.01
Dark 2	0.45 ± 0.01	0.36 ± 0.01	0.39 ± 0.01	0.34 ± 0.01

4.5 Determination of Water Use Efficiency

Experiments **4.2.1.1** and **4.2.2.1** found that EO_2 and the *drp1e* T-DNA knockout lines GK08 and SK206 displayed consistently lower transpiration during periods of light, both under ambient and elevated CO_2 compared to Col-. Experiments **4.2.1.2** and **4.2.2.2** showed that EO_2 and the same *drp1e* lines exhibited elevated carbon assimilation rates during periods of light and under treatment with elevated CO_2. Together, these findings indicate that EO_2 and the *drp1e* lines may have improved water use efficiency (WUE) compared to Col-0. EO_2 and the *drp1e* mutant lines GK08 and Sk206 were treated to a long-term WUE experiment and were grown on water-saturated medium inside sealed containers for a period of 6 weeks. The plants were then harvested, dried and the plant dry weight/weight of water lost was calculated to determine the WUE of each line. It was found that EO_2 ($p<0.01$) and SK206 ($p<0.01$) displayed significantly increased water use efficiency compared to Col-0. GK08 displayed substantially increased WUE compared to Col-0, however this was not found to be significantly different.

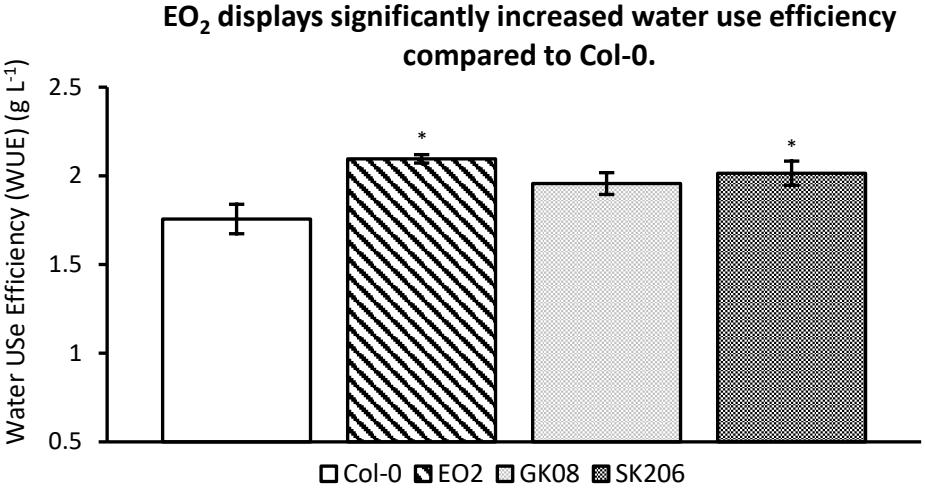

Figure 4.J) EO_2 and SK206 display significantly increased water use efficiency (WUE) compared to Col-0 ($P<0.01$). GK08 displayed increased WUE compared to Col-0, however this was not found to be significant ($p=0.074$) (two-tailed t-test). 10hr day, 110-120 µmol m-2s-1 PPFD; 70% RH, 380-400ppm CO2, 22^{o}C day/20^{o}C night.

Table 4.B) Water use efficiency of Col-0, EO_2 and *drp1e* lines

Line	**Col-0**	**EO_2**	**GK08**	**SK206**
WUE (g L^{-1})	1.76 ± 0.08	2.10 ± 0.02	1.96 ± 0.06	2.01 ± 0.07

4.6 Summary and Discussion

Infra-Red Gas Analysis (IRGA) experiments found that the inhibited stomatal response to elevated atmospheric [CO_2] that was observed in EO_2 and the *drp1e* lines translated into a lack of reduction in transpiration rate over an ambient to elevated [CO_2] transition. IRGA experiments over a light-dark transition found that EO_2 exhibited a wild type response to dark, however the EO_2 exhibited a more rapid response to darkness. The ambient to high [CO_2] and light to dark IRGA experiments established that EO_2 and the *drp1e* T-DNA knockout lines exhibited consistently lower transpiration rates than Col-0 under both ambient and elevated [CO_2] and during both light and dark periods. Analysis of carbon assimilation rates from these IRGA experiments established that EO_2 and the *drp1e* lines had consistently increased carbon assimilation rates over periods of light, under both ambient and elevated [CO_2], compared to the Col-0. However, during periods of darkness the carbon assimilation rate of EO_2 fell to similar negative values as Col-0, indicating that the source of the difference in carbon assimilation rate is unlikely to be respiratory. Stomatal development assays found that EO_2 and the *drp1e* lines had lower stomatal density compared to Col-0 when grown at ambient [CO_2]. The stomatal index of EO_2 and *drp1e* lines did not change when grown under 1500ppm CO_2, however the stomatal density of EO_2 was found to increase in response to growth under 1500ppm CO_2. The consistently decreased transpiration rate of EO_2 and the *drp1e* lines was further confirmed by gravimetric transpiration assay over a 38-hour diurnal cycle. As the mutant lines had been found to exhibit consistently decreased transpiration rates and consistently increased carbon assimilation rates compared to Col-0, it was hypothesised that this could translate to increased water use efficiency (WUE). Cumulative water loss experiments then confirmed this theory, as both EO_2 and SK206 were found to have significantly improved WUE compared to Col-0 and GK08 displayed increased, but not significant, WUE. The lower stomatal density of EO_2 and the *drp1e* lines at ambient [CO_2] could account for the consistently lower transpiration rate of these lines compared to Col-0 but appears contradictory to the increased carbon assimilation rates shown in these lines. It may therefore be that changes to the carbon dioxide sensing and signalling apparatus at a molecular level are responsible for the increased carbon assimilation rates through an unknown mechanism.

Chapter 5 – DRP1E in Carbon Dioxide Induced Stomatal Closure Signalling Pathways.

5.1 Identification of Putative DRP1E Interactions with the Current CO_2 Signalling Model

The DRP1E mutant EO_2 has been shown to exhibit a reduced stomatal closure in response to elevated atmospheric carbon dioxide ($[CO_2]_{atm}$) conditions, yet responds normally to exogenously applied abscisic acid (ABA) or calcium (Ca^{2+}) and exhibits no visible morphological phenotype, but has an increased stomatal density when grown under elevated $[CO_2]_{atm}$. Infra-red gas exchange experiments showed that EO_2 exhibited no significant response to elevated $[CO_2]$ and found that EO_2 had constitutively decreased transpiration rate and increased carbon assimilation rate during periods of light, which returned to WT levels during periods of darkness.

In light of the results presented in previous chapters, it is possible to consolidate these findings against the literature outlined in Chapter 1 to identify potential interactions of DRP1E with carbon dioxide-specific closure pathways.

5.1.1 DRP1E is Unlikely to Inhibit CO_2 Induced Stomatal Closure Through a Role in Cytokinesis

The reportedly normal cell plate formation and expansion in *drp1e* lines and lack of an aberrant phenotype **(Collings *et al*, 2008)** make it unlikely that the EO_2 reduced stomatal closure response to elevated atmospheric $[CO_2]$ can be attributed to the role of DRP1E in cytokinesis. The increased stomatal density of EO_2 during growth in elevated $[CO_2]$ may potentially provide a link to the role of DRP1E in cytokinesis, however this is unlikely to be due to the carbon dioxide-specific phenotype of EO_2.

5.1.2 A Mitochondrial Phenotype is Unlikely to Cause Stomatal Insensitivity to CO_2 in EO_2

Jin *et al*, 2003 report an elongated mitochondrial phenotype in 63% of *drp1e* mutant protoplasts and multiple sources report GFP-DRP1E localisation to mitochondria **(Jin *et al*, 2003; Tang *et al*, 2006)**, although this localisation pattern has not been demonstrated consistently **(Minami *et al*, 2015)**. **Goh *et al*, 2011** report increased oxygen consumption in intact *drp1e* mutant leaves during periods of darkness, with a return to wild type (WT) oxygen production rates under both 60 µmol $m^{-2}s^{-1}$ and 900 µmol $m^{-2}s^{-1}$ light. **Goh *et al*, 2011** further report substantially increased cytosolic ATP concentrations ($[ATP]_{cyt}$) in *drp1e* guard cell protoplasts under dark conditions which, combined with the increased rate of oxygen consumption under dark conditions, would indicate increased mitochondrial activity in *drp1e* mutants compared to WT. Increased $[ATP]_{cyt}$ is associated with stomatal opening and inhibition of stomatal closure through increased activity of plasma membrane H^+/ATPases, thereby causing membrane hyperpolarisation through efflux of H^+ which is balanced by

inward rectifying K^+ channels KAT1 and KAT2 **(Cotelle & Leonhardt, 2016)**. This increases the solute potential of the cytosol, resulting in an increase in turgor and stomatal opening **(Cotelle & Leonhardt, 2016)**.

It is not known whether the elevated $[ATP]_{cyt}$ *drp1e* phenotype reported by **Goh *et al*, 2011** is maintained during periods of light, however a theoretical sustained increase in [ATP] is likely to result in constitutively more open stomata and affect all stomatal closure pathways, not be limited to reduced stomatal closure in response to elevated $[CO_2]_{atm}$. The stomatal aperture of EO_2 and the *drp1e* lines was consistently found to be similar or marginally smaller than Col-0 in control data and EO_2 and *drp1e* lines displayed WT stomatal responses to ABA, darkness and $CaCl_2$ (**Chapter 3**). Furthermore, all gas exchange experiments conducted in **Chapter 4** found that EO_2 and *drp1e* lines displayed consistently decreased transpiration rates and increased carbon assimilation rates, and that the carbon assimilation and transpiration rate of EO_2 returned to WT levels during periods of darkness. Although oxygen consumption rates were not measured, the carbon assimilation rate during periods of darkness can act as an indication of respiration rate, as increased respiration would result in a reduced carbon assimilation rate due to the increased CO_2 production from respiration. The findings detailed in this thesis therefore contest the results of **Goh *et al.*, 2011**, which are not corroborated elsewhere, and as such it is unlikely that DRP1E affects stomatal responses to elevated $[CO_2]$ through a putative role in mitochondrial division, morphology or respiration rate.

5.1.3 DRP1E may be Involved in Endocytosis of CO_2 Stomatal Signalling Components

The suspected role of DRP1E in endocytosis may interfere with membrane recycling in *drp1e* mutants, affecting retention and activity of membrane-bound carbon dioxide signalling proteins and thereby disrupting guard cell carbon dioxide response pathways. Interestingly RBOHD, downstream of OST1 in stomatal closure responses, and PIP2;1 have been shown to localise to sphingolipid and sterol enriched membrane microdomains **(Wang *et* al, 2013; Hao *et al*, 2014)**, which are associated with MME, rendering it possible that DRP1E may affect their distribution and membrane availability. Similarly, plasma membrane H^+/ATPases have been extracted from detergent resistant membrane (DRM) fractions alongside Clathrin Heavy Chain (CHC), Clathrin Light Chain (CLC), DRP1A and DRP1E **(Minami *et al*, 2009)**, making it possible for DRP1E-mediated endocytosis to influence persistence and activity of cell membrane H^+/ATPases. Protein interactions with components of Clathrin Mediated Endocytosis (CME) and preference for specific membrane lipids, sterols and membrane microdomains may allow for preferential endocytosis of specific membrane signalling components, which could be disturbed in *drp1e* mutants. Direct studies into the effects of CME disruption and endocytic dynamics of *drp1e* mutants in stomatal carbon dioxide responses are yet to be carried out,

however the convincing role of DRP1E in CME and the known endocytosis of carbon dioxide signalling components (**Li *et al.*, 2011; Hao *et al.*, 2014; Ueda *et al.*, 2016**) makes this a promising avenue for further research.

5.2 Endocytosis as an Avenue for Further Research

In **5.1**, the results detailed in chapters 3 & 4 were consolidated against the literature and accepted guard cell carbon dioxide signalling pathways to establish a putative literature basis for the role of DRP1E in CO_2-induced stomatal closure. This evaluation of these experimental findings against the literature identified the role of DRP1E in Clathrin Mediated Endocytosis (CME) as a likely point of convergence with carbon dioxide induced stomatal closure pathways, as a number of membrane-bound carbon dioxide signalling proteins have already been shown to be internalized in response to other environmental signals (**Li *et al.*, 2011; Hao *et al.*, 2014; Ueda *et al.*, 2016**). To investigate this hypothesis further, a series of experiments using Tyrphostin-A23, an inhibitor of CME that acts via competitive binding of the active site of the µ2-subunit in CME AP2 adapter complexes (**Banbury *et al.*, 2003; Dhonukshe *et al.*, 2007; Fujimoto *et al.*, 2010**), were designed to assess the effect of disruption of selective CME on stomatal closure. Tyrphostin-A23 (tyr-A23) is thought to selectively inhibit clathrin mediated endocytosis without impacting other compartments of the endocytic pathway (**Banbury *et al.*, 2003; Dhonukshe *et al.*, 2007**).

5.3 EO_2 Stomatal Bioassays with Tyrphostin-A23 Treatment

The EO_2 mutant and Col-0 were subjected to ABA and elevated [CO_2] stomatal bioassay of epidermal peels with additional treatment using the CME inhibitor Tyrphostin-A23. Unfortunately due to experimental time restrictions, due to the number of treatments required to ensure adequate controls, it has not at this stage been possible to conduct these experiments using the T-DNA *drp1e* knockout lines GABI-KAT_168C11.08 and SALK_206052C. However, these are obvious future experiments that would increase the validity of these results.

5.3.1 Treatment with Tyrphostin-A23 Interrupts CO_2-Induced Stomatal Closure in Col-0

To investigate the role of clathrin mediated endocytosis in CO_2-induced stomatal closure, Col-0 and EO_2 were subjected to elevated CO_2 stomatal bioassay with additional tyr-A23 treatment as described in **2.4.1.2**. As found in previous experiments, the stomatal aperture of Col-0, but not EO_2 was found to significantly reduce in response to treatment with elevated (1000ppm) atmospheric [CO_2]. Treatment with tyr-A23 for 30 minutes prior to treatment with elevated CO_2 substantially inhibited the reduction of stomatal aperture exhibited by Col-0 in response to elevated [CO_2],

causing the Col-0 to exhibit a response similar to that of EO_2. These results implicate clathrin mediated endocytosis as a key player in elevated CO_2 induced stomatal closure.

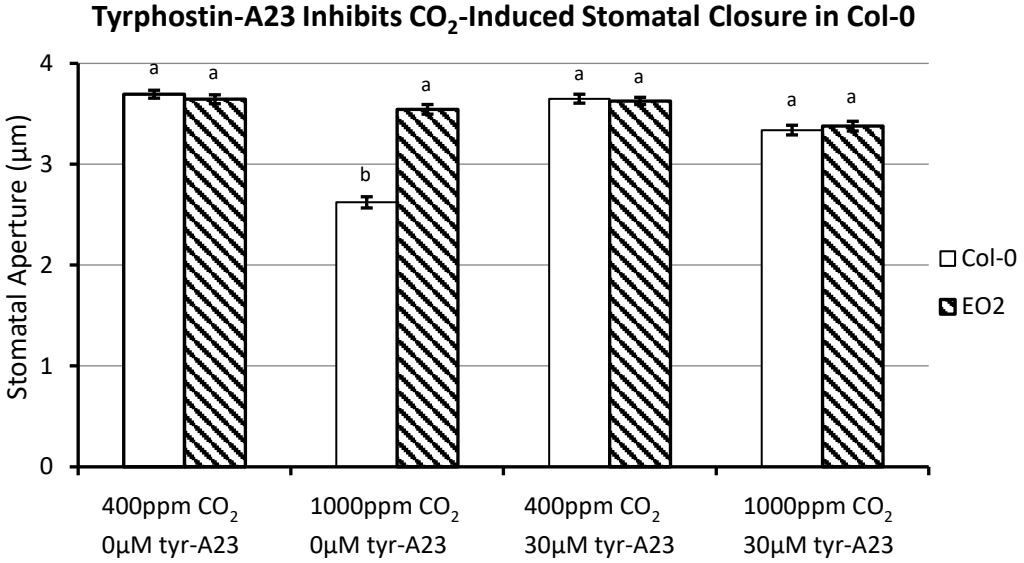

Figure 5.A) The stomatal aperture of Col-0 but not EO_2 reduces significantly ($p<0.01$) in response to treatment with elevated (1000ppm) CO_2 when not treated with tyr-A23. Treatment with tyr-A23 significantly inhibits the reduction in stomatal aperture exhibited by Col-0 in response to 1000ppm CO_2. Two-way ANOVAs found no significant different difference between lines at 400ppm CO_2, 0µM tyr-A23; 400ppm CO_2, 30µM tyr-A23; 1000ppm CO_2, 30µM tyr-A23 and EO_2 at 1000ppm CO_2, 0µM tyr-A23. This implies that cargo targeted endocytosis is involved in high CO_2 induced stomatal closure. Data values shown are mean values ± SE (n=90 from 9 biological replicates) from 3 independent experiments carried out on consecutive days. Two-tailed t-test (between treatments), 2-way ANOVA (between lines, multiple treatments). 10hr day, 120 µmol m-2s-1 PPFD; 70% RH, 380-400ppm CO2, 22°C day/20°C night.

5.3.2 ABA-Induced Stomatal Closure Proceeds During Treatment with Tyrphostin-A23

To assess the impact of inhibition of Clathrin Mediated Endocytosis on ABA-induced stomatal closure, an ABA bioassay with additional treatment with tyr-A23 was conducted using Col-0 and EO_2 as described in **2.4.1.1**. As previously found, EO_2 displayed a WT reduction ($p<0.05$) in stomatal aperture when treated with 5µM ABA, 0 µM tyr-A23. Both Col-0 and EO_2 were also found to exhibit a significant ($p<0.05$) reduction in stomatal aperture when treated with 5µM ABA, 30 µM tyr-A23 compared to treatment with 0µM ABA, 0 µM tyr-A23 or 0µM ABA, 30 µM tyr-A23, implying that ABA induced stomatal closure is not compromised by the inhibition of Clathrin Mediated Endocytosis. However, there was found to be a significant difference between the stomatal aperture of Col-0 and EO_2 when treated with 5µM ABA, 0 µM tyr-A23 compared to 5µM ABA, 30 µM tyr-A23, implying that tyr-A23 partially disrupts stomatal closure in response to ABA despite a significant closure response.

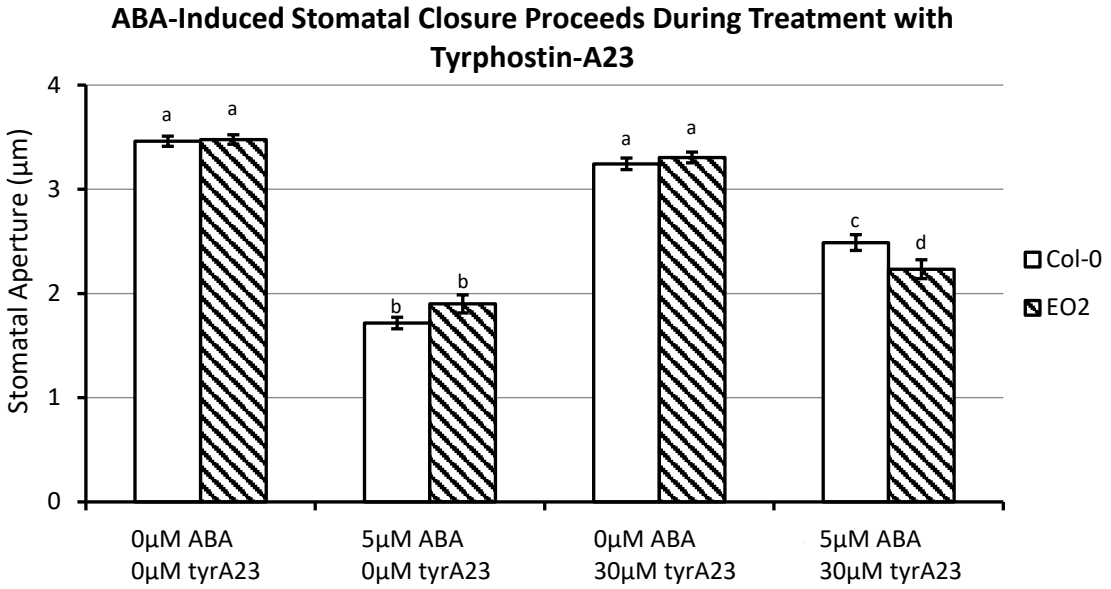

Figure 5.B) EO_2 and Col-0 display significant ($p<0.05$) stomatal closure in responses to ABA during treatment with tyr-A23. No significant difference was found between Col-0 and EO_2 at 0µM ABA, 30 µM tyr-A23 and 0µM ABA, 30 µM tyr-A23. The response of Col-0 and EO_2 when treated with 5µM ABA, 30 µM tyr-A23 was found to differ significantly ($p<0.05$) from all other treatments and the response of EO_2 was found to be significantly ($p<0.05$) different from that of Col-0 at 5µM ABA, 30 µM tyr-A23. These results indicate that disruption of clathrin mediated endocytosis partially disrupts stomatal closure in response to ABA but that plants are still able to elicit a significant response to ABA during treatment with tyr-A23. Data values shown are mean values ± SE (n=90 from 9 biological replicates) from 3 independent experiments carried out on consecutive days. Two-tailed t-test (between treatments), 2-way ANOVA (between lines, multiple treatments). 10hr day, 120 µmol m-2s-1 PPFD; 70% RH, 380-400ppm CO2, 22^{o}C day/20^{o}C night.

5.4 Confocal Microscopy Vesicle Assays Using the Styryl Membrane dye FM4-64

To further investigate the potential role of endocytosis in stomatal responses to CO_2 and ABA, outlined in **5.1** and **5.2**, a series of experiments were designed to assess the rate of cell membrane vesicle formation during CO_2 and ABA closure responses.

5.4.1 EO_2 has Consistently Reduced Endosome Numbers Compared to Col-0 and Exhibits a WT Endosome Count During ABA-Induced Stomatal Closure

Col-0 and EO_2 were subjected to confocal endosome assays as described in **2.4.2.1** with application of ABA and additional treatment with Tyrphostin-A23. EO_2 was found to have consistently lower numbers of FM4-64 labelled endosomes throughout all treatments and had, on average 18.8% ± 0.4 lower endosome numbers compared to Col-0. Treatment with ABA was found to significantly increase ($p<0.05$) labelled endosome numbers in both lines, while the application of tyr-A23 was found to reduce endosome numbers in both Col-0 and EO_2, although this was not found to be statistically significant in the un-normalised data. Endosome numbers in both EO_2 and Col-0 were found to be similar upon treatment with tyr-A23 regardless of treatment with ABA. The normalised data showed that EO_2 displayed a WT vesicle response to ABA and provided a clearer statistical analysis (**Fig 5.D**).

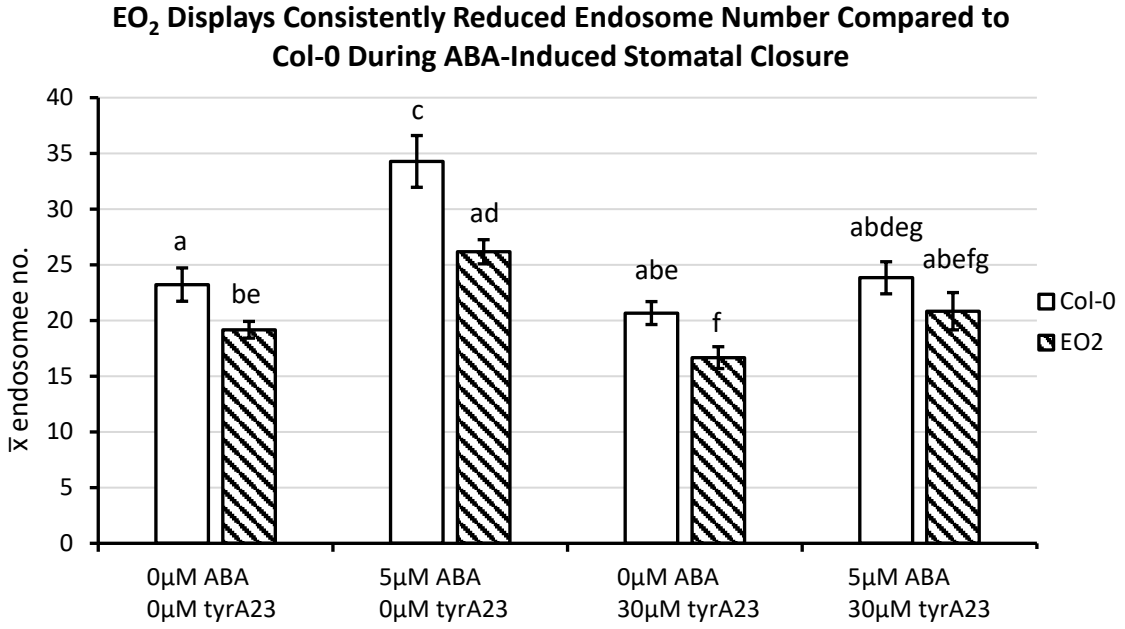

Figure 5.C) Confocal endosome assay of EO_2 and Col-0 epidermal peels in ABA induced stomatal closure, with additional treatment with tyr-A23 and the fluorescent styryl membrane dye FM4-64. The endosome number in both lines was found to increase in response to treatment with ABA ($p<0.05$), however this was abolished upon treatment with tyr-A23. EO_2 was found to have consistently decreased endosome numbers compared to Col-0, with on-average 18.8% ± 0.4 less FM4-64 labelled endosomes compared to Col-0. Statistical analysis yielded complex results which are best visualised above. Untreated Col-0 was found to have no significant difference with Col-0 at 0µM ABA, 30 µM tyr-A23 and 5µM ABA, 30 µM tyr-A23, but was significantly different from Col-0 at 5µM ABA, 0 µM tyr-A23. Untreated EO_2 was found to have no significant difference with EO_2 at 0µM

ABA, 30 µM tyr-A23 and 5µM ABA, 30 µM tyr-A23, but was significantly different from EO_2 at 5µM ABA, 0 µM tyr-A23. EO_2 and Col-0 were found to be significantly different ($p<0.05$) within each treatment except 5µM ABA, 30 µM tyr-A23. Data values shown are mean values ± SE (n=18 from 6 biological replicates) from 3 independent experiments carried out on consecutive days. Two-tailed t-test. 10hr day, 120 µmol m-2s-1 PPFD; 70% RH, 380-400ppm CO2, 22°C day/20°C night.

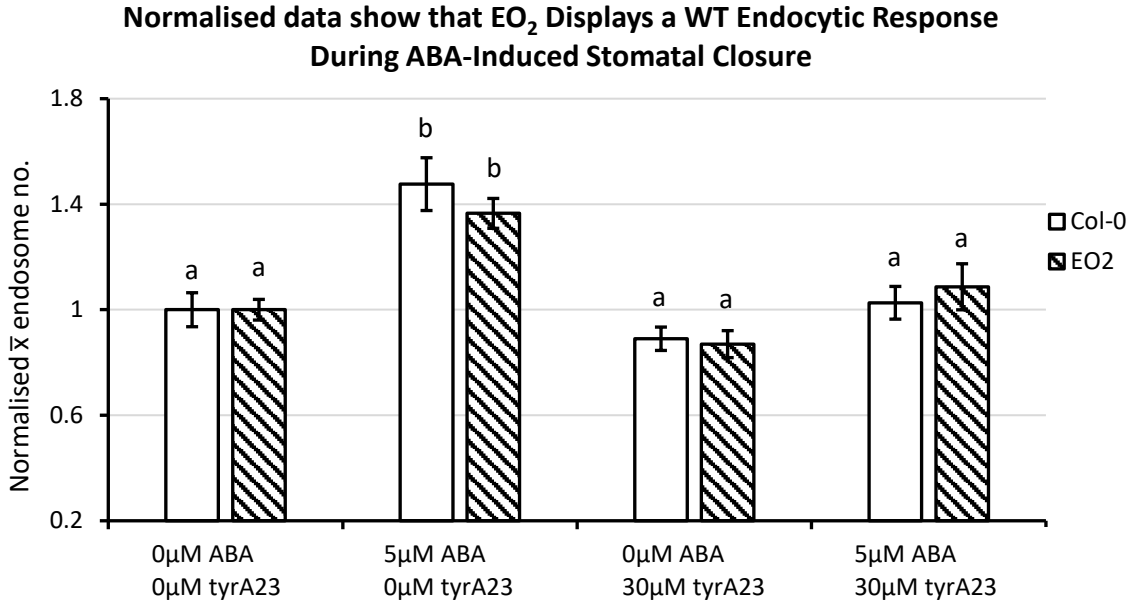

Figure 5.D) Normalised data from confocal endosome assay of EO_2 and Col-0 in ABA induced stomatal closure with additional treatment with tyr-A23 and the fluorescent styryl membrane dye FM4-64. Endosome number of both lines was still found to significantly increase when treated with ABA and was found to decrease to numbers statistically insignificant from untreated values after treatment with tyr-A23. EO_2 and Col-0 at 5µM ABA, 0 µM tyr-A23 were found to be statistically significant from Col-0 and EO_2 at all other treatments. Data values shown are mean values ± SE (n=18 from 6 biological replicates) from 3 independent experiments carried out on consecutive days. Two-tailed t-test. 10hr day, 120 µmol m-2s-1 PPFD; 70% RH, 380-400ppm CO2, 22°C day/20°C night.

5.4.2 EO_2 Continues to Exhibit a Consistently Reduced Endosome Number Compared to Col-0 and Exhibits a WT Endosome Count During CO_2-Induced Stomatal Closure

In a similar experiment to **5.3.1**, EO_2 and Col-0 were subjected to confocal endosome assays as described in **2.4.2.2**, with application of elevated (1000ppm) CO_2 and additional treatment with Tyrphostin-A23. Endosome counts in both EO_2 and Col-0 were found to marginally increase in response to treatment with elevated CO_2 ($p<0.05$). Treatment with tyr-A23 significantly ($p<0.05$) reduced endosome counts in both lines and no increase in endosome count was observed in either line upon concomitant treatment with 1000ppm CO_2. EO_2 was found to have on-average 10.4% ± 0.2 less FM4-64 labelled endosomes compared to the Col-0. The normalised data (**5.F**) found no significant difference in endosome count between EO_2 and Col-0 within any treatment.

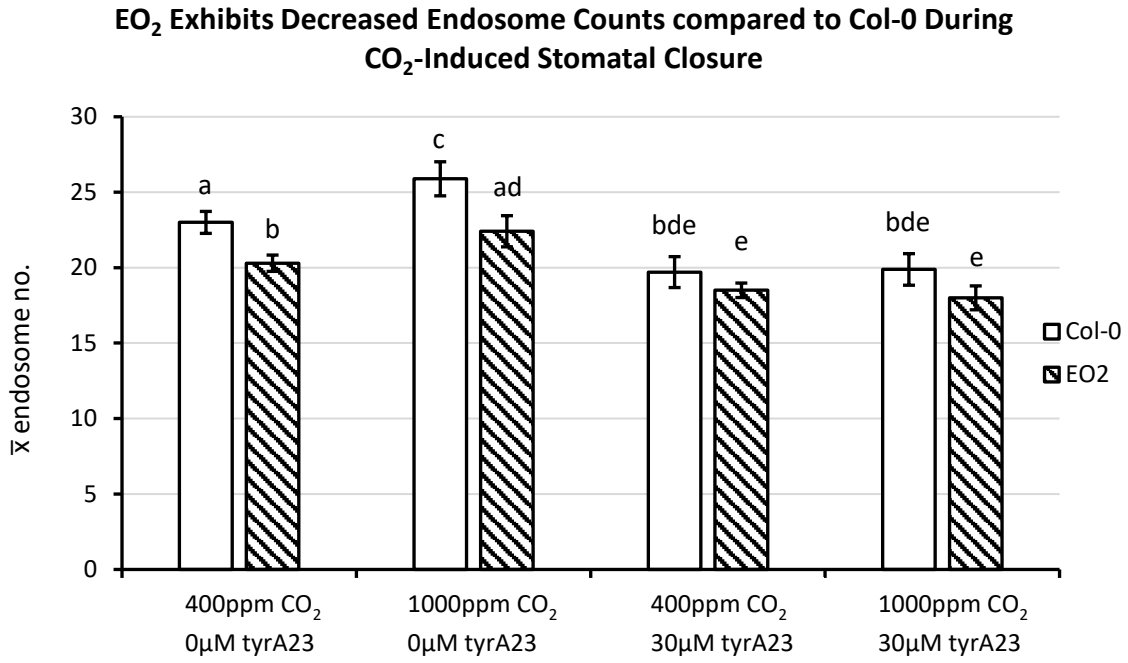

Figure 5.E) EO_2 and Col-0 confocal endosome assay with application of elevated (1000ppm) CO_2 and additional treatment with Tyrphostin-A23. Endosome count in both lines was found to increase significantly in response to the application of 1000ppm CO_2 ($p<0.05$). Treatment with tyr-A23 significantly ($p<0.05$) reduced the endosome count of both lines compared to the untreated values and application of 1000ppm CO_2 had no effect on endosome count when concomitantly treated with tyr-A23. EO_2 had a consistently decreased endosome count compared to Col-0, with an average of 10.4% ± 0.2 less FM4-64 labelled endosomes compared to the Col-0. Data values shown are mean values ± SE (n=18 from 6 biological replicates) from 3 independent experiments carried out on consecutive days. Two-tailed t-test. 10hr day, 120 µmol m-2s-1 PPFD; 70% RH, 380-400ppm CO2, 22^{o}C day/20^{o}C night.

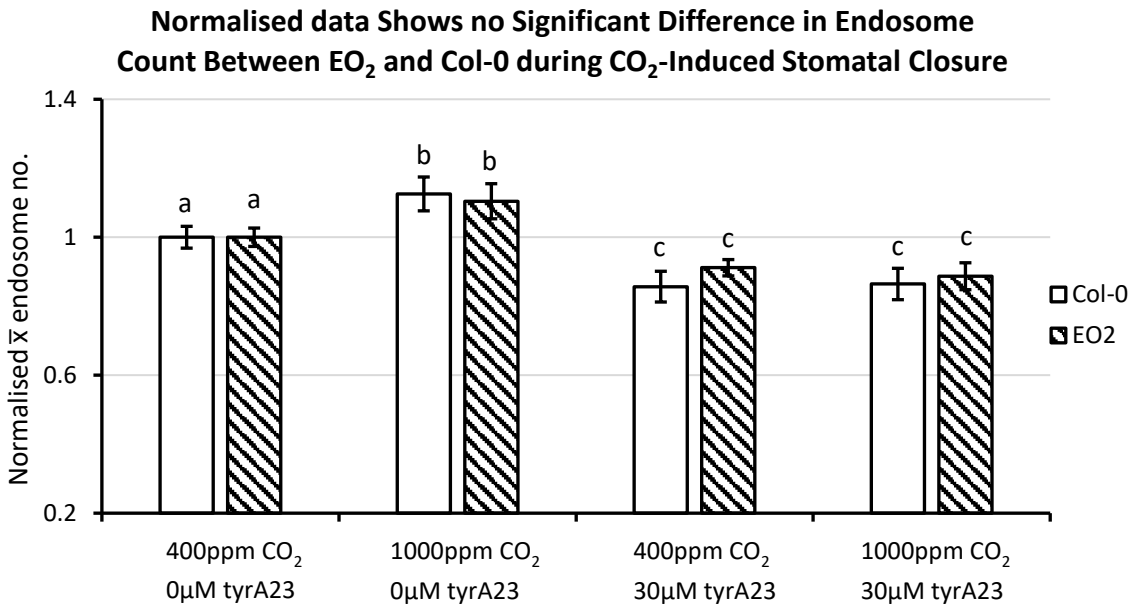

Figure 5.F) Normalised data of EO_2 and Col-0 confocal endosome assay with application of elevated (1000ppm) CO_2 and additional treatment with Tyrphostin-A23. The endosome count of both lines was found to significantly increase ($p<0.05$) upon treatment with 1000ppm CO_2 alone. The normalised endosome count of both lines was also found to significantly ($p<0.05$) decrease upon treatment with tyr-A23 and no increase in endosome count was detected upon treatment with both tyr-A23 and 1000ppm CO_2. There was no significant difference in normalised endosome count between the two lines within any treatment. Data values shown are mean values ± SE (n=18 from 6 biological replicates) from 3 independent experiments carried out on consecutive days. Two-tailed t-test. 10hr day, 120 µmol m-2s-1 PPFD; 70% RH, 380-400ppm CO2, 22^{o}C day/20^{o}C night.

5.5 Localisation of DRP1E, PIP2A and RBOHD Fluorescent Protein Fusions

Fluorescent gene constructs of DRP1E, PIP2A and RBOHD were constructed using the techniques detailed in **2.4**, in both enhanced Cyan Fluorescent Protein (eCFP) and Yellow Fluorescent Protein (YFP) variants, under the control of the viral 35S Cauliflower Mosaic Virus (35S) promotor sequence. Unfortunately, due to time restrictions stemming from the time intensive nature of creating fluorescent protein gene constructs from scratch, the findings detailed in this section are qualitative rather than quantitative and no statistical analysis has been conducted.

5.5.1 DRP1E-C/YFP Localises to Punctate Spots at the Cell Membrane and Cytoplasm

As previously reported (**Jin *et al.*, 2003; Tang *et al.*, 2006; Minami *et al.*, 2015**), DRP1E-CFP/DRP1E-YFP was found to localise to punctate spots at the cell membrane and in the cytoplasm of *Arabidopsis* protoplasts (**Fig 5.G**). The localisation of DRP1E-CFP and DRP1E-YFP was identical in all observed transformed protoplasts.

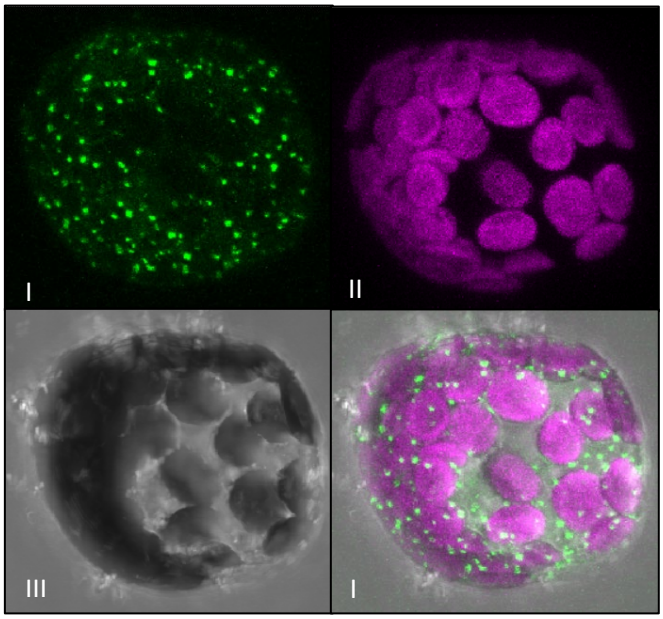

Figure 5.G) Expression of DRP1E-YFP in transformed *Arabidopsis* protoplasts.

DRP1E clearly localises to punctate spots in the cytoplasm and at the cell membrane. The localisation of DRP1E-XFP was identical in all observed transformed protoplasts and was identical for both DRP1E-CFP and DRP1E-YFP.

Images shown are max projections. I)YFP fluorescence channel; II) Autofluorescence channel; III) Brightfield; IV) Overlay of YFP fluorescence, Autofluorescence and Brightfield.

Co-expression of DRP1E-CFP and DRP1E-YFP found, through the use of FRET techniques, that DRP1E-CFP and DRP1E-YFP co-localised to the same punctate spots in the cytoplasm and at the cell membrane. This could indicate that the expressed fluorescent protein is functional, as DRP1E has

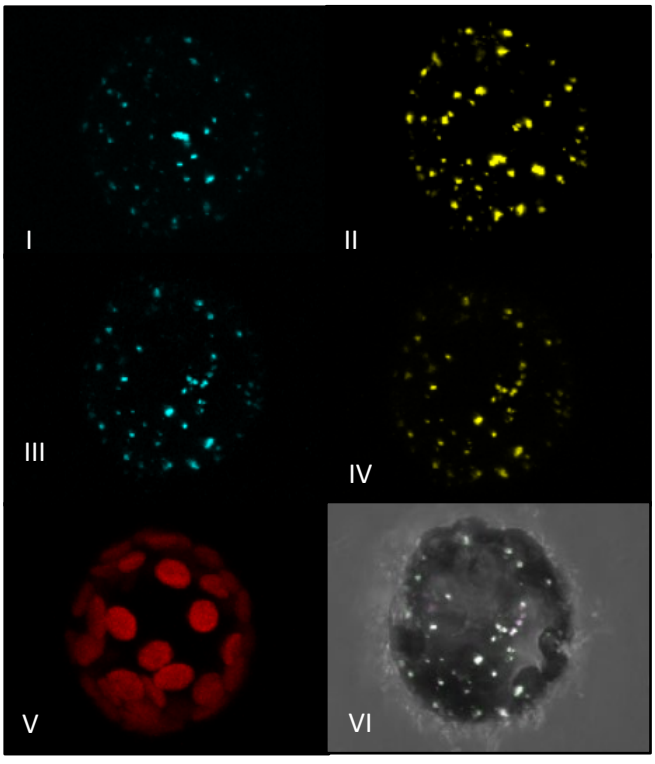

Figure 5.H) Co-expression of DRP1E-CFP and DRP1E-YFP in transformed *Arabidopsis* protoplasts.

The localisation of DRP1E-CFP and DRP1E-YFP clearly overlaps and there is obvious FRET activity, which could indicate that the DRP1E-XFP protein constructs are functional as DRP1E has previously been shown to polymerise into macromolecular helices.

Images shown are a slice from a Z-stack. I) CFP fluorescence channel; II) YFP fluorescence channel; III) CFP FRET channel; IV) YFP FRET channel; V) Autofluorescence channel; VI) Brightfield;

been shown to polymerise to form macromolecular helices (**Hong *et al.*, 2003; Praefcke and McMahon, 2004; Fujimoto *et al.*, 2010**).

5.5.2 PIP2A-C/FYP and RBOHD-YFP Gene Constructs Localise to the Cell Membrane

Expression of the created PIP2A and RBOHD fluorescent protein gene constructs found that both PIP2A and RBOHD localised to the plasma membrane as expected (**Fig 5.I**). PIP2A and RBOHD fluorescence at the cell membrane varied in intensity and appeared to form defined patches, which could indicate an association to specific membrane microdomains (**Li *et al.*, 2011; Hao *et al.*, 2014; Minami *et al.*, 2015; Ueda *et al.*, 2016**). Fluorescent protein expression of PIP2A and RBOHD appeared identical in all observed transformed protoplasts and PIP2A-CFP and PIP2A-YFP displayed identical fluorescent localisation. An RBOHD-CFP gene construct was created, however the YFP variant appeared to give significantly better fluorescence and so the RBOHD-YFP gene construct was used preferentially.

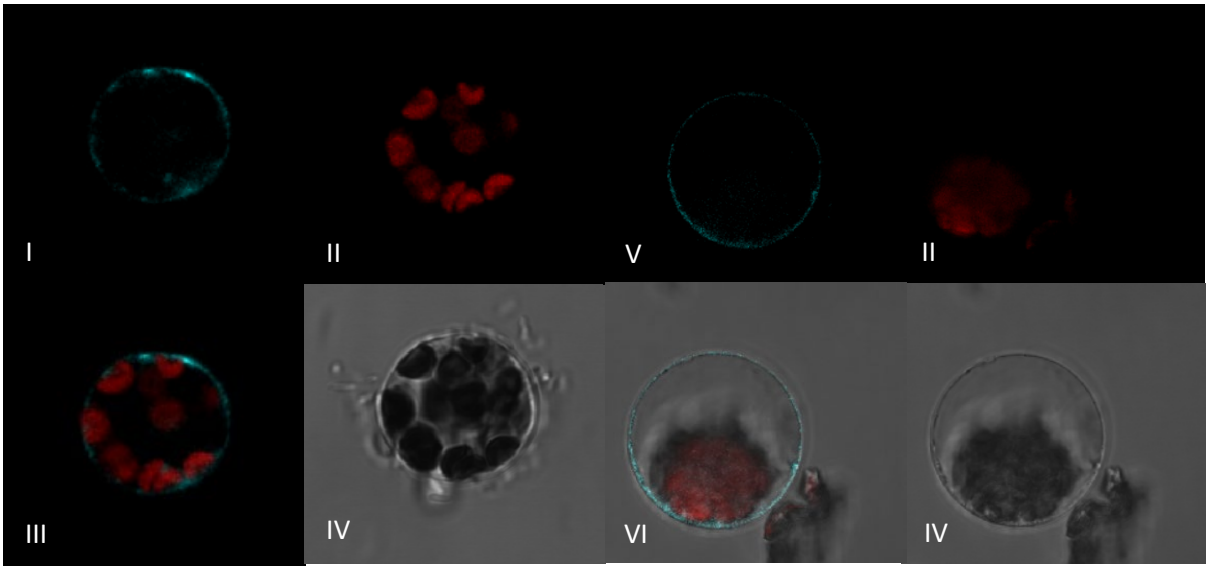

Figure 5.I) Expression of PIP2A-CFP and RBOHD-YFP in *Arabidopsis* protoplasts. Both RBOHD and PIP2A fluorescent protein fusions were found to localise non-uniformly to the plasma membrane. PIP2A-CFP and PIP2A-YFP fluorescent protein fusions exhibited the same localisation in all observed transformed protoplasts. I) PIP2A-CFP channel; II) Autofluorescence channels; III) PIP2A-CFP and Autofluorescence channel overlay; IV) Brightfield; V) RBOHD-YFP Channel; VI) RBOHD-YFP, Autofluorescence and Brightfield overlay. Images shown are from a slice of 2 separate Z-stacks.

5.5.3 PIP2A and DRP1E Appear to Co-localise at the Cell Membrane

DRP1E-YFP and PIP2A-CFP were co-expressed in *Arabidopsis* protoplasts and subjected to a confocal FRET experiment. No statistical analysis has been conducted on putative FRET interactions, however the collected images clearly indicate a FRET interaction between PIP2A-CFP and co-expressed DRP1E-YFP. Similar FRET interactions were identified in all observed transformed protoplasts.

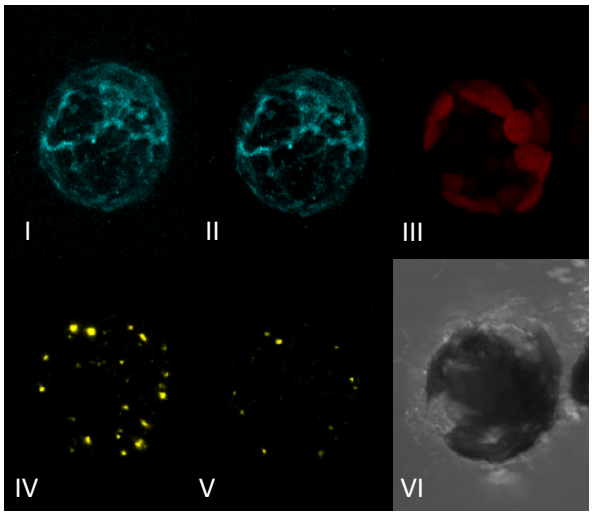

Figure 5.J) Co-expression of PIP2A-CFP and DRP1E-YFP in *Arabidopsis* protoplasts.

FRET experiments with PIP2A-CFP and DRP1E-YFP consistently found strong FRET interactions at the cell membrane, but not in the cytoplasm.

Images shown are a max projection.
I) CFP fluorescence channel; II) CFP FRET channel; III) Autofluorescence channel; IV YFP fluorescence channel; V) YFP FRET channel; VI) Brightfield;

5.6 Conclusions and Discussion

An analysis of the results detailed in chapters 3 & 4 identified the role of DRP1E in clathrin-mediated endocytosis as the most promising potential point of convergence between DRP1E and the accepted carbon dioxide specific signalling pathways that are involved in stomatal closure. Stomatal bioassay experiments on epidermal peels, with treatment of the clathrin-mediated endocytosis inhibitor Tyrophostin-A23 (tyr-A23), found that treatment with tyr-A23 severely inhibited stomatal closure in response to elevated (1000ppm) CO_2 in Col-0. Similar bioassay experiments found that treatment with tyr-A23 partially disrupted stomatal closure in response to ABA, however both Col-0 and EO_2 were able to elicit a significant ABA-induced reduction in stomatal aperture whilst treated with tyr-A23. These two experiments could indicate that clathrin mediated endocytosis plays a more significant role in CO_2 induced stomatal closure compared to ABA-induced closure.

To further investigate this possibility, a pair of confocal microscopy vesicle assays were conducted using the fluorescent styryl membrane dye FM4-64 and tyr-A23. These studies found that EO_2 guard cells displayed consistently decreased vesicle counts compared to Col-0 when treated and in untreated controls. It was found that treatment with 1000ppm CO_2 or 5µM ABA induced a significant increase in vesicle count in both Col-0 and EO_2, however treatment with tyr-A23 significantly reduced vesicle count in both Col-0 and EO_2 even when treated with CO_2 or ABA. Unexpectedly,

assessment of the normalised vesicle count found that EO_2 exhibited a WT vesicle response to both 1000ppm CO_2 and 5µM ABA, which could indicate that it is not the rate of endocytosis that is responsible for the CO_2 insensitive phenotype displayed by the EO_2 mutant and Col-0 treated with 30µM tyr-A23. This instead raises the possibility that it directed endocytosis of specifically targeted cargo proteins that leads to the carbon dioxide insensitive phenotype, rather than absolute rate of clathrin mediated endocytosis.

Preliminary studies using newly created fluorescent protein gene constructs indicate that DRP1E may interact with PIP2A at the plasma membrane and appear to confirm the findings of previous studies that DRP1E localises to punctate spots at the cell membrane and in the cytoplasm.

Chapter 6 – Discussion

6.1 Overview

The purpose of this thesis was to characterise the stomatal phenotype of the novel EO_2 mutant, which was identified as having an impaired response to elevated atmospheric carbon dioxide concentrations and a WT response to the plant hormone Abscisic Acid (ABA), to provide new insight in to carbon dioxide specific signalling in stomatal closure responses. Initial characterisation by Dr Kai Peng (**Peng, 2008**) found that EO_2 was inhibited in stomatal closure in response to elevated CO_2 but had wild type responses to exogenous ABA and calcium and had reduced stomatal density when grown under elevated CO_2. The inhibited CO_2 stomatal closure response and WT ABA response were confirmed by experiments conducted in this thesis (Chapter 3). Next generation sequencing of the EO_2 mutant population identified DRP1E as a potential candidate for the causative gene of the EO_2 stomatal phenotype and the presence of a C929T SNP in the DRP1E Coding Sequence (CDS) was confirmed by sanger sequencing. This was investigated in experiments detailed in this thesis and DRP1E was found to be allelic to the EO_2 mutation through elevated CO_2 bioassay of the F1 of EO_2 x *drp1e* crosses. The carbon dioxide insensitive stomatal response and WT ABA response of EO_2 was confirmed in two independent *drp1e* T-DNA knockout lines GABI-KAT_168C11.08 (GK08) and SALK_206052C (SK206), further confirming that *DRP1E* is the causative gene for the EO_2 mutant phenotype. The inhibited stomatal closure phenotype of *drp1e*, combined with the WT response to ABA and exogenous Ca^{2+}, make DRP1E a promising target for further research as these phenotypes indicate that DRP1E is involved specifically in carbon dioxide signalling pathways upstream of established ABA closure pathways.

6.2 Summary of Physiological Experiments

Having confirmed the CO_2-insensitive, ABA WT phenotype of EO_2 in experiments on isolated epidermal peels, it seemed logical to further investigate EO_2 gas exchange responses in intact leaves. In Chapter 4, Infra-Red Gas Analyser (IRGA) experiments found that the carbon dioxide-insensitive phenotype of EO_2 and *drp1e* mutants was conserved at a whole plant level, as these plants exhibited no significant reduction in transpiration rate after exposure to elevated atmospheric CO_2. IRGA experiments also found that EO_2 and *drp1e* mutants had consistently reduced transpiration rates and increased carbon assimilation rates during periods of light, both at ambient and elevated CO_2, although transpiration rate and carbon assimilation rate both displayed WT values during periods of darkness. Gravimetric transpiration and water use efficiency experiments found that EO_2 and *drp1e*

lines displayed increased water use efficiency (WUE) and decreased transpiration rates compared to Col-0 over a 38-hour diurnal cycle.

6.3 Summary of Endocytic Inhibitor Assays

Chapter 5 consolidated the findings of chapters 3 and 4 against the existing literature on DRP1E function and known elements of the CO_2-specific stomatal closure pathway, identifying the role of DRP1E in clathrin-mediated endocytosis (CME) as a promising avenue for further research. Stomatal bioassays using the CME inhibitor tyrphostin-A23 (tyr-A23) found that inhibition of CME severely inhibited stomatal closure in response to elevated [CO_2] but had only an intermediate effect on stomatal closure in response to ABA, as both Col-0 and EO_2 still exhibited a significant closure response to ABA that approached WT levels when treated with tyr-A23. Confocal microscopy endosome assays using the fluorescent styryl membrane dye FM4-64 found that EO_2 had a consistently lower count of FM4-64 labelled endosomes compared to Col-0 in all treatments. Confocal endosome assays found, using normalised endosome counts, that EO_2 exhibited the same proportional change in endosome count as WT in response to elevated CO_2 and ABA. It was therefore found that EO_2 displayed a WT endosomal response to ABA and elevated CO_2, which appeared contradictory to the earlier findings outlined in chapter 5. Preliminary studies using fluorescent gene constructs of DRP1E, PIP2A and RBOHD, created by the author for use in this thesis, corroborate the findings of **Jin *et al.*, 2003; Tang *et al.*, 2006; Minami *et al.*, 2015** that DRP1E localises to punctate spots in the cytoplasm. These preliminary studies further indicated that DRP1E likely associates with PIP2A at the cell membrane, as interactions were consistently observed during FRET experiments on *Arabidopsis* protoplasts co-expressing PIP2A-CFP and DRP1E-YFP.

6.4 Discussion

DRP1s have an established role in clathrin-mediated endocytosis through GTP-dependent polymerisation to form macromolecular helices, which adhere to and sever membrane tubules at clathrin coated pits, thereby producing free clathrin coated vesicles in the cytoplasm. It therefore seems highly unlikely that DRP1E would participate in guard cell CO_2 signalling pathways through direct signal transduction, however DRP1E could affect elevated CO_2-induced stomatal closure by regulation of the persistence of certain membrane-bound components of CO_2 signal transduction pathways at the cell membrane. The results of chapter 5 found that chemical inhibition of clathrin mediated endocytosis strongly affected stomatal closure in response to elevated CO_2 but only moderately affect stomatal closure induced by exogenous ABA (**5.3**). However, **5.4** found that EO_2 displayed FM4-64 labelled endosome counts not-significantly different from WT during treatment with either 1000ppm CO_2 or 5µM ABA, regardless of treatment with the CME inhibitor tyr-A23.

These results together indicate that rate of endocytosis or rate of membrane turnover are not directly responsible for the CO_2 insensitive phenotype displayed by EO_2 and *drp1e* mutants.

Gadeyne *et al.*, 2014 identified the TPLATE complex as a key player in plant clathrin mediated endocytosis and established that the *Arabidopsis* TPLATE complex is a hetero-octomeric protein complex that associates with DRP1A/C/E, DRP2A/B, all components of clathrin triskelia, actin filaments and the AP2 complex via several different TPLATE substituent proteins. Several of the proteins identified by **Gadeyne *et al.*, 2014** have as yet unknown functions and based on its role as an early binding factor in clathrin coated pit formation and as a hub for coordination of multiple elements involved in CME, it is highly likely that the TPLATE complex is involved in recruiting protein factors that specifically recognise particular cargo proteins at the cell membrane. This would allow for targeted endocytosis of specific membrane proteins, which is a logical and indeed necessary function for cell homeostasis. The results of chapter 5 showed that CME is important for correct stomatal responses to elevated CO_2 but that there is no deviance in endosome number compared to WT upon treatment with high CO_2. These results, in combination, indicate that targeted clathrin-mediated endocytosis of specific membrane bound carbon dioxide signalling components may play a significant role in stomatal responses to elevated CO_2.

As presented in **1.2.2**, in the current model for CO_2 signalling in elevated [CO_2] induced stomatal closure PIP2A redundantly allows passage of dissolved $(CO_2)_{aq}$ across the cell membrane where it is immediately converted into $(H_2CO_3)_{aq}$ by PIP2A-associated βCA4. The $(H_2CO_3)_{aq}$ dissociates to form HCO_3^- at cytosolic pH and the increase in cytosolic [HCO_3^-] stimulates RHC1 and MPK12 activity via an unknown mechanism, which both inhibit HT1 activity via independent pathways. Inhibition of HT1 by RHC1 and/or MPK12 relieves inhibition of OST1, increasing the proportion of active OST1 and promoting stomatal closure through ABA-dependent activation of SLAC1 via increased OST1 sensitivity to ABA. However MPK12 has also been shown to directly increase SLAC1 activity in response to elevated [HCO_3^-] independently of ABA (**Hu *et al.*, 2010; Xue *et al.*, 2011; Chater *et al.*, 2015; Li *et al.*, 2015; Tian *et al.*, 2015; Hashimoto-Sugimoto *et al.*, 2016; Jakobson *et al.*, 2016; Wang *et al.*, 2016**).

Of the components mentioned in the above CO_2 induced stomatal closure signalling pathway, many of the proteins are intrinsic membrane proteins or membrane-associated proteins, including PIP2A, RHC1, HT1, RBOHD, RBOHF and SLAC1 (**Figure 6A**). This provides multiple potential points of interaction between CO_2 signalling proteins and Clathrin-mediated endocytosis, which could likely act as a method of regulating CO_2 stomatal signalling pathways through selective internalisation of membrane-bound CO_2 signalling proteins.

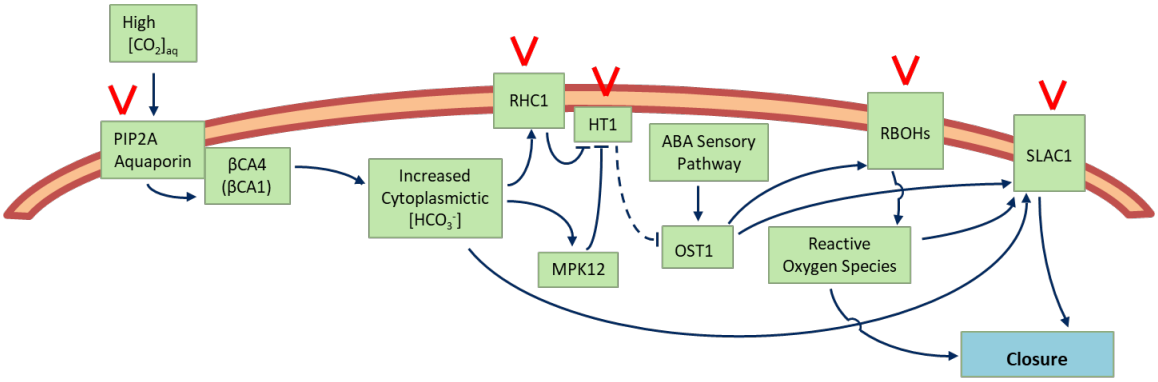

Figure 6A) Diagram of the current putative carbon dioxide signalling pathways for elevated carbon dioxide-induced stomatal closure. The intrinsic membrane proteins PIP2A, RHC1, RBOHD, RBOHF and SLAC1, and the membrane associated protein HT1 provide potential points of interaction with endocytic pathways as a means of regulating CO_2 sensory pathways through selective internalisation of relevant membrane bound signalling components. Intrinsic membrane proteins and membrane-associated protein are denoted by red markers.

The results presented in this thesis found that *drp1e* mutants displayed significantly reduced responses to elevated CO_2 and WT responses to ABA. The combination of these two phenotypes indicates that the significant interaction of DRP1E with CO_2 sensory pathways occurs upstream of integration of CO_2-specific pathways with ABA-induced stomatal closure pathways. This therefore indicates that the function and dynamics of OST1 and SLAC1 are not significantly perturbed in *drp1e* mutants, as disruption of either OST1 or SLAC1 has been shown to cause severe ABA-insensitive stomatal closure phenotypes (**Vahisalu *et al.*, 2008; Geiger *et al.*, 2009**). Furthermore, as it was found that *drp1e* mutants display reduced stomatal closure responses to elevated $[CO_2]$ (**Chapter 3, Chapter 4**), this can be taken to mean that reduced DRP1E-dependent endocytosis of certain CO_2 specific signalling components resulted in a reduced stomatal response to elevated $[CO_2]$. Decreased rates of endocytosis of certain CO_2 signalling components would result in an increase in persistence and quantity of these proteins at the cell membrane. For this to cause a reduced stomatal closure response to CO_2, this could equate to:

- An increase in persistence of negative regulators of CO_2-induced stomatal closure at the cell membrane
- Sequestering of CO_2 signalling proteins at sites of unsuccessful endocytosis events, for example in terminated CCP formation, rendering the sequestered proteins ineffective.
- Increased quantities of CO_2 signalling proteins at the cell membrane in an inhibited or inactive form, for example as poly-molecular protein rafts.

HT1 kinase acts through inhibition of OST1 kinase activity and is the only negative regulator of CO_2 induced stomatal closure identified thus far **(Tian *et al.*, 2015; Hashimoto-Sugimoto *et al.*, 2016**). An accumulation of HT1 at the cell membrane could reduce the quantity of active OST1, thereby reducing stomatal closure responses to elevated CO_2. Confocal experiments or western blot experiments on *drp1e* mutant plants transformed XFP-tagged HT1 would allow further investigation of the possibility of an accumulation of HT1 at the cell membrane.

The process of clathrin mediated endocytosis is executed in a number of steps. Firstly TPLATE and AP2 complexes are recruited to a CCP initiation site with a concentration of specifically targeted Cargo proteins, clathrin triskelia are then recruited to the CCP initiation site and polymerise, giving rigidity to the forming CCP. Actin filaments are formed at the CCP site and extrude the CCP into the cytoplasm, as further polymerisation of clathrin triskelia stabilises the CCP structure. Only after the CCP is fully extruded into the cytoplasm do DRP1s and DRP2s bind to the CCP site, restricting the membrane joining the CCP to the cell membrane into a thin tubule before enacting membrane scission to form a mature CCV within the cytoplasm. The associated CME proteins then disassociate resulting in a free cytoplasmic vesicle (**Uehlein *et al.*, 2008; Bednarek and Backues, 2010; Fujimoto *et al.*, 2010; McMahon and Boucrot, 2011; Taylor, 2011; Fujimoto and Tsutsumi, 2014; Fan *et al.*, 2015**). The late role of DRP1s in CCP formation raises the possibility of CCPs being formed but being unable to enact proper scission from the cell membrane in drp1e mutants following binding of CO_2 signalling proteins as cargo. As DRP1E has been shown to be at least partially redundant to DRP1A, this would be unlikely to affect net rates of cell membrane turnover, however as DRP1E has been shown in this thesis to display some specificity for CO_2 signalling components, this could feasibly sequester CO_2 specific signalling proteins in terminated CCP sites (**Hong *et al.*, 2003; Bednarek and Backues, 2010**). This possibility is largely speculative and it is likely that terminated CCPs would dissociate after a period of time, returning the invaginated membrane to the cell membrane, however attempted CCP formation at multiple sites could effectively decrease the quantity of active CO_2 signalling proteins at the cell membrane, thereby resulting in a reduced response to elevated [CO_2]. Sequestering of CO_2 signalling proteins in this way could also help to explain how a decrease in rates of directed endocytosis of CO_2 signalling proteins could cause a reduced response to increased CO_2, as sequestering of positive regulators of CO_2 induced stomatal closure such as PIP2A, RHC1 and the RBOHs would inhibit the CO_2 induced stomatal closure response.

A decrease in selective endocytosis of membrane bound CO_2 signalling components could lead to a build-up of CO_2 signalling proteins at the cell membrane, which could accumulate into poly-molecular protein 'rafts' in membrane microdomains, which are established sites for endocytosis. Both PIP2A and RBOHD have been shown to form poly-molecular protein 'rafts' at the cell

membrane prior to their internalisation and have been shown to have their dynamics at the cell membrane regulated by CME and MME in response to external environmental signals such as NaCl (**Li *et al.*, 2011; Hao *et al.*, 2014; Fan *et al.*, 2015**). RBOHD has been shown by **McLachlan D *et al*** (Guard Cell Group, personal communication) to be preferentially involved in CO_2 induced stomatal closure over RBOHF. Therefore 'rafting' of RBOHD on the cell membrane prior to failed endocytosis events in *drp1e* mutants could explain the reduced CO_2-induced stomatal closure response as the close proximity of the proteins could interfere with their function and result in a smaller ROS signal, leading to a reduced stomatal closure response. An accumulation of PIP2A in protein rafts at the cell membrane with associated βCA4 could explain the increased carbon assimilation rates and increased WUE observed in *drp1e* mutants in **Chapter 4**, as an accumulation of PIP2A with associated carbonic anhydrases could enhance $(CO_2)_{aq}$ diffusion into the cell and concentration of HCO_3^- in the cytoplasm.

Since PIP2A and RBOHD have previously been shown to be internalised via endocytosis and as the above reasoning identified an accumulation of these proteins at the cell membrane as potentially explaining the phenotypes observed in *drp1e* mutants in this thesis, so the dynamics of these proteins in *drp1e* mutants seems a logical direction for future research. Fluorescent protein fusions of PIP2A, RBOHD and DRP1E were created with the aim of assessing the persistence of PIP2A and RBOHD at the cell membrane in EO_2 and *drp1e* mutants and to assess the colocalization of these proteins with DRP1E at the cell membrane. Preliminary confocal microscopy and FRET experiments appeared to confirm the colocalization of DRP1E with PIP2A at the cell membrane, however these results are insufficient to provide conclusive results. Unfortunately, due to time restrictions, these fluorescent protein fusions were not used extensively and their use in a number of further experiments, discussed in **6.6**, could be powerful tools to better elucidate the role of DRP1E in carbon dioxide-specific stomatal closure responses.

6.5 Summary

In summary, this thesis reports that the *drp1e* SNP mutant and *drp1e* T-DNA lines display inhibited stomatal closure responses that are specific to CO_2 induced closure. These results link clathrin mediated endocytosis with established guard cell signalling pathways. Further experiments implicated targeted endocytosis of specific CO_2 signalling proteins as the predominant interaction between CME and CO_2 signalling, likely as a method of regulating CO_2 induced closure pathways. The membrane associated proteins HT1, PIP2A and RBOHD have been identified as potential convergence points between CO_2 signalling and CME and are promising targets for future research. The work presented in this thesis identified CME as a largely novel (**Larson *et al.*, 2017**) method of regulating stomatal movements in response to environmental stimuli, opening an exciting new area of stomatal research.

6.6 Proposals for Further Experiments

I) Completion of proper, experimentally valid, FRET experiments with PIP2A, RBOHD and DRP1E fluorescent protein fusions would provide good evidence for DRP1E playing a role in the regulation of PIP2A and RBOHD persistence at the plasma membrane. Further FRET experiments co-expressing PIP2A/RBOHD fluorescent protein fusions in *drp1e* mutant line with a *DRP1E-C929T* fluorescent protein that replicates the EO_2 point mutation could elucidate the putative interaction of DRP1E with PIP2A/RBOHD.

II) Monitoring the dynamics of fluorescently tagged PIP2A and RBOHD, after treatment with elevated CO_2, in stably transformed transgenic EO_2, WT and *drp1e* lines would provide insight as to the retention of PIP2A and RBOHD at the cell membrane. This would investigate the possibility of PIP2A or RBOHD rafting on the cell membrane in *drp1e* mutants.

III) Apoplastic confocal microscopy ROS assays using H_2DCFDA on *drp1e* mutants could investigate whether RBOHD activity is impaired in *drp1e* mutants.

IV) Confocal assays using a ratiometric fluorescent pH indicator could be conducted to monitor the rapidity of cytoplasm acidification after the application of extra-cellular bicarbonate as a means of assessing permeability of the cell membrane to $(CO_2)_{aq}$ in *drp1e* mutants. This could insight into the possibility of increased PIP2A presence at the cell membrane leading to more rapid uptake of $(CO_2)_{aq}$ in *drp1e* mutants.

V) Confocal experiments or western blot experiments on DRM fractions from cells expressing fluorescently tagged HT1 could assess the possibility of HT1 accumulation at the cell membrane in *drp1e* mutants.

References

Acharya, B. R., Jeon, B. W., Zhang, W. & Assmann, S. M. Open Stomata 1 (OST1) is limiting in abscisic acid responses of Arabidopsis guard cells. *New Phytol.* **200**, 1049–1063 (2013).

Ache, P. *et al.* GORK , a delayed outward rectifier expressed in guard cells of Arabidopsis thaliana , is a K+ selective , K+ sensing ion channel. *FEBS Lett.* **486**, 93–98 (2000).

Alonso, J. M. *et al.* Genome-Wide Insertional Mutagenesis of Arabidopsis thaliana. *Science (80-.).* **301**, 653–657 (2003).

Arimura, S. -i. *et al.* Arabidopsis ELONGATED MITOCHONDRIA1 Is Required for Localization of DYNAMIN-RELATED PROTEIN3A to Mitochondrial Fission Sites. *Plant Cell* **20**, 1555–1566 (2008).

Aung, K. & Hu, J. The Arabidopsis Tail-Anchored Protein PEROXISOMAL AND MITOCHONDRIAL DIVISION FACTOR1 Is Involved in the Morphogenesis and Proliferation of Peroxisomes and Mitochondria. *Plant Cell* **23**, 4446–4461 (2011).

Aung, K. & Hu, J. The Arabidopsis peroxisome division mutant pdd2 is defective in the dynamin-related protein3A (DRP3A) gene. *Plant Signal. Behav.* **4**, 542–544 (2009).

Aung, K. & Hu, J. Differential Roles of Arabidopsis Dynamin-Related Proteins DRP3A, DRP3B, and DRP5B in Organelle Division. *J. Integr. Plant Biol.* **54**, 921–931 (2012).

Aung, K., Zhang, X. & Hu, J. Peroxisome Division and Proliferation in Plants. *Biochmical Soc. Trans.* **38**, 817–822 (2010).

Backues, S. K., Korasick, D. A., Heese, A. & Bednarek, S. Y. The *Arabidopsis* Dynamin-Related Protein2 Family Is Essential for Gametophyte Development. *Plant Cell* **22**, 3218–3231 (2010).

Banbury, D. N., Oakley, J. D., Sessions, R. B. & Banting, G. Tyrphostin A23 inhibits internalization of the transferrin receptor by perturbing the interaction between tyrosine motifs and the medium chain subunit of the AP-2 adaptor complex. *J. Biol. Chem.* **278**, 12022–12028 (2003).

Beck, M., Zhou, J., Faulkner, C., MacLean, D. & Robatzek, S. Spatio-Temporal Cellular Dynamics of the *Arabidopsis* Flagellin Receptor Reveal Activation Status-Dependent Endosomal Sorting. *Plant Cell* **24**, 4205–4219 (2012).

Bednarek, S. Y. & Backues, S. K. Plant dynamin-related protein families DRP1 and DRP2 in plant development. *Biochem. Soc. Trans.* **38**, 797–806 (2010).

Casson, S. A. & Hetherington, A. M. Environmental regulation of stomatal development. *Curr. Opin. Plant Biol.* **13**, 90–95 (2010).

CeBiTech (Centre for Biotechnology (Germany)). GABI-Kat. *Kleinboetline et al, 2012* (2012). Available at: https://www.gabi-kat.de/db/seqsearch.php. (Accessed: 20th May 2017)

Chater, C. *et al.* Elevated CO2-Induced Responses in Stomata Require ABA and ABA Signaling. *Curr. Biol.* **25**, 2709–2716 (2015).

Collings, D. A. *et al.* Arabidopsis dynamin-like protein DRP1A: A null mutant with widespread defects in endocytosis, cellulose synthesis, cytokinesis, and cell expansion. *J. Exp. Bot.* **59**, 361–376 (2008).

Cornforth, J., Milborrow, B. & Ryback, G. Synthesis of +-Abscisin II. *Nature* **4985**, 715–715 (1965).

Costa, J. M. *et al. OPEN ALL NIGHT LONG* : The Dark Side of Stomatal Control. *Plant Physiol.* **167**, 289–294 (2015).

Cutler, S. R., Rodriguez, P. L., Finkelstein, R. R. & Abrams, S. R. Abscisic Acid : Emergence of a Core Signaling Network. *Annu. Rev. Plant Biol.* **61**, 651–682 (2010).

Danquah, A., Zelicourt, A. De, Colcombet, J. & Hirt, H. The role of ABA and MAPK signaling pathways in plant abiotic stress responses. *Biotechnol. Adv.* **32**, 40–52 (2014).

Dhonukshe, P. *et al.* Clathrin-Mediated Constitutive Endocytosis of PIN Auxin Efflux Carriers in Arabidopsis. *Curr. Biol.* **17**, 520–527 (2007).

Dodd, A. N., Kudla, J. & Sanders, D. The Language of Calcium Signaling. *Annu. Rev. Plant Biol.* **61**, 593–620 (2010).

Dutilleul, C. *et al.* Leaf Mitochondria Modulate Whole Cell Redox Homeostasis, Set Antioxidant Capacity, and Determine Stress Resistance through Altered Signaling and Diurnal Regulation. *Plant Cell* **15**, 1212–1226 (2003).

Eckardt, N. A. Aquaporins and Chloroplast Membrane Permeability. *Plant Cell Online* **20**, 499–499 (2008).

Elgass, K., Pakay, J., Ryan, M. T. & Palmer, C. S. Recent advances into the understanding of mitochondrial fission. *Biochim. Biophys. Acta* **1833**, 150–161 (2013).

ELIXIR. Primer3, v4.1.0. (2006). Available at: http://primer3.ut.ee/.

Engineer, C. B. *et al.* Carbonic anhydrases, EPF2 and a novel protease mediate CO2control of stomatal development. *Nature* **513**, 246–250 (2014).

Engineer, C. *et al.* CO2 sensing and CO2 regulation of stomatal conductance: advances and open questions. *Trends Plant Sci.* **21**, 16–30 (2016).

FABRE, N., REITER, I. M., BECUWE-LINKA, N., GENTY, B. & RUMEAU, D. Characterization and expression analysis of genes encoding alpha and beta carbonic anhydrases in Arabidopsis. *Plant. Cell Environ.* **30**, 617–629 (2007).

Fan, L., Li, R., Pan, J., Ding, Z. & Lin, J. Endocytosis and its regulation in plants. *Trends Plant Sci.* **20**, 388–397 (2015).

Ferguson, S. M. & De Camilli, P. Dynamin, a membrane-remodelling GTPase. *Nat. Rev. Mol. Cell Biol.* **13**, 75–88 (2012).

Ford, M., Jenni, S. & Nunnari, J. The Crystal Sturcture of Dynamin. *Nature* **477**, 561–566 (2014).

Friedman, J. R. & Nunnari, J. Mitochondrial form and function. *Nature* **505**, 335–343 (2014).

Fromm, S., Braun, H. & Peterhansel, C. Mitochondrial gamma carbonic anhydrases are required for complex I assembly and plant reproductive development. *New Phytol.* **211**, 194–207 (2016).

Fujimoto, M. *et al.* Arabidopsis dynamin-related proteins DRP2B and DRP1A participate together in clathrin-coated vesicle formation during endocytosis. *PNAS* **107**, 6094–6099 (2010).

Fujimoto, M. *et al.* Arabidopsis dynamin-related proteins DRP3A and DRP3B are functionally redundant in mitochondrial fission, but have distinct roles in peroxisomal fission. *Plant J.* **58**, 388–400 (2009).

Fujimoto, M., Arimura, S. I., Nakazono, M. & Tsutsumi, N. Arabidopsis dynamin-related protein DRP2B is co-localized with DRP1A on the leading edge of the forming cell plate. *Plant Cell Rep.* **27**, 1581–1586 (2008).

Fujimoto, M. & Tsutsumi, N. Dynamin-related proteins in plant post-Golgi traffic. *Front. Plant Sci.* **5**, 1–8 (2014).

Gadeyne, A. *et al.* The TPLATE adaptor complex drives clathrin-mediated endocytosis in plants. *Cell* **156**, 691–704 (2014).

Garcia-Hernandez, M. *et al.* TAIR: A resource for integrated Arabidopsis data. *Funct. Integr. Genomics* **2**, 239–253 (2002).

Geiger, D. *et al.* Activity of guard cell anion channel SLAC1 is controlled by drought-stress signaling kinase-phosphatase pair. *PNAS* **106**, 21425–21430 (2009).

Gleave, a P. A versatile binary vector system with a T-DNA organisational structure conductive to efficient intergration of cloned DNA into the plant genome. *Plant Mol. Biol.* **20**, 1203–1207 (1992).

Goh, C. H., Ko, S. M., Park, Y. Il, Kim, C. S. & Song, K. J. Regulation of Dark-Induced Stomatal Closure in Arabidopsis Dynamin-Like Protein 1E (adl1e) Mutant Leaves. *J. Plant Biol.* **54**, 112–118 (2011).

Gray, J. E. *et al.* The HIC signalling pathway links CO2 perception to stomatal development. *Nature* **408**, 713–716 (2000).

Gu, F. *et al.* The Arabidopsis CSLD5 functions in cell plate formation in a cell cycle dependent manner. *Plant Cell* **Advance Pu**, tpc.00203.2016 (2016).

Gudesblat, G. E., Torres, P. S. & Vojnov, A. A. Stomata and pathogens: Warfare at the gates. *Plant Signal. Behav.* **4**, 1114–6 (2009).

Hao, H. *et al.* Clathrin and Membrane Microdomains Cooperatively Regulate RbohD Dynamics and Activity in Arabidopsis. *Plant Cell* **26**, 1729–1745 (2014).

Harvard University. A Summary of Error Propagation. 5 (2007). doi:10.3390/s17020400

Hashimoto, M. *et al.* Arabidopsis HT1 kinase controls stomatal movements in response to CO2. *Nat. Cell Biol.* **8**, 391–397 (2006).

Hashimoto-Sugimoto, M. *et al.* Dominant and recessive mutations in the Raf-like kinase HT1 gene completely disrupt stomatal responses to CO2in Arabidopsis. *J. Exp. Bot.* **67**, 3251–3261 (2016).

He, J. *et al.* The BIG protein distinguishes the process of CO2-induced stomatal closure from the inhibition of stomatal opening by CO2. *New Phytol.* 1–10 (2018). doi:10.1111/nph.14957

Hetherington, A. M. & Woodward, F. I. The role of stomata in sensing and driving environmental change. *Nature* **424**, 901–908 (2003).

Hong, Z. *et al.* A unified nomenclature for Arabidospsis dynamin-related large GTPase based on homology and possible function. *Plant Mol. Biol.* **53**, 261–265 (2003).

Hong, Z., Zhang, Z., Olson, J. M. & Verma, D. P. A novel UDP-glucose transferase is part of the callose synthase complex and interacts with phragmoplastin at the forming cell plate. *Plant Cell* **13**, 769–79 (2001).

Hong, Z., Geisler-Lee, C. J., Zhang, Z. & Verma, D. P. S. Phragmoplastin dynamics: Multiple forms, microtubule association and their roles in cell plate formation in plants. *Plant Mol. Biol.* **53**, 297–312 (2003).

Hõrak, H. *et al.* A Dominant Mutation in the HT1 Kinase Uncovers Roles of MAP Kinases and GHR1 in CO 2 -Induced Stomatal Closure. *Plant Cell* **28**, 2493–2509 (2016).

Hsu, P.-K. *et al.* Abscisic acid-independent stomatal CO 2 signal transduction pathway and convergence of CO 2 and ABA signaling downstream of OST1 kinase. *PNAS* **115**, E9971–E9980 (2018).

Hu, H. *et al.* Carbonic anhydrases are upstream regulators of CO2-controlled stomatal movements in guard cells. *Nat. Cell Biol.* **12**, 87–93 (2010).

Hu, H. *et al.* Distinct Cellular Locations of Carbonic Anhydrases Mediate Carbon Dioxide Control of Stomatal Movements. *Plant Physiol.* **169**, 1168–1178 (2015).

Huang, J. *et al.* Arabidopsis dynamin-related proteins, DRP2A and DRP2B, function coordinately in post-Golgi trafficking. *Biochem. Biophys. Res. Commun.* **456**, 238–244 (2015).

Imes, D. *et al.* Open stomata 1 (OST1) kinase controls R – type anion channel QUAC1 in Arabidopsis guard cells. *Plant J.* **74**, 372–382 (2013).

Jakobson, L. *et al.* Natural Variation in Arabidopsis Cvi-0 Accession Reveals an Important Role of MPK12 in Guard Cell CO2 Signaling. *PLoS Biol.* **14**, 1–25 (2016).

Jin, J. B. *et al.* The Arabidopsis dynamin-like proteins ADL1C and ADL1E play a critical role in mitochondrial morphogenesis. *Plant Cell* **15**, 2357–2369 (2003).

Jurgens, G. Cytokinesis in Higher Plants. *Annu. Rev. Plant Biol.* **56**, 281–299 (2005).

Jürgens, G. Membrane Trafficking in Plants. *Annu. Rev. Cell Dev. Biol.* **20**, 481–504 (2004).

Jürgens, G. *et al.* Plant cytokinesis: a tale of membrane traffic and fusion. *Biochem. Soc. Trans.* **43**, 73–78 (2015).

Kadota, Y. *et al.* Direct Regulation of the NADPH Oxidase RBOHD by the PRR-Associated Kinase BIK1 during Plant Immunity. *Mol. Cell* **54**, 43–55 (2014).

Kang, B.-H., Busse, J. S., Dickey, C., Rancour, D. M. & Bednarek, S. Y. The Arabidopsis Cell Plate-Associated Dynamin-Like Protein, ADL1Ap, Is Required for Multiple Stages of Plant Growth and Development. *Plant Physiol.* **126**, 47–68 (2001).

Kang, B. H., Rancour, D. M. & Bednarek, S. Y. The dynamin-like protein ADL1C is essential for plasma membrane maintenance during pollen maturation. *Plant J.* **35**, 1–15 (2003).

Kang, B.-H., Busse, J. S. & Bednarek, S. Y. Members of the Arabidopsis dynamin-like gene family, ADL1, are essential for plant cytokinesis and polarized cell growth. *Plant Cell* **15**, 899–913 (2003).

Kim, T.-H., Bohmer, M., Hu, H., Nishimura, N. & Schroeder, J. I. Guard cells signal transduction network: advances in understanding abscisic acid CO2, and Ca2+ signalling. *Annu. Rev. Plant Biol.* **61**, 561–591 (2010).

Kleinboelting, N., Huep, G., Kloetgen, A., Viehoever, P. & Weisshaar, B. GABI-Kat SimpleSearch: New features of the Arabidopsis thaliana T-DNA mutant database. *Nucleic Acids Res.* **40**, 1211–1215 (2012).

Koelle, M. Easy Subcloning. 8–11 (2008).

Koelle, M. Transformation of Compenent E . coli. (1998).

Konopka, C. A., Backues, S. K. & Bednarek, S. Y. Dynamics of Arabidopsis Dynamin-Related Protein 1C and a Clathrin Light Chain at the Plasma Membrane. *Plant Cell Online* **20**, 1363–1380 (2008).

Konopka, C. A. & Bednarek, S. Y. Comparison of the Dynamics and Functional Redundancy of the Arabidopsis Dynamin-Related Isoforms DRP1A and DRP1C during Plant Development. *Plant Physiol.* **147**, 1590–1602 (2008).

Konopka, C., Schleede, J., Skop, A. & Bednarek, S. Dynmin and Cytokinesis. *Trafffic* **7**, 239–247 (2006).

Kuroiwa, T. *et al.* Structure, function and evolution of the mitochondrial division apparatus. *Biochim. Biophys. Acta* **1763**, 510–521 (2006).

Kwak, J. M. *et al.* NADPH oxidase *AtrbohD* and *AtrbohF* genes function in ROS-dependent ABA signaling in *Arabidopsis*. *EMBO J.* **22**, 2623–2633 (2003).

Lake, J. A. & Woodward, F. I. Response of stomatal numbers to CO2 and humidity: Control by transpiration rate and abscisic acid. *New Phytol.* **179**, 397–404 (2008).

Larson, E. R., Van Zelm, E., Roux, C., Marion-Poll, A. & Blatt, M. R. Clathrin Heavy Chain subunits coordinate endo- and exocytic traffic and affect stomatal movement. *Plant Physiol.* **175**, p708-720 (2017).

Lauber, M. H. *et al.* The Arabidopsis KNOLLE protein is a cytokinesis-specific syntaxin. *J. Cell Biol.* **139**, 1485–1493 (1997).

Lee, M. *et al.* The ABC transporter AtABCB14 is a malate importer and modulates stomatal response to CO2. *Nat. Cell Biol.* **10**, 1217–1223 (2008).

Lee, S. C., Lan, W., Buchanan, B. B. & Luan, S. A protein kinase-phosphatase pair interacts with an ion channel to regulate ABA signaling in plant guard cells. *PNAS* **106**, 21419–21424 (2009).

Leymarie, J., Lascève, G. & Vavasseur, A. Interaction of stomatal responses to ABA and CO2 in Arabidopsis thaliana. *Aust. J. Plant Physiol.* **25**, 785–791 (1998).

Leymarie, J., Vavasseur, A. & Lasceve, G. CO2 sensing in stomata of abi1-1 and abi2-1 mutants of Arabidopsis thaliana. *Plant Physiol.* **36**, 539–543 (1998).

Li, L. *et al.* Harpin Hpa1 Interacts with Aquaporin PIP1;4 to Promote the Substrate Transport and Photosynthesis in Arabidopsis. *Sci. Rep.* **5**, 1–17 (2015).

Li, X. *et al.* Single-Molecule Analysis of PIP2;1 Dynamics and Partitioning Reveals Multiple Modes of Arabidopsis Plasma Membrane Aquaporin Regulation. *Plant Cell* **23**, 3780–3797 (2011).

Logan, D. C., Scott, I. & Tobin, A. K. The genetic control of plant mitochondrial morphology and dynamics. *Plant J.* **36**, 500–509 (2003).

Logan, D. C. Mitochondrial fusion, division and positioning in plants: Figure 1. *Biochem. Soc. Trans.* **38**, 789–795 (2010).

Loveys, B. R. & Robinson, S. P. ABSCISIC ACID SYNTHESIS AND METABOLISM IN B A R L E Y LEAVES AND PROTOPLASTS. *Plant Sci.* **49**, 23–30 (1987).

Ludwig, M. Evolution of carbonic anhydrase in C4plants. *Curr. Opin. Plant Biol.* **31**, 16–22 (2016).

Lukowitz, W., Gillmor, C. S. & Scheible, W.-R. Positional Cloning in Arabidopsis. Why It Feels Good to Have a Genome Initiative Working for You. *Plant Physiol.* **123**, 795–806 (2000).

Ma, Y. *et al.* Regulators of PP2C Phosphatase Activity Function as as Abscisic Acid Sensors. *Science (80-.).* **324**, 1064–1067 (2009).

Maierhofer, T. *et al.* Site and kinase-specific phosphorylation-mediated activation of SLAC1 , a guard cell anion channel stimulated by abscisic acid. *Plant Biol.* **7**, 1–12 (2014).

Mano, S., Nakamori, C., Kondo, M., Hayashi, M. & Nishimura, M. An Arabidopsis dynamin-related protein, DRP3A, controls both peroxisomal and mitochondrial division. *Plant J.* **38**, 487–498 (2004).

Mansfield, T. A. & Jones, R. A. Effects of Abscisic Acid on Potassium Uptake and Starch Content of Stomatal Guard Cells. *Planta* **101**, 147–158 (1971).

Marchler-Bauer, A. *et al.* CDD/SPARCLE: Functional classification of proteins via subfamily domain architectures. *Nucleic Acids Res.* **45**, D200–D203 (2017).

Martin, V. *et al.* Recombinant plant gamma carbonic anhydrase homotrimers bind inorganic carbon. *FEBS Lett.* **583**, 3425–3430 (2009).

Matrosova, A. *et al.* The HT1 protein kinase is essential for red light-induced stomatal opening and genetically interacts with OST1 in red light and CO2-induced stomatal movement responses. *New Phytol.* **208**, 1126–1137 (2015).

Mcainsh, M. R., Brownlee, C. & Hetherington, A. M. Abscisic acid-induced elevation of guard cell cytosolic Ca 2 + precedes stomatal closure. *Lett. to Nat.* **343**, 186–188 (1990).

McAinsh, M. R., Evans, N. H., Montgomery, L. T. & North, K. A. Calcium signalling in stomatal responses to pollutants. *New Phytol.* **153**, 441–447 (2002).

Mcainsh, M. R., Clayton, H., Mansfield, T. A. & Hetherington, A. M. Changes in Stomatal Behavior and Guard Cell Cytosolic Free Calcium in Response to Oxidative Stress ’. *Plant Physiol.* **111**, 1031–1042 (1996).

McAusland, L. *et al.* Effects of kinetics of light-induced stomatal responses on photosynthesis and water-use efficiency. *New Phytol.* **211**, 1209–1220 (2016).

McMahon, H. T. & Boucrot, E. Molecular mechanism and physiological functions of clathrin-mediated endocytosis. *Nat. Rev. Mol. Cell Biol.* **12**, 517–533 (2011).

Melcher, K. *et al.* A gate – latch – lock mechanism for hormone signalling by abscisic acid receptors. *Nature* **462**, 602–608 (2009).

Merilo, E. *et al.* PYR/RCAR Receptors Contribute to Ozone-, Reduced Air Humidity-, Darkness-, and CO2-Induced Stomatal Regulation. *Plant Physiol.* **162**, 1652–1668 (2013).

Merlot, S. *et al.* Constitutive activation of a plasma membrane H+-ATPase prevents abscisic acid-mediated stomatal closure. *EMBO J.* **26**, 3216–3226 (2007).

Merlot, S. *et al.* Use of infrared thermal imaging to isolate Arabidopsis mutants defective in stomatal regulation. *Plant J.* **30**, 601–609 (2002).

Miart, F. *et al.* Spatio-temporal analysis of cellulose synthesis during cell plate formation in Arabidopsis. *Plant J.* **77**, 71–84 (2014).

Mickelbart, M. V. & Marler, T. E. Growth, gas exchange, and mineral relations of black sapote (Diospyros digyna Jacq.) as influenced by salinity. *Sci. Hortic. (Amsterdam).* **72**, 103–110 (1998).

Milbarrow, B. & Robinson, D. Factors Affecting the Biosynthesis of Abscisic Acid. *J. Exp. Bot.* **24**, 537–548 (1973).

Minami, A. *et al.* Arabidopsis dynamin-related protein 1E in sphingolipid-enriched plasma membrane domains is associated with the development of freezing tolerance. *Plant J.* **83**, 501–514 (2015).

Mittelheuser, C. J. & Van Steveninck, R. Stomatal Closure and Inhibition of Transpiration by RS-Abscisic acid. *Nature* **221**, 281–282 (1969).

Miyagishima, S. *et al.* A plant-specific dynamin-related protein forms a ring at the chloroplast division site. *Plant Cell* **15**, 655–665 (2003).

Miyagishima, S., Kuwayama, H., Urushihara, H. & Nakanishi, H. Evolutionary linkage between eukaryotic cytokinesis and chloroplast division by dynamin proteins. *PNAS* **105**, 15202–7 (2008).

Musa-aziz, R., Chen, L., Pelletier, M. F. & Boron, W. F. Relative CO2 /NH 3 selectivities of AQP1, AQP4, AQP5, AmtB, and RhAG. *PNAS* **106**, 5406–5411 (2008).

Musa-Aziz, R., Occhipinti, R. & Boron, W. F. Evidence from simultaneous intracellular- and surface-pH transients that carbonic anhydrase II enhances CO 2 fluxes across Xenopus oocyte plasma membranes. *Am. J. Physiol. Physiol.* **307**, C814–C840 (2014).

Mustilli, A., Merlot, S., Vavasseur, A., Fenzi, F. & Giraudat, J. Arabidopsis OST1 Protein Kinase Mediates the Regulation of Stomatal Aperture by Abscisic Acid and Acts Upstream of Reactive Oxygen Species Production. *Plant Cell* **14**, 3089–3099 (2002).

NCBI (National Centre for Biotechnology Information). Conserved Domain Search (CDS). *Marchler-Bauer et al 2017* (2017). Available at: https://www.ncbi.nlm.nih.gov/Structure/cdd/wrpsb.cgi.

NCBI (National Centre for Biotechnology Information). Align Sequences Nucleotide BLAST. (2009). Available at: https://blast.ncbi.nlm.nih.gov/Blast.cgi?PAGE_TYPE=BlastSearch&BLAST_SPEC=blast2seq&LINK_LOC=align2seq#.

NEB (New England Biolabs). NEBase Changer. (2011). Available at: http://nebasechanger.neb.com/#.

Negi, J. *et al.* CO2 regulator SLAC1 and its homologues are essential for anion homeostasis in plant cells. *Nature* **452**, 483–486 (2008).

Ng, S. *et al.* A Membrane-Bound NAC Transcription Factor, ANAC017, Mediates Mitochondrial Retrograde Signaling in Arabidopsis. *Plant Cell* **25**, 3450–3471 (2013).

Nie, Z. & Randazzo, P. Arf GAPs and membrane traffic. *J. Cell Sci.* **119**, 1203–1211 (2006).

Osteryoung, K. W. & Nunnari, J. The Division of Endosymbiotic Organelles. *Science (80-.).* **302**, 1698–1704 (2003).

Osteryoung, K. W. & Pyke, K. A. Division and Dynamic Morphology of Plastids. *Annu. Rev. Plant Biol.* **65**, 443–472 (2014).

Otegui, M. S., Mastronarde, D. N., Kang, B. H., Bednarek, S. Y. & Staehelin, L. A. Three-dimensional analysis of syncytial-type cell plates during endosperm cellularization visualized by high resolution electron tomography. *Plant Cell* **13**, 2033–2051 (2001).

Otegui, M. S. & Staehelin, L. A. Electron tomographic analysis of post-meiotic cytokinesis during pollen development in Arabidopsis thaliana. *Planta* **218**, 501–515 (2004).

Pan, R. & Hu, J. The conserved fission complex on peroxisomes and mitochondria. *Plant Signal. Behav.* **6**, 870–872 (2011).

Pantin, F. *et al.* Developmental priming of stomatal sensitivity to abscisic acid by leaf microclimate. *Curr. Biol.* **23**, 1805–1811 (2013).

Park, S. *et al.* Abscisic Acid Inhibits PP2Cs via the PYR/PYL family of ABA-binding START Proteins. *Science (80-.).* **324**, 1068–1071 (2009).

Pei, Z. *et al.* Calcium channels activated by hydrogen peroxide mediate abscisic acid signalling in guard cells. *Lett. to Nat.* **406**, 731–734 (2000).

Peng, K. CO2 signalling in stomatal guard cells. *PhD thesis, Univ. Bristol* (2008).

Praefcke, G. J. K. & McMahon, H. T. The dynamin superfamily: Universal membrane tubulation and fission molecules? *Nat. Rev. Mol. Cell Biol.* **5**, 133–147 (2004).

QIAGEN. DNeasy ® Plant Handbook DNeasy Plant Mini Kit and tissues , or fungi Sample & Assay Technologies QIAGEN Sample and Assay Technologies. 22–25 (2012).

QIAGEN. Quick-Start Protocol QIAquick PCR Purification Kit. 12–13 (2010).

Ramachandran, R. *et al.* The dynamin middle domain is critical for tetramerization and higher-order self-assembly. *EMBO J.* **26**, 559–566 (2007).

Reubold, T. F. *et al.* Crystal structure of the dynamin tetramer. *Nature* **525**, 404–408 (2015).

Saito, S. & Uozumi, N. Guard Cell Membrane Anion Transport Systems and Their Regulatory Components: An Elaborate Mechanism Controlling Stress-Induced Stomatal Closure. *Plants* **8**, (2019).

Samuels, L., Giddings, T. & Staehelin, A. Cytokinesis in Tobacco BY-2 and Root Tip Cells : *J. Cell Biol.* **130**, 1345–1357 (1995).

Sandoval, J. F., Yoo, C. Y., Gosney, M. J. & Mickelbart, M. V. Growth of Arabidopsis thaliana and Eutrema salsugineum in a closed growing system designed for quantification of plant water use. *J. Plant Physiol.* **193**, 110–118 (2016).

Sasaki, T. *et al.* Closing Plant Stomata Requires a Homolog of an Aluminum-Activated Malate Transporter. *Plant Cell Physiol.* **51**, 354–365 (2010).

Sato, A. *et al.* Threonine at position 306 of the KAT1 potassium channel is essential for channel activity and is a target site for ABA-activated SnRK2 / OST1 / SnRK2 . 6 protein kinase. *Biochem. J.* **424**, 439–448 (2009).

Sharma, B., Molden, D. & Cook, S. Water use efficiency in agriculture: Measurement, current situation and trends Managing water and fertilizer for sustainable agricultural intensification

40 Managing water and fertilizer for sustainable agricultural intensification. in *Managing water and fertilizer for sustainable agricultural intensification* 39–64 (2015).

Sheahan, M. B., McCurdy, D. W. & Rose, R. J. Mitochondria as a connected population: Ensuring continuity of the mitochondrial genome during plant cell dedifferentiation through massive mitochondrial fusion. *Plant J.* **44**, 744–755 (2005).

SIGnAL (SALK Institute Genomic Analysis Laboratory). T-DNA Primer Design. (2005). Available at: http://signal.salk.edu/tdnaprimers.2.html.

Sirichandra, C. *et al.* Phosphorylation of the Arabidopsis AtrbohF NADPH oxidase by OST1 protein kinase. *FEBS Lett.* **583**, 2982–2986 (2009).

Smirnova, E., Shurland, D. L., Newman-Smith, E. D., Pishvaee, B. & Van Der Bliek, A. M. A model for dynamin self-assembly based on binding between three different protein domains. *J. Biol. Chem.* **274**, 14942–14947 (1999).

SnapGene. SnapGene Resources. (2017). Available at: www.snapgene.com/resources. (Accessed: 20th July 2018)

Song, J., Lee, M. H., Lee, G.-J., Yoo, C. M. & Hwang, I. Arabidopsis EPSIN1 Plays an Important Role in Vacuolar Trafficking of Soluble Cargo Proteins in Plant Cells via Interactions with Clathrin, AP-1, VTI11, and VSR1. *Plant Cell* **18**, 2258–2274 (2006).

Soto, D. *et al.* Functional characterization of mutants affected in the carbonic anhydrase domain of the respiratory complex i in Arabidopsis thaliana. *Plant J.* **83**, 831–844 (2015).

Tagliavia, C. Isolation and characterization of CO 2 response mutants in Arabidopisis thaliana. *PhD thesis, Univ. Bristol* (2006).

TAIR (The Arabidopsis Information Resource). TAIR. (2018). Available at: https://www.arabidopsis.org/index.jsp.

Tallman, G. Are diurnal patterns of stomatal movement the result of alternating metabolism of endogenous guard cell ABA and accumulation of ABA delivered to the apoplast around guard cells by transpiration? *J. Exp. Bot.* **55**, 1963–1976 (2004).

Tang, D., Ade, J., Frye, C. A. & Innes, R. W. A mutation in the GTP hydrolysis site of Arabidopsis dynamin-related protein 1E confers enhanced cell death in response to powdery mildew infection. *Plant J.* **47**, 75–84 (2006).

Taylor, N. G. A role for Arabidopsis dynamin related proteins DRP2A/B in endocytosis; DRP2 function is essential for plant growth. *Plant Mol. Biol.* **76**, 117–129 (2011).

Thoms, S. & Erdmann, R. Dynamin-related proteins and Pex11 proteins in peroxisome division and proliferation. *FEBS J.* **272**, 5169–5181 (2005).

Tian, W. *et al.* A molecular pathway for CO2 response in Arabidopsis guard cells. *Nat. Commun.* **6**, 1–10 (2015).

Tõldsepp, K. *et al.* Mitogen-activated protein kinases MPK4 and MPK12 are key components mediating CO 2 -induced stomatal movements. *Plant J.* **96**, 1018–1035 (2018).

Torres, M. A. & Dangl, J. L. Functions of the respiratory burst oxidase in biotic interactions, abiotic stress and development. *Curr. Opin. Plant Biol.* **8**, 397–403 (2005).

Ueda, M., Tsutsumi, N. & Fujimoto, M. Salt stress induces internalization of plasma membrane aquaporin into the vacuole in Arabidopsis thaliana. *Biochem. Biophys. Res. Commun.* **474**, 742–746 (2016).

Uehlein, N. *et al.* Function of Nicotiana tabacum Aquaporins as Chloroplast Gas Pores Challenges the Concept of Membrane CO2 Permeability. *Plant Cell* **20**, 648–657 (2008).

Umezawa, T., Sugiyama, N., Mizoguchi, M., Hayashi, S. & Myouga, F. Type 2C protein phosphatases directly regulate abscisic acid-activated protein kinases in Arabidopsis. *PNAS* **106**, 17588–17593 (2009).

Vahisalu, T. *et al.* SLAC1 is required for plant guard cell S-type anion channel function in stomatal signalling. *Nature* **452**, 487–491 (2008).

Verma, D. P. S. & Hong, Z. The ins and outs in membrane dynamics: Tubulation and vesiculation. *Trends Plant Sci.* **10**, 159–165 (2005).

Viotti, C. *et al.* The Endoplasmic Reticulum is the Main Membrane Source for Biogenesis of the Lytic Vacuole in Arabidopsis. *Plant Cell* **25**, 3434–3449 (2008).

Vitha, S., McAndrew, R. S. & Osteryoung, K. W. FtsZ ring formation at the chloroplast division site in plants. *J. Cell Biol.* **153**, 111–119 (2001).

Vlad, F. *et al.* Protein Phosphatases 2C Regulate the Activation of the Snf1-Related Kinase OST1 by Abscisic Acid in Arabidopsis. *Plant Cell* **21**, 3170–3184 (2009).

Waidyarathne, P. & Samarasinghe, S. Boolean Calcium Signalling Model Predicts Calcium Role in Acceleration and Stability of Abscisic Acid-Mediated Stomatal Closure. *Sci. Rep.* **8**, 1–16 (2018).

Wang, C. *et al.* Reconstitution of CO_2 Regulation of SLAC1 Anion Channel and Function of CO_2 -Permeable PIP2;1 Aquaporin as CARBONIC ANHYDRASE4 Interactor. *Plant Cell* **28**, 568–582 (2016).

Wang, M. *et al.* Family-wide expression characterization of Arabidopsis beta-carbonic anhydrase genes using qRT-PCR and Promoter::GUS fusions. *Biochimie* **97**, 219–227 (2014).

Wang, T. L., Donkin, M. E. & Martin, E. S. The Physiology of a Wilty Pea : Abscisic Acid Production under Water Stress. *J. Exp. Bot.* **35**, 1222–1232 (1984).

Wang, W. H. *et al.* The reduced state of the plastoquinone pool is required for chloroplast-mediated stomatal closure in response to calcium stimulation. *Plant J.* **86**, 132–144 (2016).

Wang, Y., Holroyd, G., Hetherington, A. M. & Ng, C. K. Y. Seeing 'cool' and 'hot' - Infrared thermography as a tool for non-invasive, high-throughput screening of Arabidopsis guard cell signalling mutants. *J. Exp. Bot.* **55**, 1187–1193 (2004).

Webb, A. & Hetherington, A. Convergence of the abscisic acid, CO2, and extracellular calcium signal transduction pathways in stomatal guard cells. *Plant Physiol.* **114**, 1557–1560 (1997).

Wilmer, C. & Fricker, M. *Stomata*. (Springer Netherlands, 1996).

Wolf, O., Jeschke, W. D. & Hartung, W. Long distance transport of abscisic acid in NaCl-treated intact plants of Lupinus albus. *J. Exp. Bot.* **41**, 593–600 (1990).

Woodward, F. I. Stomatal numbers are sensitive to increases in CO2 from pre-industrial levels. *Nature* **327**, 617–618 (1987).

Xie, Y. J. *et al.* Evidence of Arabidopsis salt acclimation induced by up-regulation of HY1 and the regulatory role of RbohD-derived reactive oxygen species synthesis. *Plant J.* **66**, 280–292 (2011).

Xu, Z., Jiang, Y., Jia, B. & Zhou, G. Elevated-CO2 Response of Stomata and Its Dependence on Environmental Factors. *Front. Plant Sci.* **7**, 1–15 (2016).

Xue, S. *et al.* Central functions of bicarbonate in S-type anion channel activation and OST1 protein kinase in CO2signal transduction in guard cell. *EMBO J.* **30**, 1645–1658 (2011).

Yoo, C. Y., Pence, H. E., Hasegawa, P. M. & Mickelbart, M. V. Regulation of transpiration to improve crop water use. *CRC. Crit. Rev. Plant Sci.* **28**, 410–431 (2009).

Yoo, C. Y. *et al.* The Arabidopsis GTL1 Transcription Factor Regulates Water Use Efficiency and Drought Tolerance by Modulating Stomatal Density via Transrepression of SDD1. *Plant Cell* **22**, 4128–4141 (2010).

Zhang, J., Jia, W., Yang, J. & Ismail, A. M. Role of ABA in integrating plant responses to drought and salt stresses. *F. Crop. Res.* **97**, 111–119 (2006).

Zhang, X. & Hu, J. The Arabidopsis Chloroplast Division Protein DYNAMIN-RELATED PROTEIN5B Also Mediates Peroxisome Division. *Plant Cell* **22**, 431–442 (2010).

Zhang, X. C. & Hu, J. P. FISSION1A and FISSION1B proteins mediate the fission of peroxisomes and mitochondria in Arabidopsis. *Mol. Plant* **1**, 1036–1047 (2008).

Zhang, X. & Hu, J. Two small protein families, DYNAMIN-RELATED PROTEIN3 and FISSION1, are required for peroxisome fission in Arabidopsis. *Plant J.* **57**, 146–159 (2009).

Zinchuk, V., Zinchuk, O. & Okada, T. Quantitative Colocalization Analysis of Multicolor Confocal Immunofluorescence Microscopy Images: Pushing Pixels to Explore Biological Phenomena. *Acta Histochem. Cytochem.* **40**, 101–111 (2007).

Zoulias, N., Harrison, E. L., Casson, S. A. & Gray, J. E. Molecular control of stomatal development. *Biochem. J.* **475**, 441–454 (2018).